TECHNISCHE UNIVERSITÄT MÜNCHEN

Wissenschaftszentrum Weihenstephan für Ernährung, Landnutzung und Umwelt

Lehrstuhl für Entwicklungsgenetik

Cellular mechanisms of sensory organ regeneration in the lateral-line system of zebrafish

Oriol Viader-Llargués

Vollständiger Abdruck der von der Fakultät Wissenschaftszentrum Weihenstephan für Ernährung, Landnutzung und Umwelt der Technischen Universität München zur Erlangung des akademischen Grades eines

Doktors der Naturwissenschaften

genehmigten Dissertation.

Voristzende:	Prof. Dr. Harald Luksch
Prüfer der Dissertation:	1. Prof. Dr. Wolfgang Wurst
	2. Prof. Dr. Virginie Lecaudey

Die Dissertation wurde am 26.09.2018 bei der Technischen Universität München eingereicht und durch die Fakultät Wissenschaftszentrum Weihenstephan für Ernährung, Landnutzung und Umwelt am 05.02.2019 angenommen.

Table of Contents

Summary

Understanding the mechanisms that guide the precise rearrangement of cells during regeneration has fascinated scientists for centuries. Unfortunately, mammals have only modest regenerative abilities when compared to our counterparts in the animal kingdom. In an attempt to improve our own approach to regenerative medicine, biologists have turned to the study of species that are endowed with more efficient regeneration.

In my thesis, I have undertaken work to gain a global perspective on how multiple cellular behaviors coordinate to drive organ regeneration. To this end, I have used a multidisciplinary approach that combines pharmacology, laser-mediated microsurgery, long-term live imaging and cell-lineage tracing, and machine-learning analytical methods. As experimental system, I used the neuromasts of the superficial lateral line of larval zebrafish. Neuromasts have manageable numbers of total cells, and an invariant distribution of their three constituent cell types: hair, sustentacular and mantle cells. Laying on the surface of the fish, they are amenable to physical access and non-invasive live-imaging.

I started by testing the effect of recurrent hair-cell ablations on the efficiency of their own regeneration and on the maintenance of organ architecture in both larval and adult zebrafish. I found that neuromasts are able to repeatedly regenerate hair cells without dismantling the global architecture of the organ, even in the absence of spatially-patterned Notch signaling. By maintaining a broad but weak expression domain of Atoh1a, neuromasts ensure the availability of a large pool of primed progenitors, and the rapid re-routing of sustentacular cells to a hair-cell progenitor fate. By forcing the production of neuromasts with imbalances of cell-type proportions, I

showed that neuromasts are able quickly return to homeostatic conditions, demonstrating remarkable architectural resilience.

Following these observations, I developed a novel experimental framework to generate damage of increasing severity in all neuromast cell types and followed the regenerative response of the remaining cells with high spatiotemporal resolution. With the help of machine-learning analytical methods, my data unveiled a process by which multiple individual cells coordinate to behave as a collective and recapitulate original organ architecture. I found that neuromasts do not contain specialized stem cells that predominantly participate in regeneration, but rather that its prevalent cell type, the sustentacular cells, is able to transiently switch from quiescence to proliferation and differentiation upon neuromast injury. Additionally, my results indicate that sustentacular cells are equipotent and coordinate their cell cycles during regeneration. Finally, machine-learning algorithms identified mediolateral position within the growing organ and distance to neighboring mantle cells as the best predictors of cell-fate acquisition. My original findings allowed me to propose a self-regulatory mechanism that guides the regenerative process to identical outcome despite the intrinsically stochastic nature of damage.

Zusammenfassung

Seit Jahrhunderten faszinieren Wissenschaftler die Mechanismen, welche die präzise Anordnung von Zellen während der Regeneration steuern. Verglichen mit weiteren Vertretern des Tierreichs, haben Säugetiere jedoch sehr begrenzte regenerative Eigenschaften. Daher wandten sich Biologen anderen Modellorganismen zu, die mehr Regenerationspotential aufweisen, um die Regeneration des Gewebes mit den gewonnenen Erkenntnissen der regenerativen Medizin zu verbessern.

In meiner Doktorarbeit habe ich Versuche durchgeführt, um einen universellen Überblick zu erhalten, wie vielseitige zelluläre Verhaltensweisen koordiniert werden, welche die Organregeneration steuern. Um dies zu erreichen, habe ich einen multidisziplinären Ansatz verfolgt, welcher Pharmakologie, laser vermittelte Mikrochirurgie, Langzeit-Live-Bildgebung und Zelllinien-Tracing sowie analytische Methoden des maschinellen Lernens kombiniert. Als experimentelles System dienten die Neuromasten der oberflächlichen Seitenlinienorgane von Zebrafischlarven. Neuromasten haben eine überschaubare Gesamtanzahl von Zellen und eine statische Verteilung ihrer drei Zelltypen: Haar-, Sustentakular- und Mantelzellen. Außerdem liegen diese auf der Oberfläche des Fisches, sind daher physikalisch messbar und können für nicht-invasive Live-Bildgebung genutzt werden.

Ich testete zuerst die Wirkung von wiederkehrenden Ablationen von Haarzellen auf die Leistungsfähigkeit ihrer Regeneration und auf die Aufrechterhaltung der Organarchitektur, sowohl bei Larven als auch bei adulten Zebrafischen. Dadurch stellte ich fest, dass Neuromasten in der Lage sind, Haarzellen immer wieder zu regenerieren, ohne die universelle Organarchitektur zu zerstören, selbst in der Abwesenheit von strukturiert angeordneten Notch-Signalen. Durch die

Aufrechterhaltung einer breiten, wenn auch schwachen Expressionsdomäne von Atoh1a sichern Neuromasten die Verfügbarkeit eines großen Vorrats von geprimten Vorläuferzellen und die schnelle Umwandlung von Sustentakular-Zellen zu Vorläufer-Haarzellen. Indem ich die Herstellung von Neuromasten mit einem Ungleichgewicht von Zelltyp spezifischen Eigenschaften erzwang, zeigte ich, dass Neuromasten schnell zu homöostatischen Zuständen zurückkehren können, was eine bemerkenswerte architektonische Belastbarkeit zeigt.

Basierend auf diesen Beobachtungen, entwickelte ich einen neuartigen experimentellen Ansatz, um in allen Neuromast-Zelltypen Schäden mit zunehmenden Ausmaßen auszulösen und der regenerativen Reaktion der verbleibenden Zellen mit hoher räumlicher und zeitlicher Auflösung zu folgen. Mit Hilfe von Analysemethoden, welche maschinelles Lernen nutzen, konnte ich mit meinen Daten einen Prozess entschlüsseln, bei dem sich mehrere einzelne Zellen in einem Zusammenschluss koordinieren und sich wie ein Kollektiv verhalten, um die ursprüngliche Organarchitektur wiederherstellen. Des weiteren fand ich heraus, dass Neuromasten keine spezialisierten Stammzellen enthalten, die vorwiegend an der Regeneration beteiligt sind, sondern, dass ihr vorherrschender Zelltyp, die Sustentakularzellen, in der Lage ist, bei Verletzung von Neuromasten vorübergehend aus einem Ruhezustand zu Proliferation und Differenzierung überzugehen. Darüber hinaus zeigten meine Ergebnisse, dass die Sustentakular-Zellen äquipotent sind und ihre Zellzyklen während der Regeneration koordinieren. Abschließend, wurde durch maschinelle Lernalgorithmen die mediolaterale Lage innerhalb des wachsenden Organs und die Entfernung zu benachbarten Mantelzellen als die optimalsten Indikatoren identifiziert, um das Schicksal einer Zelle vorherzusagen. All diese Ergebnisse ermöglichten mir,

einen sich selbst regulierenden Mechanismus zu suggerieren, der den regenerativen Vorgang zu einem gleich bleibenden Ergebnis verhilft, unabhängig von der Art der Verletzung, welche an sich stochastischer Natur ist.

An abridged version of the work presented in this thesis has been published in international peer-reviewed journals and is freely available online within the following articles:

Pinto-Teixeira, F.*, Viader-Llargués, O.*, Torres-Mejia, E., Turan, M., Gonzalez-Gualda, E., Pola-Morell, L., & López-Schier, H. (2015). Inexhaustible hair-cell regeneration in young and aged zebrafish. *Biol Open*, 4(7), 903-909. doi:10.1242/bio.012112

* equally contributing authors

Viader-Llargués, O., Lupperger, V., Pola-Morell, L., Marr, C., & López-Schier, H. (2018). Live cell-lineage tracing and machine learning reveal patterns of organ regeneration. *eLife*, 7. doi:10.7554/eLife.30823

1. Introduction

1.1. **Hallmarks of regeneration**

Regeneration is commonly defined as the structural and functional reconstruction of a lost cell, tissue, organ or body part. This complex process involves the generation of several differentiated cell types, the repositioning of cells to precise locations, the reestablishment of three-dimensional structures and the restoration of mechanisms that allow intercellular communication. The ability to regenerate, however, is capriciously distributed among the animal kingdom. Even within a given species, regeneration is strongly dependent on the nature of the tissues and becomes frequently less efficient as an individual ages (**Figure 1**). Invertebrates like *Hydra* and planaria are able to regenerate entire animals from small body fragments (as small as 1/300th for planaria) (Bosch, 2007; Morgan, 1898), whereas mammals have a strikingly limited capacity to regenerate vital organs or body parts. It is likely that regeneration has been favorably selected by evolution during the emergence of multi-cellular organisms, as a mechanism to maintain specific sizes and morphologies that were essential for the execution of various vital functions. Yet, it is commonly accepted that, evolutionarily, this ability represents an ancestral trait that has been partially lost in many lineages, including the amniotes or "higher vertebrates" but remained or re-appeared in the anamniotes or "lower vertebrates" (Dinsmore, 1991). Thus, research attention has focused on animals with exceptional regenerative abilities, in order to reveal the underlying cellular and molecular mechanisms that may be conserved among some species and lost in others.

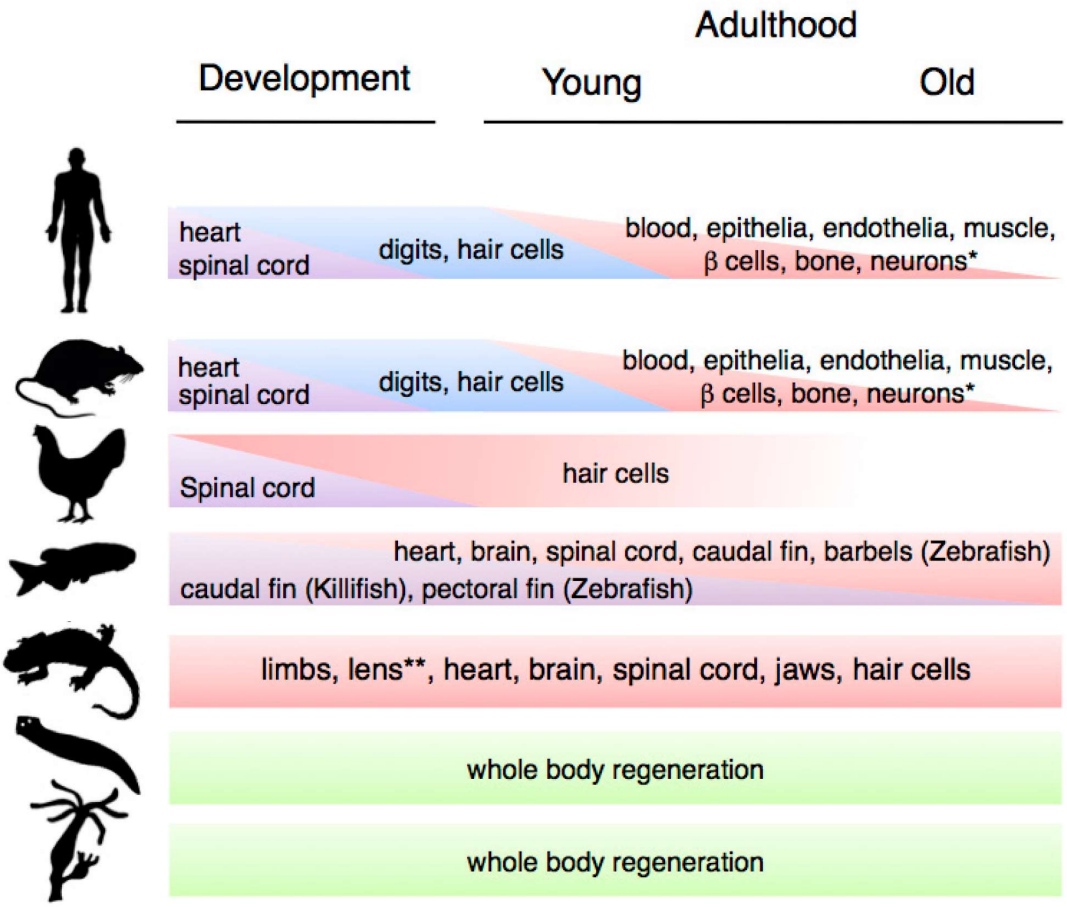

Figure 1. Differences in regenerative capacity in the animal kingdom through phylogeny and aging. From top to bottom: human, mouse, chicken, zebrafish, salamander, planarian and Hydra. Mammalian aging is characterized by a progressive decline in regenerative capacity, whereas other models like hydra, planarians, salamanders (axolotls and newts) and zebrafish maintain their ability to regenerate complex organs throughout their lifespan. *The ability to regenerate these systems is present in most other animal groups; **Regeneration of the lens is observed throughout the lifespan in newts, but it only occurs during axolotl development. Adapted from Yun (2015)

For many years, investigation of regeneration in lower vertebrates was mainly entrusted to developmental and evolutionary biologists. Today, these experimental models are becoming an essential complement to the modern field of stem-cell research. Yet, the complex processes that govern of growth and tissue patterning

during organ regeneration is not yet fully understood. Ultimately, by understanding how regeneration occurs naturally in these organisms, we may be able to extract mechanistic information to devise strategies to promote regeneration of mammalian organs damaged by trauma, disease or aging and to optimize regenerative medicine in humans.

1.2. **Regenerative modalities**

The classification of regeneration in different modalities has been, and continues to be, a controversial subject. This stems from the fact that, in general, classifications are only valid when the processes are well-understood and can be evenly compared. However, the categorization of regenerative processes into well-defined, mutually exclusive modalities becomes infinitely difficult because many of them are still so poorly understood that cannot be assigned to a particular group.

Nevertheless, at least four regenerative modalities have been identified and are commonly accepted (Carlson, 2007a):

a) Physiological regeneration refers to the natural replacement of worn-out cells or structures and is responsible for tissue homeostasis in the absence of trauma (often referred to as homeostatic cell turnover). It is characteristic of intestinal epithelia or the hematopoietic system.

b) Reparative regeneration represents what is popularly understood as the process after injury that replaces the structure and the functionality of a lost cell, tissue, organ or body part with exceptional accuracy. This includes two different modalities: Epimorphic regeneration, which requires the formation of a

blastema of undifferentiated cells preceding the development of the regenerated part. The classic example is the regeneration of an amputated limb of a salamander or newt. The rest of regenerative processes that do not involve the formation of a blastema are termed, accordingly, as cell, tissue or organ regeneration. Reparative regeneration without blastema can occur by a wide variety of means and are usually compliant with the extent and location of the injury or trauma. Some examples are hair cells, heart or muscle regeneration in zebrafish.

c) Hypertrophy is a particular case of regeneration that is often characterized by an increase in functional mass, rather than a restoration of external form. A classic example of this modality is the regeneration observed in the mammalian liver after the chirurgical resection of hepatic lobes.

d) Morphallaxis is a regenerative modality confined mostly to invertebrate organisms like planarians or *Hydra*. In this case, the reconstruction of a body part involves the complete reorganization of the remaining structures such as the relocation of entire organs.

1.3. **Stem cells in regeneration**

Despite semantic considerations, one aspect prevails: to understand any regenerative mechanism it is crucial to understand how the cells that participate in the process coordinate two different behaviors: proliferation and differentiation. In many cases, these two processes are performed simultaneously and precisely coordinated by stem cells (Greulich & Simons, 2016). These cells have been classically described by their ability to simultaneously self-renew and to produce cells that differentiate into

terminal cell types (Carlson, 2007b; Xin *et al.*, 2016). Adult organs have adopted two main strategies to ensure a cellular source during regeneration: One is to maintain a specialized population of tissue or organ-specific progenitors, normally called adult stem cells, ready to be mobilized upon specific requirements. The other is to transiently dedifferentiate cells committed to particular cell-types so that these can achieve the ability to differentiate into other cell types (multipotency). Irrespectively of the source of the cells that perform it, "stemness" behavior is imperative for the successful outcome of any regenerative process.

The turnover of adult stem cells varies greatly among tissues (Wabik & Jones, 2015). Adult stem cells are defined as slow-cycling or quiescent cells that constitute a specialized population that resides in a spatially defined microenvironment within the organ, referred to as "niche". These cells respond to inputs from their local environment and are responsible for the homeostasis of the organ. During homeostasis, the proliferation rate of stem cells is matched by that of cell loss from the lineage(s) they support, such that total cell number and cell-type proportions remain constant (Greulich & Simons, 2016). Upon acute injury, however, these cells must quickly respond to regenerate the lost tissue, by switching to a high proliferation mode (Wabik & Jones, 2015). The regulation of this switch requires an exquisitely refined tuning of cell behaviors, as the simultaneous engagement of all cells residing in the niche could lead to exhaustion of the stem-cell pool and impair the future capacity of the organ to cope with injury, resulting in organ failure (Blanpain & Fuchs, 2014). Thus, the maintenance of quiescence is especially relevant, as it prevents stem-cell depletion whilst decelerating the natural accumulation of oncogenic mutations in their nuclear and mitochondrial DNA (Greco & Guo, 2010).

Four fundamental questions in regenerative biology are the current focus of intense attention: 1) how do stem cells maintain the delicate equilibrium between quiescence and proliferation, 2) how do these cells sense three-dimensional, large-scale disruptions of organ integrity to adapt their regenerative response to the extent and location of injuries 3) how does a seemingly homogenous cell population is able to generate a diversity of cell types, and 4) how are cell lineage choices computed during the decision-making processes.

1.4. **Zebrafish as a model organism to study regeneration**

The teleost *Danio rerio* (zebrafish) is a tropical freshwater fish native from the Ganges region in eastern India and southeastern Himalayas, named after the blue horizontal stripes that extend from its gills to the caudal fin tip. In the wild, they inhabit slow-moving shallow waters with high content of slit and vegetables.

Although the regenerative potential of teleost fish was first discovered by the French naturalist Broussonet in 1786 (Broussonet, 1786), it was not until around 40 years ago that the zebrafish was established as a routine model for animal experimentation. Based on goldfish experiments, Broussonet concluded that caudal fins display a regenerative advantage over other fins, a finding that certainly influenced regenerative biology until today, since research continues to use the caudal fin to elucidate the molecular and cellular mechanisms governing vertebrate regeneration (**Figure 2**).

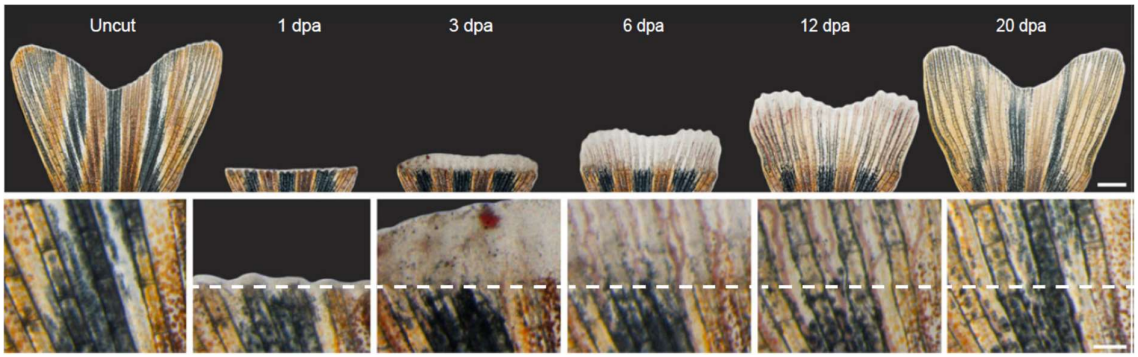

Figure 2. Blastema formation during caudal fin regeneration in zebrafish. Amputation of the caudal fin triggers a regenerative response that restores original tissue architecture. Top panel: Time-lapse images; 1 day-post-amputation (dpa), the white tissue above the amputation contains wound epidermis and a few undifferentiated cells. At 3dpa, the mass of undifferentiated cells forms a blastema. At 6dpa, the blastema extends rapidly and starts to display bone structures and pigmentation. At 12dpa, fin regeneration is at its advanced stage. 20dpa, the size of the regenerated fin matches its original size and striped pattern. The white margin of tissue remains at the tip for homeostatic growth/regeneration. Bottom panels: Higher magnifications of the of the fin surface at the amputation site (white dashed line) at the respective time points. Scale bars: (top) 1000µm; (bottom) 200µm. Adapted from Pfefferli and Jazwinska (2015).

The popularity of the zebrafish as an experimental model has been growing exponentially since the 1970s, when the biologist George Streisinger, aware of the exhaustion of the phage as a genetic system, decided to continue his work on a vertebrate model that was easy to manipulate genetically (Varga, 2018). His colleagues at the University of Oregon soon became zebrafish enthusiasts, as it proved particularly attractive for studying embryonic development of the vertebrate nervous system (Kimmel, 1972; Streisinger *et al.*, 1981). A few years later, the zebrafish became the first vertebrate model to be used for large-scale forward genetic screens, carried out by two independent laboratories in Boston and Tübingen (Driever *et al.*, 1996; Haffter *et al.*, 1996). Together with later mutagenesis screens (Amsterdam *et al.*, 1999; Golling *et al.*, 2002; Mullins *et al.*, 1994), these studies led to the discovery of more than 2000 single-allele mutated genes linked to unique phenotypes in a wide variety of biological

processes. Until today, numerous reverse genetics technologies have been developed to directly test the function of a gene of interest. These genome editing tools include zinc finger nucleases (ZFNs) (Doyon *et al.*, 2008; Meng *et al.*, 2008) TAL-effector nucleases (TALENs) (Huang *et al.*, 2011), and perhaps most importantly, the clustered regulatory interspaced short palindromic repeat (CRISPR)/Cas9 endonuclease (Varshney *et al.*, 2015). In fact, the CRISPR/Cas9 system have made reverse genetic approaches available to virtually every zebrafish laboratory, even to those with modest resources or lack of molecular biology expertise.

The zebrafish present several advantages compared to other experimental animal model systems for several reasons. These include high fecundity, rapid and external development and optical transparency during embryonic and larval stages. These conditions make them amenable for non-invasive live-imaging and genetic tractability. Additionally, the zebrafish reach sexual maturity at 3-4 months of age, allowing a relatively short time for the generation of mutant and transgenic lines.

The sequencing of the zebrafish genome was completed in 2013, revealing that it contains homologues of approximately 70% of human genes and that 80% of those are involved in disease etiology (Howe *et al.*, 2013). As a vertebrate, many of its organs share remarkable anatomical and physiological similarities to those in humans. However, most adult mammals are naturally less capable of regenerating their organs than the zebrafish. In fact, the zebrafish is endowed with an outstanding capacity to regenerate size and shape of several organs, including fins (Nechiporuk & Keating, 2002), heart (Poss *et al.*, 2002), retina (Vihtelic & Hyde, 2000), spinal cord (Becker *et al.*, 1997), telencephalon (Kroehne *et al.*, 2011), skin (Richardson *et al.*, 2013), melanocytes (Yang *et al.*, 2004), hair cells (Harris *et al.*, 2003), pancreas (Moss *et al.*,

2009), liver (Sadler *et al.*, 2007), and kidney (Diep *et al.*, 2011). Because of its remarkable regenerative abilities and amenability for genetic manipulation and state-of-the-art live imaging, the zebrafish is emerging as an excellent model to understand the biology of adult stem cells and vertebrate organ regeneration.

1.5. **Case-study: Brief history of hair-cell regeneration**

One of the fields that has largely benefited from the use of the zebrafish as an experimental animal model is that interested in understanding why mammals are unable to efficiently regenerate auditory and vestibular hair-cells after their loss. Hair cells are specialized receptors responsible for the transduction of external mechanical stimuli into chemical signals. These signals are in turn converted into electrical impulses by afferent neurons and transmitted to the brain via ascending neuronal pathways (Hudspeth, 1989). Hair cells are unique to vertebrates, and can be found in the inner ear, comprising the auditory and vestibular systems, as well as in the lateral line system of some aquatic vertebrates such as the zebrafish (Hudspeth, 1989; Nicolson, 2005). The survival and homeostasis of hair-cells is essential for the life-long function of these mechano-sensory organs. However, a wide range of genetic mutations and external insults negatively affect hair-cell survival and often lead to their death. These include infections, high sound-pressure levels and numerous ototoxic agents such as heavy metals, aminoglycoside antibiotics or anti-neoplastic therapies (Chen & Fechter, 2003; Huth *et al.*, 2011; Langer *et al.*, 2013). In mammals, hair-cells are almost exclusively produced during embryogenesis and display very limited regenerative capacity. Hence, the postembryonic loss of these cells leads to irreversible hearing loss and balance disorders (Chardin & Romand, 1995; Davis *et al.*, 1989). On

the contrary, the production of sensory hair-cells continues long after birth in many non-mammalian vertebrates, a feature that allows them to efficiently regenerate lost hair cells (Behra *et al.*, 2009; Hernandez *et al.*, 2007; Williams & Holder, 2000). Postembryonic addition of hair cells was first discovered in amphibians and cartilaginous fish as part of their ongoing growth (Balak *et al.*, 1990; Corwin, 1981, 1985). Continuous turnover of vestibular hair cells was also observed in birds, as well as regeneration of both vestibular and auditory hair cells after damage by acoustic trauma (Corwin & Cotanche, 1988; Cruz *et al.*, 1987; Ryals & Rubel, 1988). This natural process has fueled an intense interest in elucidating the underlying mechanisms of regeneration, as well as for the design of therapeutic approaches to restore hearing and balance in humans through the postembryonic stimulation of hair-cell production in the inner ear.

Because of its exceptional accessibility and visibility, a substantial part of hair-cell regeneration investigation has relied on the lateral-line system of the zebrafish. In the recent years, this system has become a highly valuable experimental model for understanding the cellular and molecular foundations of hair-cell regeneration (Grant *et al.*, 2005; Harris *et al.*, 2003; Hernandez *et al.*, 2007; López-Schier & Hudspeth, 2006; Ma *et al.*, 2008; Pinto-Teixeira *et al.*, 2013; Williams & Holder, 2000).

1.1. The lateral-line system of the zebrafish

1.1.1. Anatomy of the lateral line and its functional units

The lateral-line is a sensory system present in fish and amphibia responsible for the detection of pressure changes and water disturbances in the vicinity of the fish body,

mediating the so-called "touch-at-a-distance" sense (Dijkgraaf, 1963). The ability to sense this information is vital for the performance of several complex motor behaviors including navigation, prey tracking and predator avoidance, rheotaxis (orientation of the body against direction of the flow), schooling and sexual courtship (Coombs & Montgomery, 1999; Montgomery *et al.*, 2000; Montgomery *et al.*, 1997).

The lateral line system consists of two major branches; the anterior lateral-line, that extends towards the head, and the posterior lateral-line, which extends along the trunk until the tip of the tail (**Figure 3**). Of note, the latest has concentrated the major part of the current investigation on the development, organization and regeneration of the system. These branches comprise a collection of independent small organs that are the ultimate mechano-sensing units of the lateral line. These organs, called neuromasts, are distributed on the surface of the animal skin in a species-specific pattern and are functionally analogous to the inner ear (Ghysen & Dambly-Chaudière, 2007).

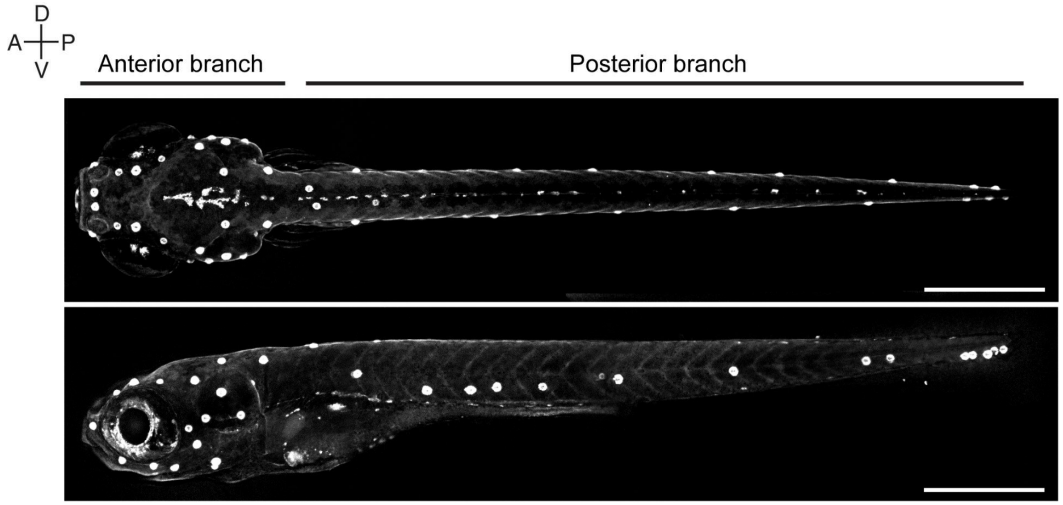

Figure 3. Distribution of anterior and posterior branches of the zebrafish lateral line. Top (above) and lateral (below) views of a 7dpf zebrafish larvae from the *Tg[SqGw57A]* transgenic line. Cytosolic GFP (white) labels neuromast supporting cells, highlighting their position along the fish body. Scale bars: 500 μm.

Mature neuromasts consist of a circular epithelium of 60 to 70 cells that contains approximately 18 centrally-located, mechanotransducing hair cells and 40 to 50 supporting cells surrounding them (**Figure 4**A). Lateral line hair-cells share physiological, cellular and molecular properties with those in the inner ear (Nicolson, 2005). Each hair-cell projects a hair-bundle that trespasses the skin and is embedded into a gelatinous cupula that bends in response to water movements (Ghysen & Dambly-Chaudière, 2007). The hair bundle is composed of hundreds of actin-based stereocilia arranged in rows of increasing length and a single microtubule-based kinocilum located adjacent to the tallest stereocilia (**Figure 4**B). In consequence, hair cells are oriented in a specific direction along the plane of the epithelium in what is a striking example of planar cell polarization (PCP) (**Figure 4**B). Hair cells are innervated by neurons that transmit electrical stimuli to the central nervous system and efferent neurons that signal in the opposite direction to modulate hair-cells'

sensitivity. The axons from afferent neurons extend along the myoseptum forming a nerve and the somas coalesce into a small ganglion located adjacent to the otic vesicle (Metcalfe *et al.*, 1985).

Each neuromast develops two equally-numbered populations of intermingled hair cells that are oriented along the same axis but facing opposite directions (**Figure 4**C). Thus, the morphological polarization of hair cells underlies the bidirectional sensitivity of these organs; bending of the cupula towards a given direction, depolarizes one half of the hair cells and hyperpolarizes the other, and vice versa (Hudspeth, 1989). Interestingly, two types of neuromasts have been described according to their orientation relative to the body's axis. Those with hair cells oriented along the anteroposterior axis are called horizontal neuromasts whereas those with hair cells oriented along the dorsoventral axis are called vertical neuromasts (**Figure 4**D) (López-Schier *et al.*, 2004).

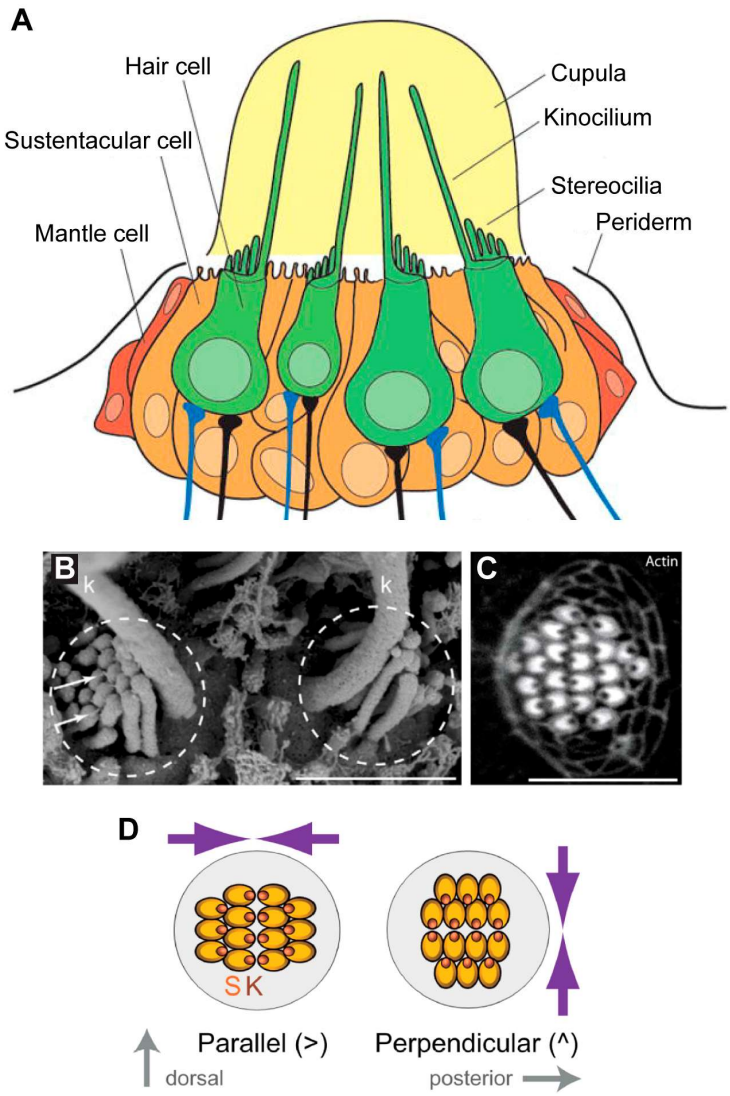

Figure 4. Cellular organization of lateral line neuromasts. (**A**) Schematic representation of a neuromast cross-section showing the organization of the different cell types and organ structures. Hair cells occupy the center of the organ and extend their mechanotransducing organelle through the periderm, towards a gelatinous cupula. Sustentacular cells surround and intermingle with the hair cells. Mantle cells conform the outermost cell layer and delimitate the periphery of the organ. (**B**) Scanning electron microscopy (SEM) images of two hair bundles with confronting polarities. Kinocilia (k) are extrinsically located next to the highest stereocilia (arrows). Scale bar: 1µm (**C**) Actin staining with rhodamine-phalloidin reveals two equally-numbered groups of hair cells with opposing polarities oriented along the same axis. Scale bar: 10µm. (**D**) The orientation of a neuromast is determined by the polarization of its hair cells. Parallel neuromasts are mechanosensitive in the anteroposterior direction, and perpendicular neuromasts in the dorsoventral direction. Adapted from Chiu *et al.* (2008); Kindt *et al.* (2012); López-Schier *et al.* (2004); Pujol-Marti and López-Schier (2013).

Differences in location and shape divide this last group in two sub-types: sustentacular and mantle cells (Ghysen & Dambly-Chaudière, 2007). Sustentacular cells form the bulk of the epithelium and are located underneath and surrounding the hair cells. They intermingle with hair cells by extending membrane processes towards the apex of the neuromast. Finally, a thin layer of mantle cells encircles the organ, outlining the outer perimeter of the neuromast (Chezar, 1930). Gene-expression analysis by *in situ* hybridization (Froehlicher *et al.*, 2009) and two independent mRNA profiling screens demonstrated that sustentacular and mantle cells are molecularly-distinguishable subpopulations (Jiang *et al.*, 2014; Steiner *et al.*, 2014).

1.1.2. Development of the posterior lateral line

The posterior lateral line originates from the posterior lateral-line placode, an epidermal thickening that appears caudal to the otic vesicle by 18 hours post fertilization (hpf) (Kimmel *et al.*, 1995). Within the next hour, the placode delaminates and splits into two groups. An anterior group of approximately 20 cells remains stationary and differentiates into the afferent neurons ganglion, whereas a large posterior group, containing around 100 cells, forms the posterior lateral-line primordium. This cohesive cluster of cells starts migrating under the skin along the myoseptum towards the tip of the tail (Metcalfe *et al.*, 1985). During migration, the primordium periodically deposits clusters of cellular rosettes of approximately 20 cells, each of them a prospective neuromast (**Figure 5**A). By 48hpf, the primordium reaches the tip of the trunk leaving behind a line of 7-8 discrete neuromasts connected by a thin thread of interneuromast cells. At around 40hpf, a second placode gives rise to two new

primordia (Sapède *et al.*, 2002). One of them follows the same route as the first primordium and deposits 3 to 4 additional neuromasts along the same trail and the other migrates dorsally generating a dorsal lateral line (**Figure 5**B).

The lateral-line primordium is strongly polarized along its anteroposterior axis; its cells experience progressive changes in behavior and morphology as they move from the leading end to the trailing domain (**Figure 5**C). Cells at the migratory front are flatter and display mesenchymal morphology whereas cells in the adjacent trailing domain start acquiring apicobasal polarity as they become apically constricted for the assembly in epithelial rosettes (Lecaudey *et al.*, 2008). The territorialization of cell behaviors in the primordium is governed by a complex self-regulatory network that results in high levels of Wnt/β-catenin activation at the leading edge and high levels of FGF at the trailing domain (**Figure 5**C) (Aman & Piotrowski, 2008; Lecaudey *et al.*, 2008; Nechiporuk & Raible, 2008). Several recent comprehensive reviews describe in detail the molecular bases of collective migration, rosettogenesis and neuromast deposition by the posterior lateral-line primordium and will not be discussed here (Chitnis *et al.*, 2012; Harding *et al.*, 2014; Ma & Raible, 2009).

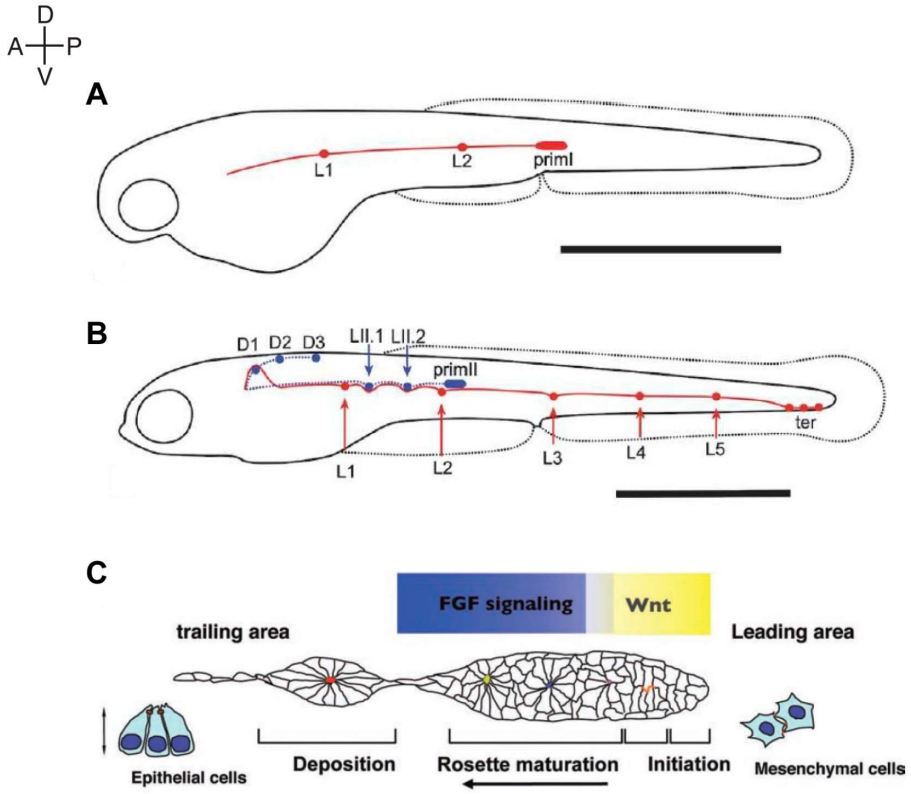

Figure 5. Lateral line primordium migration. During its migration along the myoseptum, the primordium deposits small clusters of cells in stereotyped positions that will mature into neuromasts, as well as a thin thread of interneuromast cells. (**A**) At 32hpf, the primordium is half-way through the trunk and deposited two prospective neuromasts. (**B**) At 3dpf, the first primordium reached the tip of the tail where it fragments in two or three terminal neuromasts. At ~40hpf, a second placode delaminates and splits into two new primordia; One follows the same path as the first and deposits perpendicular neuromasts, and a dorsal primordium that migrates dorsally and deposits two or three neuromasts behind the head of the fish. (**C**) Schematic representation of a migrating primordium. Cells at the leading edge, exposed to high levels of Wnt signaling, display a mesenchymal morphology. As cells move towards the trailing domain, dominated by FGF signaling, they progressively acquire epithelial morphology and began to assemble into epithelial rosettes. Eventually, a rosette is detached from the primordium and becomes a prospective neuromast. Adapted from Chitnis *et al.* (2012); Ghysen and Dambly-Chaudière (2007). Scale bars: 1mm.

After their deposition, posterior neuromasts migrate ventrally to its final location below the myoseptum (Ledent, 2002; Nuñez *et al.*, 2009; Sapède *et al.*, 2002). Interestingly, neuromasts derived from the first primordium are oriented in the

anteroposterior axis, whereas neuromasts derived from the second and dorsal primordia are oriented in the dorsoventral axis (López-Schier *et al.*, 2004; Nuñez *et al.*, 2009). A few hours after deposition, cellular rosettes differentiate into mature neuromasts.

1.1.3. Postembryonic generation of lateral-line neuromasts

After an initial phase of embryonic development (up to 3 days-post fertilization, dpf), zebrafish continue to grow as larvae (3dpf to 1 month) and juvenile (1 to 3 months) until they reach sexual maturity and their final size (around 30mm, without the caudal fin) (Kimmel *et al.*, 1995). During this period of continued growth, and unlike other sensory systems like the eyes or the olfactory bulbs, neuromast's size does not increase proportionally with body size, but rather the number of neuromasts increases.

In the transition from embryo to larvae, interneuromast cells derived from the first primordium begin to aggregate and proliferate and give rise to intercalary neuromasts (**Figure 6**A-C) (Nuñez *et al.*, 2009). This occurs precociously in the absence of the glial cells that accompany the afferent neurons, called Schwann cells (**Figure 6**D,E) (Grant *et al.*, 2005; López-Schier & Hudspeth, 2005). It has been recently reported that this occurs because Schwann cells prevent the activation of Wnt/β-catenin in interneuromast cells via inhibitory ErbB signaling (Lush & Piotrowski, 2014; Sánchez *et al.*, 2016).

Another interesting example of postembryonic neuromast generation that occurs in early juvenile stages is the formation of stitches. Stitches are dense linear arrays of 10 to 20 neuromasts that extend dorsoventrally that are formed through budding of a founder neuromast (**Figure 6**F-G) (Ledent, 2002). Although the budding process has been analyzed by live-imaging video-microscopy, the precise contribution of the different neuromast cell types to the generation of a new organ remains enigmatic (Wada *et al.*, 2013; Wada *et al.*, 2010). Interestingly, the neuromasts in a stitch maintain the orientation of its founder neuromast (**Figure 6**H) and are innervated by the same neurons through repeated branching (Ledent, 2002).

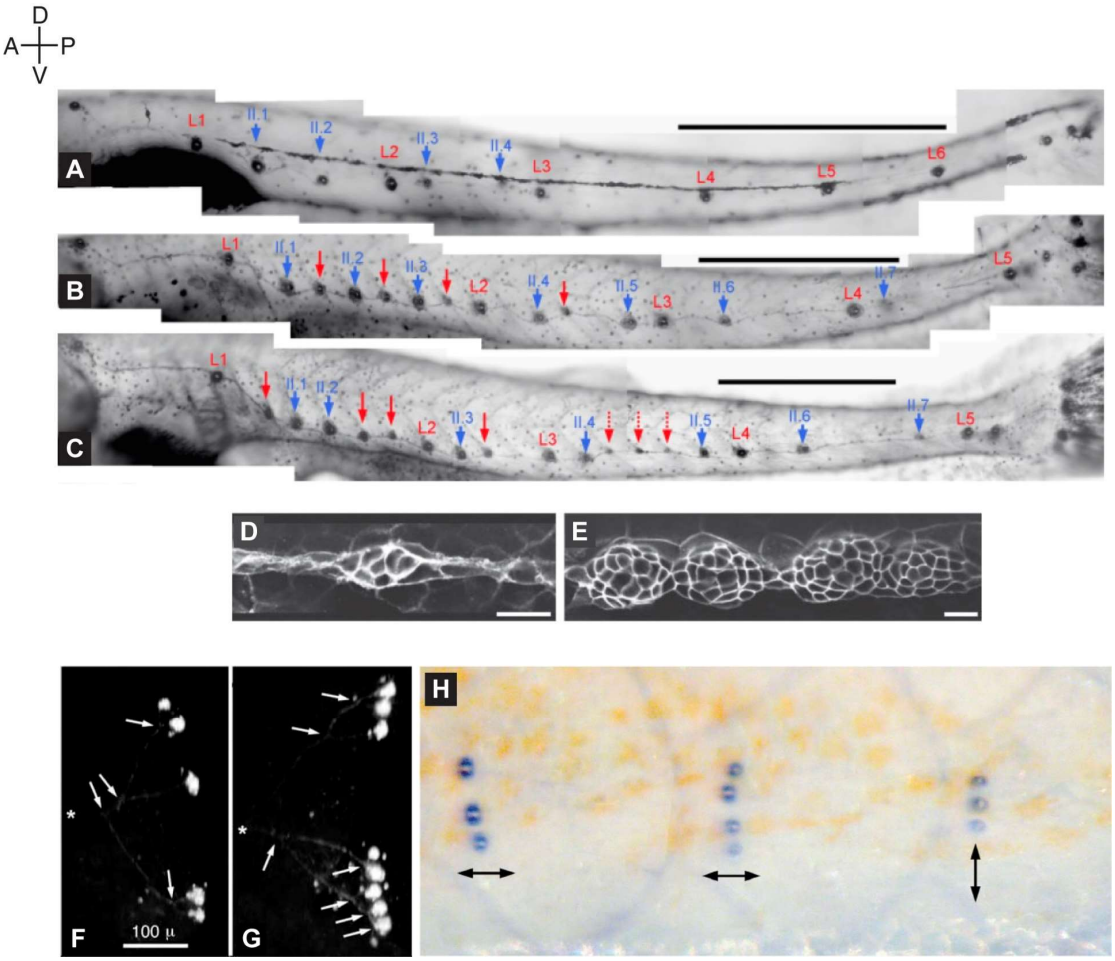

Figure 6. Postembryonic development of the lateral line. (**A**) At 6dpf the posterior lateral line presents only primordium-derived neuromasts (red and blue numbering). (**B**) At 12dpf, the first intercalary neuromasts are generated through the proliferation and aggregation of interneuromast cells (red arrows). (**C**) At an early juvenile stage (5.5mm) intercalary neuromast continue to be formed. The pattern of a neuromast per somatic border is nearly complete. Scale bars: 1mm. (**D**) Interneuromast cells of a *neurogenin 1* (*ngn1)* mutant lacking both neurons and Schwann cells begin to coalesce precociously (52hpf). (**E**) By 72hpf, these cell clusters resolve into new neuromasts generating extra intercalary neuromasts. Scale bars: 10µm. (**F,G**) Formation of neuromast stitches by budding of founder neuromasts. Sibling neuromasts are innervated by the same neurons (arrow point to neuronal bifurcations). (**H**) Stitches in a late-juvenile specimen (17.5mm). Neuromasts from the same stitch are oriented in the same polarity axis. Adapted from (**A-C**) Nuñez *et al.* (2009) (**D,E**) López-Schier and Hudspeth (2005) (**F,G**) Ledent (2002) (**H**) Ghysen and Dambly-Chaudière (2007).

1.1.4. Neuromast maturation and homeostasis

The acquisition of different cell fates within a neuromast requires the orchestrated integration of several intercellular signaling pathways. The specification of the first pair of hair cells in newly deposited neuromasts depends on an FGF-dependent activation of *atoh1a* in a central progenitor cell (Nechiporuk & Raible, 2008). The localized source of FGF activity is most likely the effect of ligand accumulation in the luminal cavity of neuromast rosettes (Durdu *et al.*, 2014). The same FGF signaling center initiates also the expression of DeltaA, which activates the Notch receptor in adjacent prospective non-sensory supporting cells, preventing them from expressing *atoh1a* (Matsuda & Chitnis, 2010). Subsequently, Atoh1a activates the expression of another Notch ligand, DeltaD, reinforcing the Notch-mediated suppression of *atoh1a* in neighboring cells, and allowing them to differentiate into supporting cells (Matsuda & Chitnis, 2010). The first cell that stabilizes the expression of *atoh1a* is specified as hair-cell progenitor and becomes the new source of FGF signaling by upregulating the FGF ligand FGF10, and simultaneously inhibiting the expression of its receptor FGFR1

(Lecaudey *et al.*, 2008; Matsuda & Chitnis, 2010). At this stage, hair-cell progenitor identity becomes FGF-independent and relies solely on its own auto-regulation. This is possible through the Atoh1a-dependent activation of *atoh1b* expression, which helps maintain the expression of the *atoh1a* by a cross-activation mechanism (Matsuda & Chitnis, 2010). Meanwhile, Notch signaling remains active in the surrounding cells, which continue to express FGFR1 and therefore remain competent to receive FGFR1 activation signals. The newly formed hair-cell progenitor, as a source of FGF and DeltaD, is now capable of activating *atoh1a* expression and to promote the specification of additional hair-cell progenitors in its vicinity. By specifying the fate of prospective hair cells and supporting cells, the interaction between FGF and Notch signaling marks the first event of neuromast cell diversification.

Because of their exposure to the environment, hair cells in neuromasts are slowly but continuously lost and replaced (Cruz *et al.*, 2015; Williams & Holder, 2000). To maintain their physiological function, neuromasts must strike a balance between allowing continuous hair-cell production and preventing uncontrolled cell proliferation, which may lead to tissue-architectural problems. One way to achieve this balance is to restrict different cellular behaviors to specific locations within the organ. Several studies have identified the presence of distinct cellular territories in fully-grown neuromasts. In particular, genetic analyses have defined polar (dorsal-ventral) and equatorial (anterior-posterior) areas with, respectively, low and high expression of the transgenic marker SqEt20, which is, in turn, complementary to the activity domains of the endogenous enzyme alkaline phosphatase (Villablanca *et al.*, 2006; Wibowo *et al.*, 2011). Further investigation showed that the levels of Notch signaling also define neuromast regionalization (Ma *et al.*, 2008; Wibowo *et al.*, 2011). In this

context, the Notch receptor Notch3 is strongly enriched in equatorial areas and is absent in the central and polar areas, where DeltaA and Atoh1a are expressed. These observations lead to the conclusion that equatorial territories under sustained high levels of Notch activity are non-permissive environments where the acquisition of hair-cell progenitor identity is inhibited, whereas polar areas, with low or no Notch activity, allow the expression of Atoh1a and thus, the specification of these progenitors (Wibowo *et al.*, 2011). However, during homeostasis, neuromasts display low cell proliferation rates that appear to be directly regulated by a negative feedback loop that depends on the relative proportion of hair cells within the organ (Wada & Kawakami, 2015). In fact, pharmacological activation of canonical Wnt/β-catenin in mature neuromasts stimulates production of both supporting and hair cells (Head *et al.*, 2013; Jacques *et al.*, 2014). The observation of a central-located *dkk2* expression domain suggests that this secreted Wnt inhibitor is expressed by either hair cells or their direct progenitors to maintain low levels of Wnt/β-catenin signaling throughout the neuromast and thus, prevent cell proliferation in the absence of cell loss (Wada *et al.*, 2013).

1.1.5. Basis of hair-cell regeneration in the lateral line

Cellular basis

Lateral-line hair cells are especially susceptible to harmful compounds present in water. For instance, a brief treatment with aminoglycoside antibiotics or copper sulfate is enough to eliminate their entire population. Such approach has become the most common strategy to ablate hair cells and study their regeneration in zebrafish (Harris *et al.*, 2003; Hernández *et al.*, 2006; Hernandez *et al.*, 2007; Owens *et al.*, 2007; Song

et al., 1995; Williams & Holder, 2000). After the complete ablation of lateral line hair cells, neuromasts mount a rapid regenerative response that recovers all lost sensory cells in a period of around 72 hours (Harris *et al.*, 2003; Hernandez *et al.*, 2007; López-Schier & Hudspeth, 2006; Williams & Holder, 2000). Although it has been shown that birds and amphibians can regenerate hair cells via direct supporting cell trans-differentiation (Adler & Raphael, 1996; Baird *et al.*, 2000; Roberson *et al.*, 1996; Roberson *et al.*, 2004; Rubel *et al.*, 2013), this mechanism of phenotypic conversion has been rarely observed in zebrafish (Hernandez *et al.*, 2007; Millimaki *et al.*, 2010). Indeed, studies using BrdU incorporation into DNA and time-lapse imaging have persuasively shown that zebrafish replace lost hair cells primarily through the division and subsequent differentiation of inner supporting cells, most likely sustentacular cells (López-Schier & Hudspeth, 2006; Ma *et al.*, 2008; Mackenzie & Raible, 2012; Romero-Carvajal *et al.*, 2015; Wibowo *et al.*, 2011). In accordance with the above conclusion, treatment of zebrafish after hair-cell ablation with cell cycle inhibitors completely prevent hair-cell regeneration in neuromasts, indicating that a trans-differentiation is rare or non-existent (Mackenzie & Raible, 2012; Wibowo *et al.*, 2011). Hair-cell progenitors are initially identified in the central and dorsoventral areas of the neuromast, where a terminal differentiating division gives rise to a new pair of confronting hair cells (**Figure 7**) (López-Schier & Hudspeth, 2006; Ma *et al.*, 2008; Romero-Carvajal *et al.*, 2015; Wibowo *et al.*, 2011). Strikingly, coherent planar polarization is also reestablished during this process (**Figure 7**, last panel) (Wibowo *et al.*, 2011). Although no directed cellular migration has been observed during hair-cell regeneration, stochastic cell movement might be determinant for the re-positioning of prospective sensory progenitors to permissive areas (Romero-Carvajal *et al.*, 2015; Wibowo *et al.*, 2011).

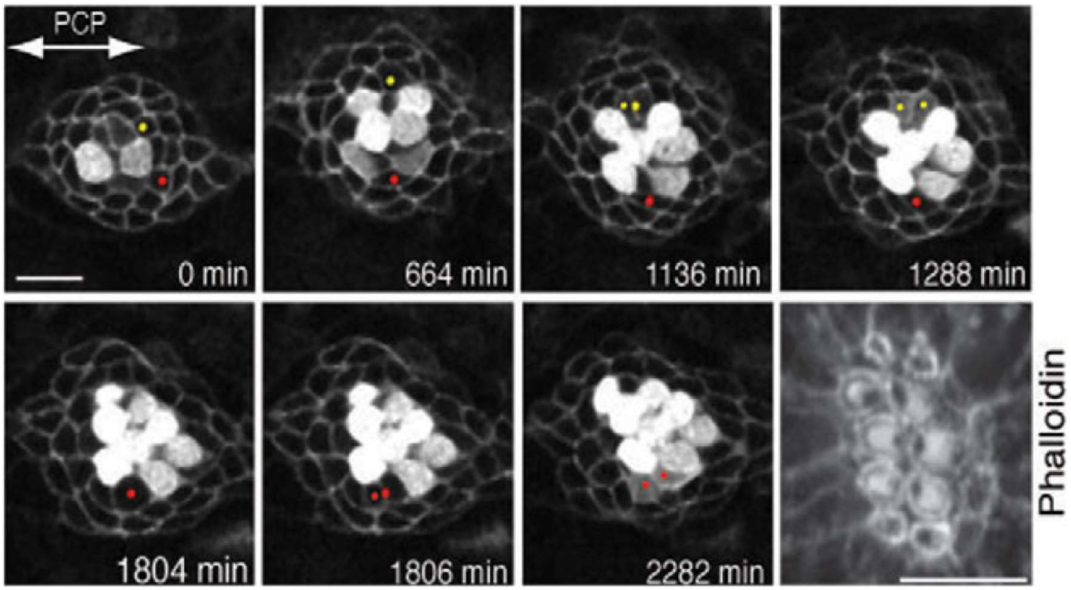

Figure 7. Hair cell regeneration in lateral line neuromasts. Hair cell precursors appear sequentially at the dorsal and ventral areas of a neuromast and divide into a pair of regenerated hair cells. Regenerated hair cells recover the original axis of planar cell polarity during the process. Adapted from Wibowo *et al.* (2011).

Molecular basis

The steady equilibrium of molecular pathways that sustains physiological levels of hair-cell replacement during non-traumatic periods must undergo significant rearrangements in order to cope with a massive loss of hair cells. To promote a rapid production of new sensory cells, neuromasts must reactivate several developmental mechanisms. Immediately after hair-cell ablation, ligands of the Notch and FGF signaling pathways are transiently down-regulated (Jiang *et al.*, 2014; Rubbini *et al.*, 2015). In parallel, *atoh1a* and delta ligands are strongly up-regulated in central sustentacular cells (Ma *et al.*, 2008; Wibowo *et al.*, 2011). The short window of Notch inactivity leads to the loss of dkk2 expression and thus, releases the inhibition on the

Wnt/β-catenin pathway as revealed by the expression of wnt2 and wnt10a (Romero-Carvajal *et al.*, 2015). The most significant changes in the activity levels of these signaling pathways occur in the first 24 hours, during which period neuromasts replace up to 8 hair cells (Harris *et al.*, 2003; López-Schier & Hudspeth, 2006). Afterwards, they progressively return to the original balance and hair-cell regeneration continues at a lower rate (Jiang *et al.*, 2014). An additional signaling pathway that has been found to play a major role in hair-cell regeneration is the retinoic acid (RA) pathway. The activation of RA signaling is crucial for heart and fin regeneration in adult zebrafish (Blum & Begemann, 2012; Kikuchi *et al.*, 2011) as well as for the regeneration of amputated limbs and several organs in other vertebrates such as axolotl, salamander, chick and mouse (Cunningham & Duester, 2015). Recently, it has been shown that the RA ligand *aldh1a2* is expressed in mantle cells of the zebrafish lateral line neuromasts, as revealed by the expression of a fluorescent reporter driven by the *aldh1a2* regulatory regions (Pittlik & Begemann, 2012). Additionally, the RA receptor *rarga* is expressed throughout the neuromast, indicating that this signaling pathway might be important for neuromast homeostasis (Rubbini *et al.*, 2015). In fact, the RA ligand *aldh1a3* and the receptor *rarab* are strongly up-regulated in central supporting cells upon hair-cell loss. In accordance with these observations, the expression of a dominant negative form of the RA receptor *rarαa* (dnRAR), prevents hair-cell regeneration in lateral line neuromasts and in the inner ear by blocking proliferation of supporting cells. One possible explanation is that dnRAR impairs the down-regulation of the cell cycle inhibitor *p27kip* (also known as *cdkn1bb*) that normally occurs after hair-cell ablation, a step that might be essential for allowing supporting cells to enter S-phase and thus, proceed to cell division (Rubbini *et al.*, 2015). Surprisingly, blocking Notch signaling

also down-regulates *p27kip* (Romero-Carvajal *et al.*, 2015), suggesting that Notch and RA might be acting synergistically during regeneration of sensory cells.

1.2. Aims of the thesis

1.2.1. To study the mechanisms underlying the inexhaustible regeneration of hair cells and the maintenance of organ architecture

Previous studies have thoroughly addressed the regeneration of hair cells in the lateral line (Behra *et al.*, 2009; López-Schier & Hudspeth, 2006; Ma *et al.*, 2008; Steiner *et al.*, 2014; Wibowo *et al.*, 2011; Williams & Holder, 2000). These studies have revealed that hair-cell progenitors originate from inner supporting cells and that their spatial specification is regulated by levels of Notch activity. However, the repercussion of this regeneration on the maintenance of other cell types and whether the regenerative capacity of neuromasts diminishes with age or after recurrent damage remains unknown. Another unresolved aspect of hair-cell regeneration, is to understand if hair-cell progenitors represent a separate cell population and if this occupies a well-defined region within the neuromast.

Here, I intend to shed light into these questions by forcing recurrent hair-cell regeneration in larval and adult zebrafish, pharmacologically modulating known intercellular signaling pathways and assessing the recovery of spatial landmarks that define neuromast three-dimensional architecture.

1.2.2. To exploit the regenerative potential of lateral line neuromasts and reveal cellular principles that govern the morphological recovery of complex tissues during regeneration

The postembryonic generation of neuromasts has been observed during physiological growth (Grant *et al.*, 2005; Ledent, 2002; López-Schier & Hudspeth, 2005; Nuñez *et al.*, 2009; Wada *et al.*, 2013) and during regeneration of the caudal fin (Dufourcq *et al.*, 2006). These observations support the notion that at least some cells in the lateral line have the potential to produce entire neuromasts *de novo*. However, while the lateral line has been extensively used to understand hair-cell replacement, the regeneration of non-sensory cells has remained largely unexplored and neuromast stem cells are yet to be identified.

Here, I aim at establishing a new experimental assay that allows a precise and reproducible method to perform ablations of different extent and location with near single-cell resolution and follow the recovery of neuromast's architecture. By testing injuries of different size and location, I should be able to determine the cells that are ultimately responsible for the regeneration of a complete neuromast.

Finally, a fundamental question of regenerative biology is how individual cell behaviors are regulated and tuned to generate organs of predictable size and shape. Even more, how do multiple cells performing simultaneous decisions operate collectively to achieve balanced cell proliferation and differentiation and regenerate complex structures. To answer these questions, I am introducing here a multi-disciplinary approach that combines long-term live imaging, lineage tracing at cellular resolution, and pharmacological manipulations together with the computational analytical power of unbiased machine learning algorithms.The neuromasts of the superficial lateral line

in zebrafish are ideal for these purposes because they are discrete and have a stereotypic localization along the animal's body that varies only marginally between individuals and during larval growth (Ledent, 2002). This feature allows the unambiguous identification of a target organ throughout the experimental period, and the comparison between corresponding organs in different animals.

2. Results

2.1. **Definition of neuromast architecture**

To study the regeneration of neuromasts and their constituent organs structures and cell populations, I decided to identify several architectural landmarks that can be posteriorly used as milestones of regeneration's precision. I used a comprehensive collection of transgenic lines expressing genetically encoded fluorescent-protein markers that allow the unambiguous visualization of cell identity, distribution, and numbers *in vivo*, and serve as a direct and dynamic readout of organ architecture.

The first architectural landmark is represented by the diversity of cell types in the organ (**Figure 8**A). The second is defined by the invariant spatial distribution of the three cell types in neuromasts, which generates a radial symmetry in the epithelium (**Figure 8**B). Finally, neuromasts also have an axis of bilateral symmetry defined by the planar polarization of the hair cells, and also by the position of the polar and equatorial areas, underlined, respectively, by the domains of alkaline phosphatase activity and the expression of the SqEt20 transgene (Villablanca *et al.*, 2006; Wibowo *et al.*, 2011) (**Figure 8**C) .In addition, a string of interneuromast cells connects each neuromast along the entire lateral-line system providing continuity to the epithelium.

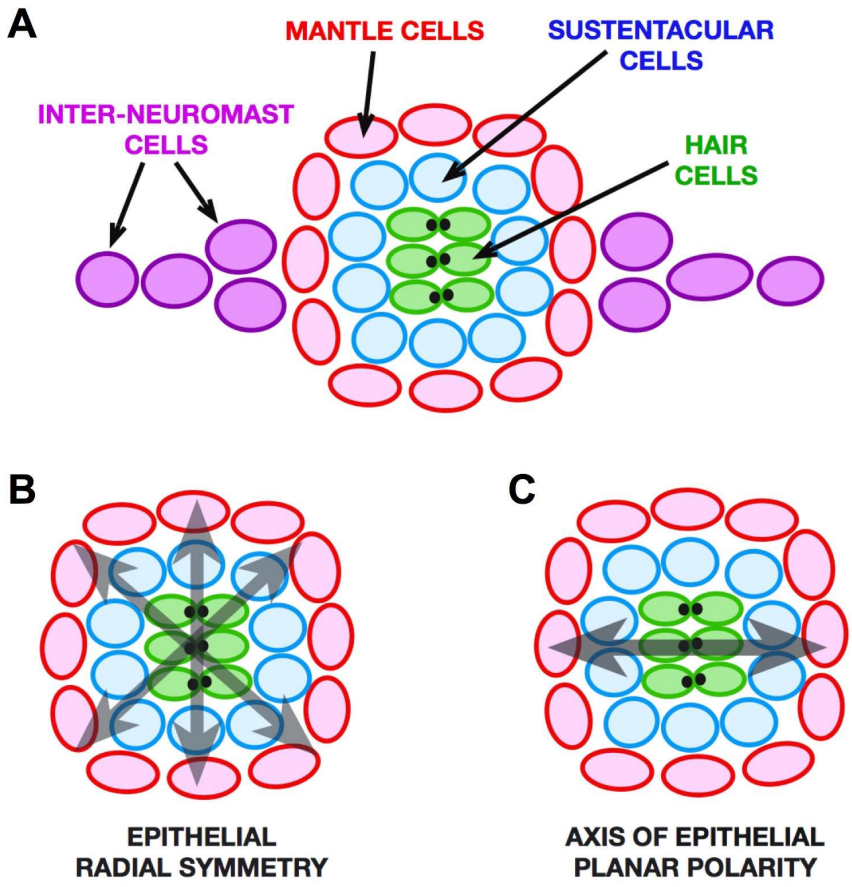

Figure 8. Geometric organization of neuromasts. (**A-C**) Schematic 2D representation of a neuromast depicting (**A**) marker-identifiable epithelial cell types. Grey arrows depict, respectively, (**B**) radial symmetry and (**C**) epithelial planar polarity.

2.2. Characterization of a new sustentacular cell fluorescent marker

I established a new transgenic line called *Tg[SqGw57A]* to better characterize neuromast cell diversity *in vivo*. The line was generated by the genomic insertion of a gene-trapping vector carrying a green-fluorescent protein (Kondrychyn *et al.*, 2011). By combining the line with mantle and hair-cell markers, I concluded that SqGw57A expresses EGFP in neuromast supporting cells (including both sustentacular and mantle cells), but not in hair cells or interneuromast cells (**Figure 9**A,B). Thus, the line can be used a *bona fide* marker for the supporting cell population and is likely to highlight the cells that will be canalized into hair-cell progenitor fate.

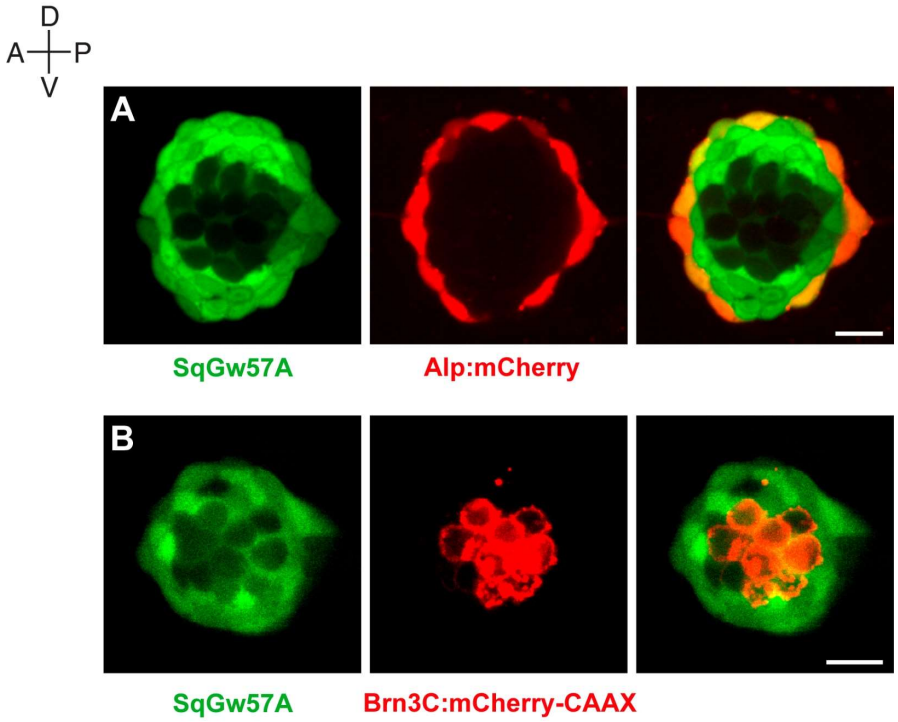

2.3. Cell proportions during neuromasts homeostasis

Figure 9. Characterization of Tg[SqGw57A] line. (**A**) Transgene expression co-localizes with the mantle cell marker Alpl:mCherry. (**B**) Unlabeled cells correspond to hair cells, as revealed by the Brn3C:mCherry-CAAX marker. Scale bars: 10 μm

To clarify the issue of neuromast's cell diversity and relative proportions of cell types in homeostatic neuromasts, I periodically imaged 10 zebrafish larvae from 5dpf to

12dpf in the triple transgenic line *Tg[Cldnb:lynGFP; SqGw57A; Alpl:mCherry]*. The green-fluorescent line *Tg[Cldnb:lyn-EGFP]* is used as a pan-lateral line marker that labels all cell membranes irrespectively of their cell type (Haas & Gilmour, 2006; López-Schier & Hudspeth, 2006). The *Tg[SqGw57A]* line highlights neuromast supporting cells, thus exposing centrally-located hair cells, whereas the red-fluorescent *Tg[Alpl:mCherry]* line labels mantle and interneuromast cells (Steiner et al., 2014), revealing the exact number of sustentacular cells. By quantifying the cell type numbers and their relative proportions, I found that the balance of cell types remains largely constant from 5dpf onwards, with around 35-40 sustentacular (~60%), 10-12 mantle (~15%), and 14-16 (~25%) hair cells (**Figure 10**).

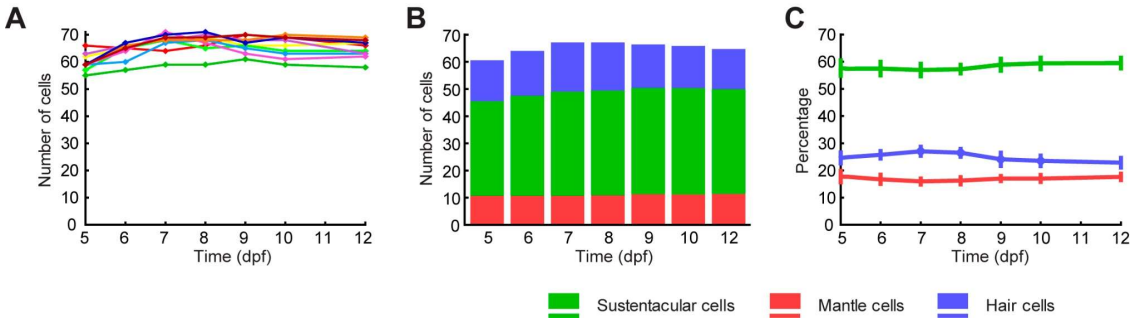

2.4. **Hair-cell regeneration and neuromast architecture remain unaffected by aging and**

Figure 10. Cell type proportions during neuromast homeostasis. (**A**) The number of total neuromast cells remains constant from 5 to 12dpf. (**B-C**) Neuromast cell type proportions are already established by 5dpf and do not vary during the following 6 days. Time-points in **C** represent mean±s.d. (N=10).

recurrent loss of hair cells

A single treatment with the ototoxic aminoglycoside antibiotic neomycin readily ablates every functional hair cell in the superficial lateral line of the zebrafish larva (Harris *et al.*, 2003; López-Schier & Hudspeth, 2006; Pinto-Teixeira *et al.*, 2013). Subsequently, neuromasts enter a regenerative process that is largely complete by 72

hours post (neomycin) treatment (hpt) (Ma *et al.*, 2008; Wibowo *et al.*, 2011). Strikingly, the first pair of hair cells appears as soon as 8 hpt (Wibowo *et al.*, 2011), suggesting that the fast onset of regeneration could be explained by the presence of a subpopulation of "primed" cells that are quickly routed towards a hair-cell progenitor fate upon the loss of hair cells. Therefore, a frequent and rapid sequence of hair-cell ablations should deplete the epithelium from primed cells, leading to regenerative decline. To test this idea, I subjected *Tg[SqEt4]* zebrafish larvae to 6 consecutive hair-cell ablations with neomycin and counted hair cells 24 hours after each treatment. The *Tg[SqEt4]* line expresses EGFP in hair-cell progenitors and mature hair cells (López-Schier & Hudspeth, 2006; Parinov, Serguei *et al.*, 2004; Wibowo *et al.*, 2011). Neuromasts showed invariable hair-cell regeneration after each ablation (**Figure 11**A), indicating that the pool of available hair-cell progenitors is not limited to a few cells. Thus, to maintain this inexhaustible regenerative capacity at constant kinetics, each organ must persistently produce at least 4 progenitors per day, representing approximately 10% of the supporting cells.

To test whether the capacity to regenerate hair cells diminishes with age, and if the repeated and frequent loss of hair cells affects neuromast's epithelial architecture, I performed 6 consecutive neomycin treatments, with intervening 48-hour periods of rest between treatments to allow partial regeneration, on 2-year old *Tg[SqEt4]* and *Tg[Alpl:mCherry; SqEt20]* zebrafish (**Figure 11**B,C). The *Tg[SqEt20]* line highlights neuromast regionalization by displaying stronger transgene expression in equatorial mantle cells than in polar mantle cells (Wibowo *et al.*, 2011). Interestingly, I found that hair cells regenerated efficiently after the 6th injury cycle and that epithelial architecture was properly restored, based on the equatorial position of the SqEt20

labeling (**Figure 11**B-G). These results demonstrate that neuromasts are endowed with invariant and enduring capacity to regenerate hair cells from larval to adult stages, and that the organ is able to assimilate these changes without losing its epithelial structure.

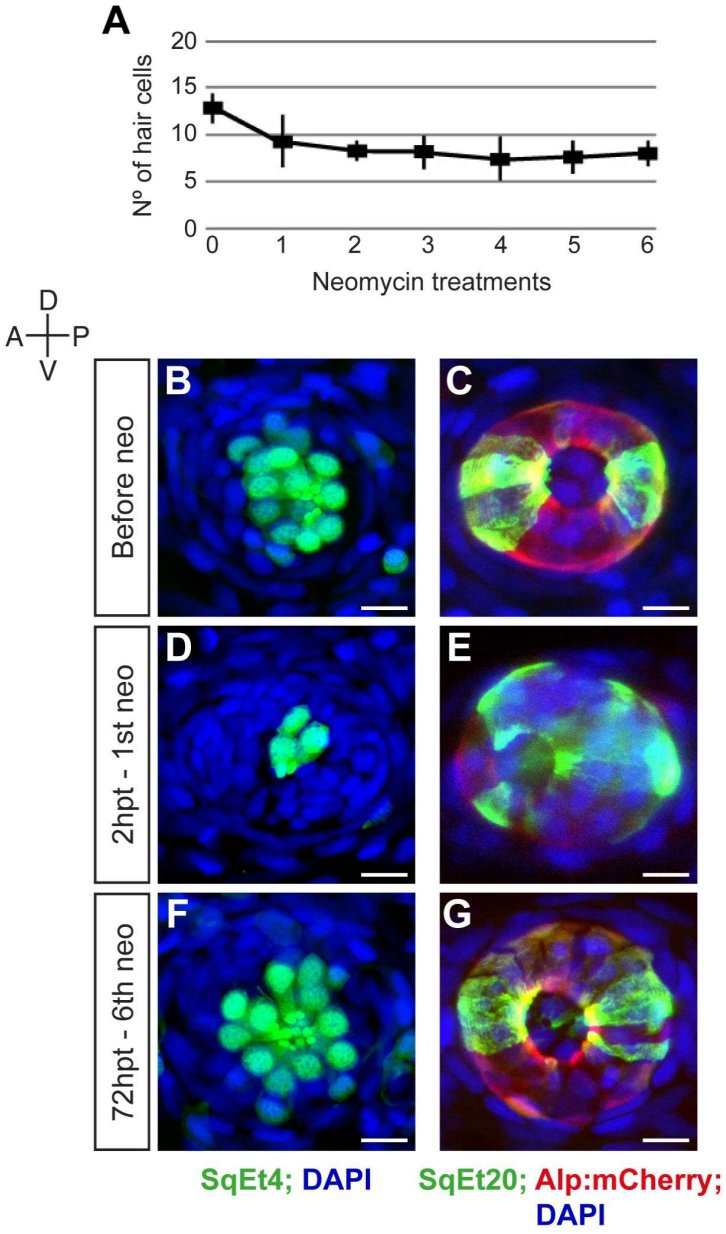

Figure 11. Hair cell regeneration and neuromast architecture in larvae and adult zebrafish. (**A**) Number of hair cells (mean±s.d.) per neuromast 24h after each neomycin treatment, over the course of 6 consecutive treatments. (**B-C**) Before neomycin, hair cells occupy the center of the organ and equatorial regions are highlighted by the SqEt20 marker. (**D-E**) Hair cells are eliminated upon neomycin treatment and neuromast regionalization is partially impaired. (**F-G**) Hair cells regenerate after 6 consecutive ablations and SqEt20 regions recover their original position. N=10 neuromast, 2 fish. Scale bars: 10 µm. Images were kindly given by Laura Pola-Morell.

2.5. **Atoh1a is transiently and broadly expressed in the epithelium**

Hair cells require Atoh1a for their development. Ma and colleagues showed that Atoh1a is expressed in broad areas of the epithelium during the first 24h of regeneration (Ma *et al.*, 2008). Using the double-transgenic line *Tg[Atoh1a:tdTomato; SqEt4*] to simultaneously visualize Atoh1a expression and hair cells, I extended these previous observations by finding a broad but weak Atoh1a expression domain in the supporting cells that surround the core of sensory cells, which stabilizes and becomes stronger in hair-cell progenitors and in young hair cells (**Figure 12**A). This pattern of Atoh1a expression substantiates the prediction that neuromasts may use a large pool of supporting cells to generate hair-cell progenitors to sustain regeneration upon recurrent severe damage, and suggests that the expression of Atoh1a occurs by default in supporting cells. To further test this hypothesis, I ablated hair cells and abrogated Notch signaling by treating zebrafish larvae with the γ-secretase inhibitor DAPT (Ma *et al.*, 2008; Wibowo *et al.*, 2011). The uniform loss of Notch signaling stabilized Atoh1a in a broader area of the neuromast (**Figure 12**B), and generated supernumerary hair cells.

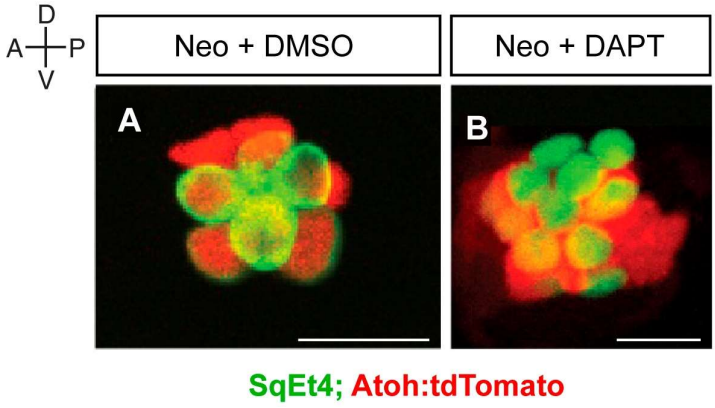

Figure 12. Atoh1a expression during Notch inhibition. Neuromasts from a neomycin-treated *Tg[SqEt4; Atoh1a:dTomato]* larvae (**A**) without, and (**B**) with Notch inhibition with DAPT, showing supernumerary hair cells and stronger and broader Atho1a expression. Scale bars: 10 μm.

2.6. **Complete characterization of Sox2 expression in the lateral line**

Sox2 is a transcription factor at the apex of the gene-expression cascade that establishes sensory competence in the inner ear neuroepithelium at the earliest stages of hair-cell development and is important for precursor cell maintenance (Kiernan *et al.*, 2005; Millimaki *et al.*, 2010; Neves *et al.*, 2013). In the zebrafish, Sox2 is expressed in the supporting cells of the inner ear and lateral line neuromasts and is down-regulated in differentiated hair cells. Thus, the domain of Sox2-expressing supporting cells is unequivocally the source of hair-cell progenitors (Hernandez *et al.*, 2007). In fact, the morpholino-mediated knockdown of *sox2* mRNA translation selectively impairs regeneration but not development of hair cells in the inner ear (Hernandez *et al.*, 2007; Millimaki *et al.*, 2010). Despite the thorough characterization of this gene in the lateral line, it was still unclear if Sox2 was expressed in all mantle cells and in interneuromast cells. To shed light into this issue, I used a Sox2-directed antibody and imaged homeostatic neuromasts with confocal resolution. As expected, Sox2 was expressed in the sustentacular cells around a core of unlabeled hair cells (**Figure 13**A). In a combinatorial staining with the mantle cell marker Alpl:mCherry I found that Sox2 is expressed in the entire mantle cell population, as well as in all interneuromast cells (**Figure 13**B-D). These observations hint about the possibility that all neuromast supporting cells, as well as interneuromast cells, might be able to become hair-cell progenitors in yet unknown specific biological contexts.

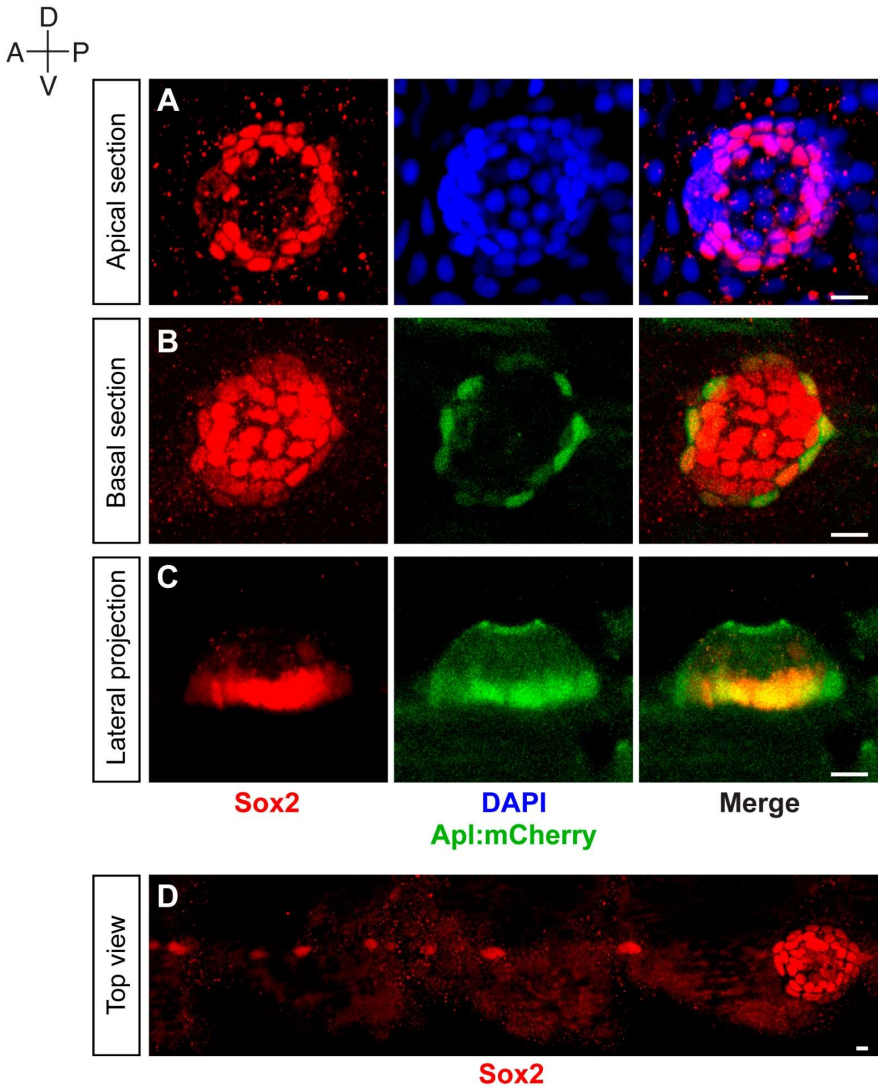

Figure 13. Sox2 in the lateral line. (**A**) A top-apical section of a 5dpf neuromast immunostained for Sox-2 and counterstained with the nuclear dye DAPI reveal a core of central unlabeled cells corresponding to hair cell cells. (**B-C**) Top-basal and lateral sections show that mantle cells are Sox2-positive, based on the co-localization with the Alpl:mCherry transgene. (**D**) A thread of immunostained cells reveals that Sox2 is also expressed in interneuromast cells. Scale bars: 10 μm. Image in panel D was kindly given by Elen Torres-Mejía.

2.7. **PCP and territories are not affected by loss of Notch signaling and recurrent hair-cell ablations.**

It has been reported that the expression levels of Notch signaling components may underlie the maintenance of neuromast regionalization (Ma *et al.*, 2008; Wibowo *et al.*, 2011). To further investigate this hypothesis, I used the γ-secretase inhibitor DAPT to inhibit Notch signaling and assessed organ architecture by revealing the position of the alkaline phosphatase activity domains and the planar polarization of hair cells. In order to subject the organs to a strong regenerative stress, I killed all hair cells with a neomycin treatment, abrogated Notch signaling with DAPT during the following 48 hours, and subsequently killed all hair cells two more times, separated by a 48-hour resting period (**Figure 14**A). The lifting of Notch signaling produced supernumerary hair cells compared to control neuromasts (**Figure 14**F) (13±1 vs 21±3, mean±s.d.). However, neither the polar position of the alkaline phosphatase domains (**Figure 14**B,C) nor the planar polarization of the regenerated hair cells (**Figure 14**D,E) were qualitatively different from the DMSO-treated larvae in any of the time points (N=8 neuromasts per time point, 3 fish). This indicates that intercellular Notch signaling is not directly responsible for neuromast regionalization and highlights once more the striking architectural resilience of the organ.

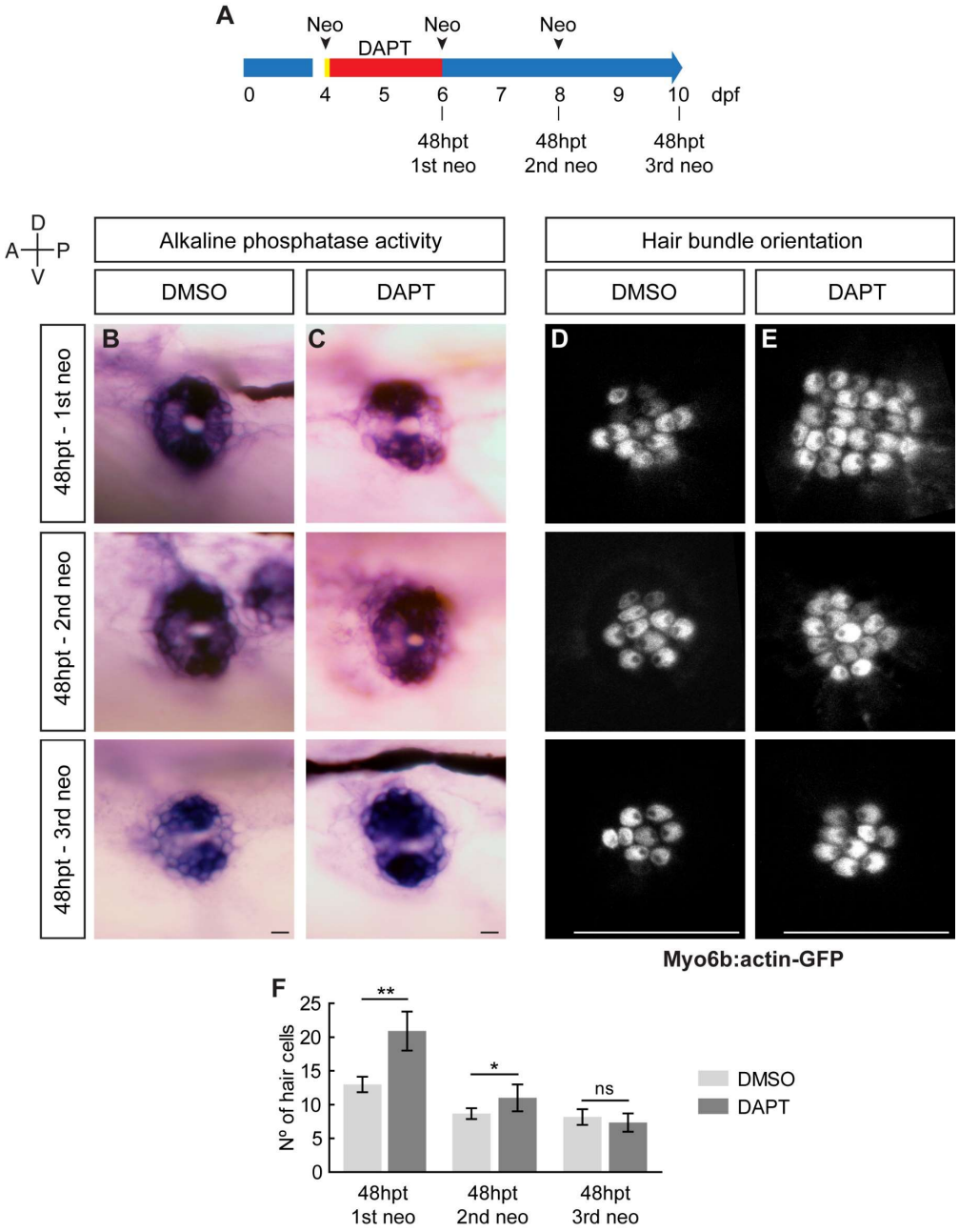

Figure 14. Notch blockade does not affect neuromast regionalization nor PCP. (**A**) Experimental design. (**B**) Location of alkaline phosphatase domains in DMSO-treated larvae remains unaffected after the 1st, 2nd and 3rd consecutive neomycin treatments. (**C**) Pharmacological inhibition of Notch does not affect the location of alkaline phosphate domains even after the 3rd ablation of hair cells. (**D**) Hair cell PCP is unperturbed after 3 consecutive ablation-regeneration cycles. (**E-F**) DAPT-treated larvae overshoot hair cell regeneration after the 1st (p=0,0067, Mann Whitney test) and 2nd (p=0,0334, Mann Whitney test) neomycin treatments but maintain the original axis of PCP as revealed by the orientation of hair bundles. Scale bars: 10 μm.

2.8. **Neuromast proportions are reversibly affected by imbalances of Notch signaling**

Despite the fact that neuromast regionalization is not affected by the loss of Notch signaling, the excessive production of hair cells must undoubtedly have an impact to the relative proportion between cell types, another important architectural landmark. It has been proposed that a feedback inhibition of supporting-cell proliferation via Notch signaling maintains a constant cellular population in neuromasts (Ma *et al.*, 2008). Thus, to test functional links between intercellular communication and cell type proportions, I again examined neuromasts with defective Notch activity. In order to boost the hair-cell regenerative capacity of neuromasts, I treated zebrafish larvae with neomycin, incubated them in DAPT for 24 hours and repeated the neomycin treatment for a second time (**Figure 15**A). Cell type numbers were quantified and compared to DMSO-treated neuromasts at 1, 3 and 7dpt to follow the long-term effect of cell type proportions imbalances. Expectedly, 1dpt DAPT-treated neuromasts revealed an imbalance of cell type proportions (**Figure 15**B-B"). However, they also revealed that the increase of hair-cell proportions occurs at the expense of sustentacular cells but not mantle cells, thus, reinforcing previous conclusions that superfluous hair cells are produced by abnormal fate acquisition of cells that would otherwise remain sustentacular. On the other hand, DMSO-treated neuromasts, experienced opposite proportional changes, likely because the hair-cell population had only partially regenerated 1dpt (**Figure 15**B,E). At 3dpt, neuromasts that were depleted from Notch signaling had lost some of the superfluous hair cells but still display an increased proportion compared to control organs. However, they have completely regenerated the sustentacular cells that were lost during the overproduction of hair cells (**Figure 15**C). Strikingly, these organs gradually recovered normal proportions during the 7

days that followed the inhibition of Notch signaling (**Figure 15**D,F), to become virtually undistinguishable from controls (**Figure 15**E).

Figure 15. Notch blockade produces a reversible imbalance of cell type proportions. (**A**) Experimental strategy of hair-cell elimination and inhibition of Notch signaling. (**B**) 1dpt, DAPT-treated neuromasts produced supernumerary hair cells at the expense of sustentacular cells and not mantle cells. (**B'-B"**) Representative examples of regenerating control (DMSO) and Notch-inhibited (DAPT) neuromasts. (**C**) 3dpt, the number of hair cells had slightly decreased and sustentacular cells had replenished their population to control levels. (**D**) 7dpt, hair cell numbers kept decreasing, matching almost control numbers. The number of sustentacular and mantle cells was indistinguishable from control neuromasts. Bars show mean±s.d. Hair cells: 1dpt p=0.0080, 3dpt p=0.0054, 7dpt p=0.0139. Sustentacular cells: 1dpt p=0.0078. All p-values derive from Mann-Whitney tests. (**E**) Hair cell elimination in control neuromasts produced a minor cell type imbalance 1dpt due to the still uncompleted regeneration of hair cells, that is quickly restored by 3dpt. (D) The same elimination in Notch-inhibited neuromasts resulted in a strong imbalance of cell types 1dpt as a consequence of an excessive hair cell production at the expense of sustentacular cells. However, cell type proportions gradually recover their original conditions in the following 6 days. Time points are mean ±s.d. DAPT: N_{1dpt}=6, N_{3dpt}=7, N_{7dpt}=8. DMSO: N_{1dpt}=5, N_{3dpt}=5, N_{7dpt}=5. ns: non-significant. Scale bars: 10 µm.

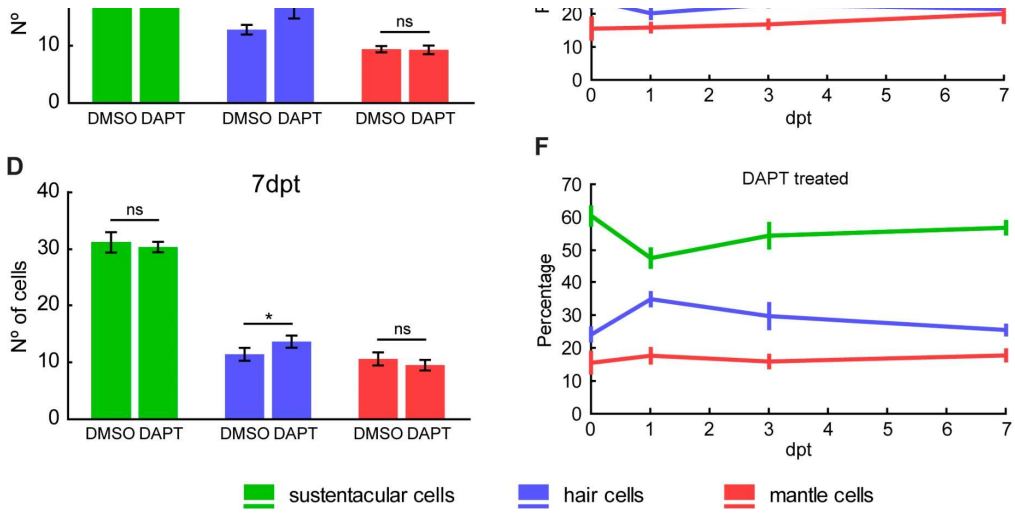

Together, these results strongly support the idea that neuromasts can autonomously organize cell type proportions after transient inhibition of Notch-mediated

intercellular communication, which is suggestive of architectural plasticity in the epithelium.

2.9. **Wnt/β-catenin actively regulates organ dimensions during development and homeostasis**

Previous work by other laboratories demonstrated that the Wnt/β-catenin pathway is another key component of the genetic network that maintains the equilibrium between progenitor and differentiated cell fates in the inner ear and the lateral line (Jacques *et al.*, 2014; Jacques *et al.*, 2012; Shi *et al.*, 2014; Shi *et al.*, 2012). While the inhibition of Notch increases hair-cell regeneration at the expense of supporting cells due to failure of lateral inhibition, the activation of Wnt facilitates hair-cell regeneration by promoting the proliferation of supporting cell without affecting hair-cell differentiation (Head *et al.*, 2013; Romero-Carvajal *et al.*, 2015). To further explore neuromasts' plasticity and the resilience of cell type proportions, I forced the production of hypertrophic neuromasts by treating zebrafish larvae from 2 to 6dpf with 1-azakenpaullone (AZK), a GSK3 inhibitor that blocks degradation of β-catenin leading to Wnt over-activation. AZK-treated neuromasts (**Figure 16**A,B) grew to an average of 146±14 total cells (mean±s.d, N=10), approximately a 2,5-fold increase compared to control DMSO-treated neuromasts (**Figure 16**C) (61±2, mean±s.d., N=15). Interestingly, cell type numbers in hypertrophic neuromasts did not increase in identical proportions (**Figure 16**D). While, on average, sustentacular cells experienced a 2,75-fold increase, hair cells only increased 2,05 fold and mantle cells 1,6 fold, suggesting that the establishment of cell type proportions may be directly dependent on the dimensions of the organ.

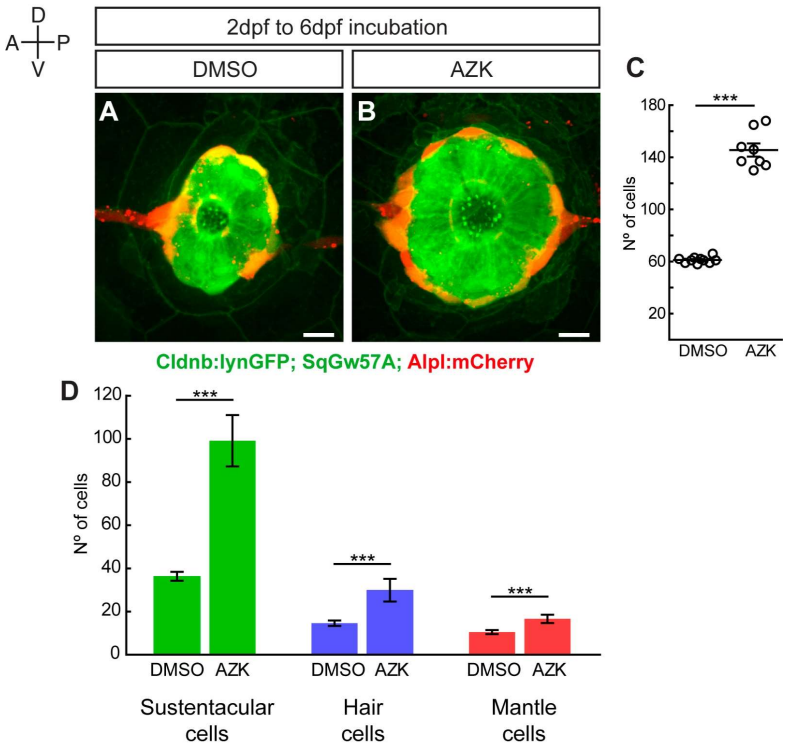

Figure 16. Development of hypertrophic neuromasts by pharmacological activation of Wnt/β-catenin signaling. (**A**) Control (DMSO) neuromast at 6dpf. (**B**) Hypertrophic neuromast generated by prolonged 1-azakenpaullone (AZK) treatment. (**C**) Control neuromasts developed a total 61±2 cells and hypertrophic neuromasts a total of 146±14 cells. p< 0.0001. (**D**) All cell types experienced statistically significant increments in their total counts. Sustentacular cells; DMSO: 36±1, AZK: 99±4. p< 0.0001. Hair cells; DMSO: 15±1, AZK: 30±2. p< 0.0001. Mantle cells; DMSO: 11±1, AZK: 17±1. p< 0.0001. Cell numbers represent mean±s.d. All p-values derive from unpaired t-tests. N_{DMSO}=10, N_{DAPT}=8. Scale bars: 10 μm.

To test the reversibility of cell type imbalances, zebrafish with hypertrophic neuromasts were transferred into drug-free medium and let recover for a 7-day period. After the inhibition of Wnt/β-catenin was lifted, neuromasts' size decreased rapidly (**Figure 17**A-C) by losing mostly sustentacular cells and, to a lesser extent, hair cells.

Surprisingly, hypertrophic neuromasts did not lose virtually any mantle cell during the partial recovery of organ size (**Figure 17**D). These observations suggest that Wnt/β-catenin is actively controlling organ size by promoting sustentacular cell proliferation and that the maintenance of organ size and cell type proportions is a strongly favored

biological process that may have evolved as a defense mechanism against developmental or regenerative flaws for organs to maintain their original architecture.

2.10. **Setup of laser-mediated regeneration assay**

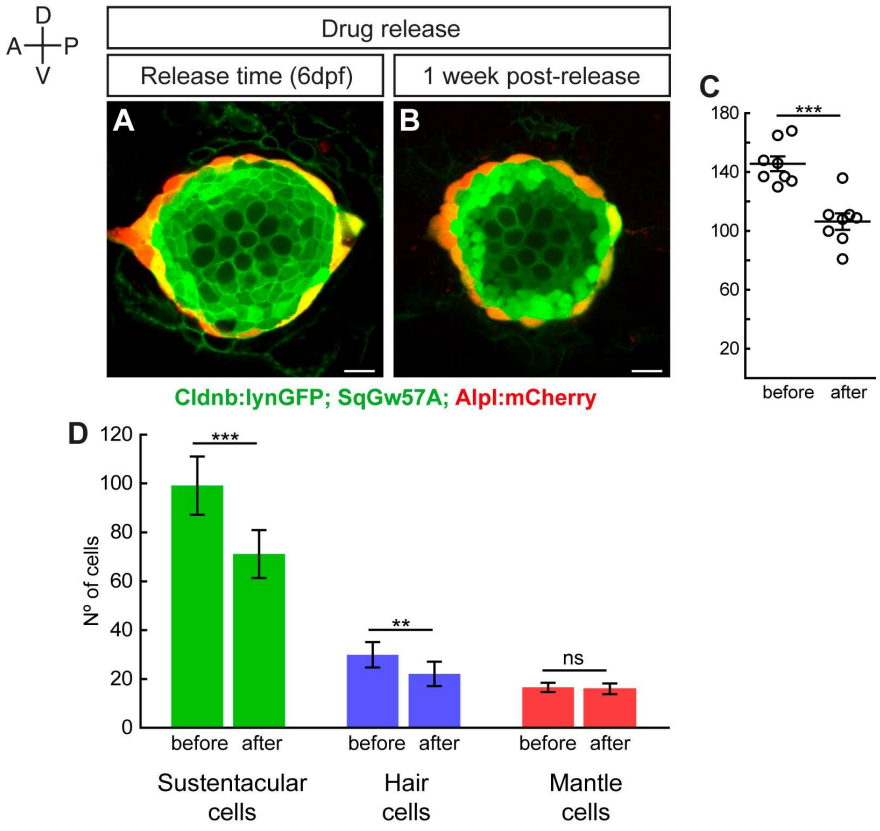

Figure 17. Hypertrophic neuromasts shrink upon lifting of Wnt/β-catenin over-activation. (**A**) Hypertrophic neuromast at the end of AZK treatment, right before moving the specimen to drug-free medium. (**B**) The same neuromast 1 week after the lifting of AZK, showing notably less sustentacular and hair cells. (**C**) The total cell number in hypertrophic neuromasts decreased from 146±14 cells to 109±16 in 6 days (N=8). (D) Neuromast shrinking was mainly due to a reduction of the number sustentacular cells (from 99±12 to 71±9, p< 0.0001), followed by that of hair cells (from 30±5 to 22±5, p=0,0024). The number of mantle cells remained virtually identical during the entire period (from 17±2 to 16±2, p=0,4238). Cell numbers represent mean±s.d. All p-values derive from unpaired t-tests. ns: non-significant. Scale bars: 10 µm.

During many years, the use of neuromasts as an *in vivo* model for regeneration, has been limited to the investigation of hair-cell loss and recovery because of the difficulty

to cause targeted damage to other cell types in a reliable and reproducible manner. This fact, together with the unavailability of comprehensive combinations of cell type-specific transgenic markers, led to a delay in the understanding of the regenerative potential of other neuromast cell types. However, it has become evident that these small organs are endowed with an outstanding capacity to maintain and recover their three-dimensional architecture after acute disruptions of cell composition and intercellular signaling.

To gain a detailed and quantitative understanding of whole-organ regeneration I sought to develop a new experimental assay that combines controllable and reproducible tissue damage with single cell resolution and simultaneous long-term imaging. Neuromasts' external location allows a non-invasive physical access to the entire organ as well as numerous options for live imaging setups. To control tissue damage, I took advantage of a high power ultraviolet laser beam (355 nm) coupled to a high numerical-aperture objective (N.A. = 1.2) that was used simultaneously for imaging and aiming at single or multiple target cells. All laser ablations were controlled 4 hours-post-injury (hpi), after the cellular debris accumulated during necrotic cell death is cleared from the damaged area, to verify the precise outcome of the injury. The regenerative response of the remaining neuromast structures or cells was determined by periodic evaluations of cell type composition, proportions and distribution during the course of 7 days-post-injury (dpi).

2.11. **Complete neuromast elimination is irreversible in larval zebrafish**

I began by completely ablating entire neuromasts in 6dpf *Tg[Cldnb:lynGFP; Alpl:mCherry]* zebrafish larvae (**Figure 18**A-E), and followed the response of flanking interneuromast cells for 7dpi. At 4hpi, a transient wound developed at the site of injury (**Figure 18**B). 1 dpi, the damaged area was occupied by a thread of interneuromast cells (**Figure 18**C). None of the removed neuromasts regenerated after 7 days nor signs of regeneration were observed (N=22) (**Figure 18**D-E), revealing that interneuromast cells resolve damage but are unable to drive *de novo* organogenesis.

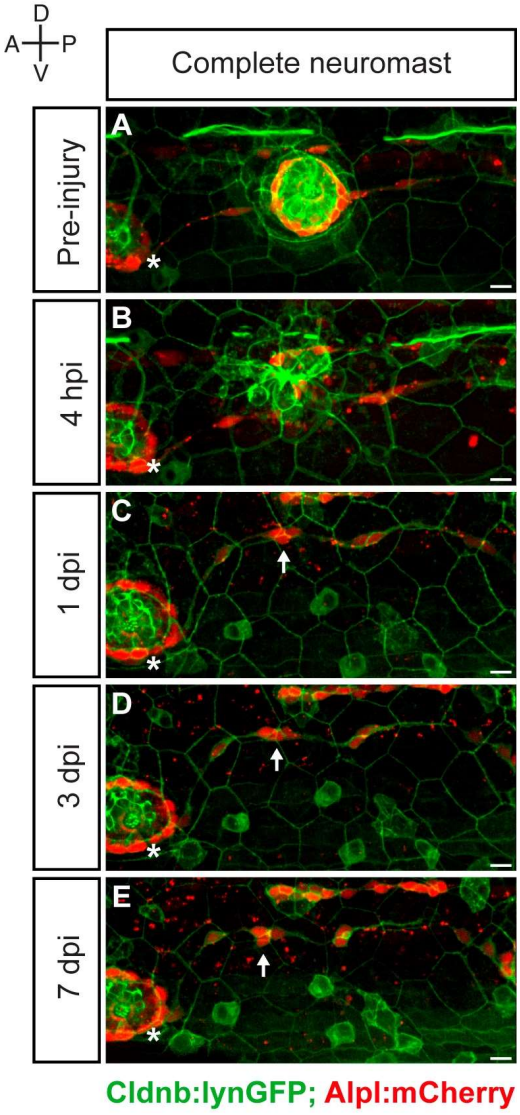

Figure 18. Zebrafish larvae do not regenerate completely ablated neuromasts. (**A-E**) Confocal images of a 7-day follow-up of the complete ablation of a neuromast. (**A**) The site of damage was identified over subsequent days by the position of an intact reference neuromast (white asterisk). (**B**) Laser-mediated neuromast ablation produced a wound at 4 hours-post-injury (hpi). (**C-E**) This wound was replaced by a thread of mCherry(+) cells (white arrow) at 1 day-post-injury (dpi), and did not change over the subsequent 6 days. Scale bars: 10 µm.

Previously published data supports the notion that primordium migration is slightly slowed down in *Tg[Cldnb:lynGFP]* zebrafish larvae (Nuñez et al., 2009). Thus, to rule out a putative transgene-specific phenotype of this line during regeneration, I performed identical ablations using the *Tg[Sox2:EGFP]*, a live fluorescent reporter of Sox2 expression that labels neuromast supporting cells and interneuromast cells (Shin *et al.*, 2014). Before using the line, I confirmed that transgene expression matched my previous immunostaining results (**Figure 19**A). An identical outcome was obtained using this new supporting cell marker (N=9) (**Figure 19**B).

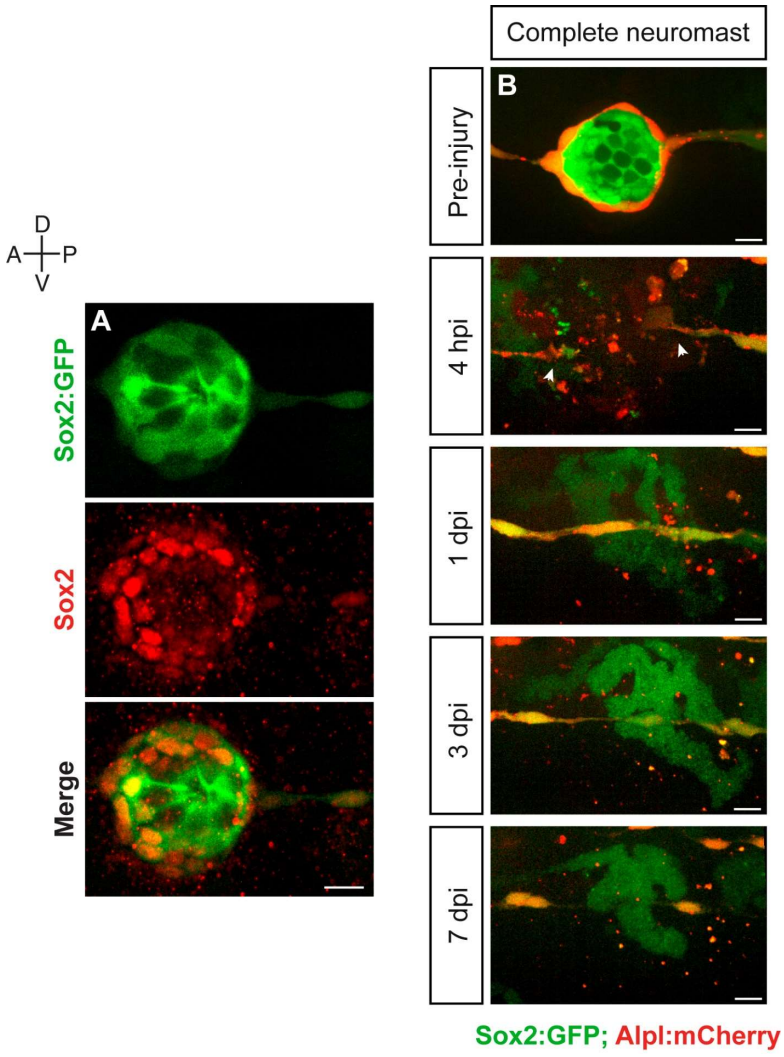

Figure 19. Validation of *Tg[Sox2:GFP]* line and injury model. (**A**) Counterstaining with Sox2 antibody in a neuromast from *Tg[Sox2:GFP]* zebrafish shows co-localization in supporting and interneuromast cells. (**B**) 7-day follow-up of complete neuromast ablation in the double transgenic line *Tg[Sox2:GFP; Alpl:mCherry]*. Scale bars: 10 μm.

2.12. ErbB signaling does not inhibit INCs proliferative behavior

The observation that interneuromast cells flanking the injury cannot support neuromast regeneration is intriguing because embryonic loss of Schwann cells permits the formation of supernumerary neuromasts that originate from the interneuromast cells (Grant *et al.*, 2005; López-Schier & Hudspeth, 2005). This occurs because these glia signal via ErbB to block the proliferation and aggregation of interneuromast cells into epithelial rosettes that are the precursors of neuromasts (Lush & Piotrowski, 2014). Therefore, I tested the hypothesis that the irreversibility of whole-organ elimination is

due to a repressive activity of the Schwann cells. To this end, I used the quintuple transgenic line *Tg[2o2A;UAS:EGFP; SILL:Cherry; SqET4; Alpl:mCherry]* that allows the simultaneous visualization of Schwann cells (green) around afferent neurons (red), and the target neuromast (mantle cells in red and hair cells in green) with its neighboring interneuromast cells (red) (**Figure 20**A) (Xiao *et al.*, 2015). I simultaneously ablated a target neuromast and its neighboring Schwann cells without affecting adjacent interneuromast cells (**Figure 20**B). Counter to my expectations, the absence of Schwann cells did not result in neuromast regeneration (**Figure 20**C-E) in any of the experimental specimens (n=9). In complementary experiments, I used the small chemical compound AG1478, which inhibits the tyrosine-kinase activity of ErbB. Zebrafish embryos incubated in AG1478 from 30hpf to 3dpf developed more than twice the normal number of neuromasts (**Figure 20**F), similar to previous reports (Lush & Piotrowski, 2014; Rojas-Muñoz *et al.*, 2009). Surprisingly, however, the incubation of 5dpf larvae for 5 consecutive days did not result in the overproduction of neuromasts, suggesting that embryonic and larval interneuromast cells respond differently to ErbB signaling (**Figure 20**G). Yet, I incubated 5dpf zebrafish with AG1478 after the complete ablation of a neuromast (**Figure 20**H-J). In 10 out of 11 experiments, this treatment did not trigger interneuromast-cell proliferation and organ regeneration (**Figure 20**H,I). Together, these results reveal that the complete elimination of a neuromast in larval zebrafish is irreversible.

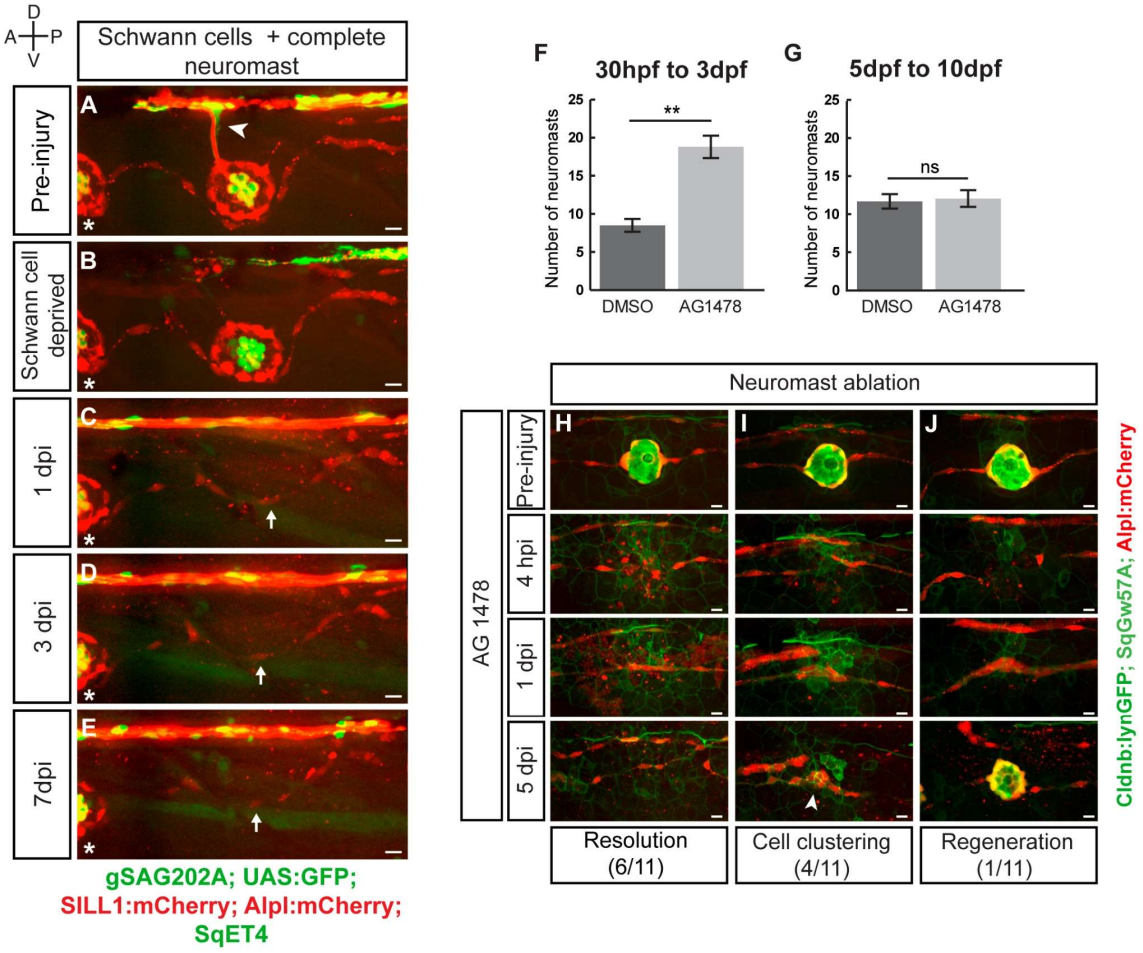
D
A
P
V
Schwann cells + complete neuromast
Pre-injury
Schwann cell deprived
1 dpi
3 dpi
7dpi
A
B
C
D
E
gSAG202A; UAS:GFP;
SILL1:mCherry; Alpl:mCherry;
SqET4
F
30hpf to 3dpf
Number of neuromasts
**
DMSO
AG1478
G
5dpf to 10dpf
Number of neuromasts
ns
DMSO
AG1478
Neuromast ablation
AG 1478
Pre-injury
4 hpi
1 dpi
5 dpi
H
I
J
Resolution (6/11)
Cell clustering (4/11)
Regeneration (1/11)
Cldnb:lynGFP; SqGw57A; Alpl:mCherry

Figure 20. Schwann cell-derived ErbB2 does not inhibit neuromast regeneration. (**A**) Schwann cells (arrowhead) follow the afferent neuron exiting the main axonal branch towards the target neuromast. A reference neuromast (white asterisk) serves as a spatial landmark. (**B**) Schwann-cell ablation was followed by axon severing to prevent Schwann-cell regrowth towards the target neuromast. (**C-E**) The complete ablation of the target neuromast results in a thin trail of interneuromast cells (white arrows) covering the damaged area (n=9). In these cases, the quintuple-transgenic line *Tg[202A;UAS:EGFP; SILL:Cherry; SqET4; Alpl:mCherry]* was used. (**F**) ErbB signaling inhibition from 30hpf to 3dpf produced larvae with significantly more neuromasts per fish than controls (p=0.0067, Mann-Whitney test, DMSO n=6, AG1478 n=6). (**G**) ErbB signaling inhibition from 5dpf to 10dpf did not produce extra neuromasts (p= 0.4192, Mann-Whitney test, N_{DMSO}=10, N_{AG1478}=15). (**H-J**) Examples of a 5-day follow-up of completely ablated neuromasts under constant incubation with 3µm of AG1478 (n=11). (**H**) In more than 50% of the cases, interneuromast cells resolved the ablation of a neuromast by forming a thin trail of cells (arrowhead) but did not produce a new neuromast. (**I**) Example of interneuromast cell clustering upon the injury site (arrowhead). (**J**) In one of eleven cases, a neuromast regenerated presumably from interneuromast cells. ns: non-significant. Scale bars: 10 µm.

2.13. **Interneuromast cells do not regenerate after laser-mediated ablations**

To further test the quiescent behavior of interneuromast cells, I tested their regeneration directly by ablating them partially and completely. Surprisingly, neither the ablation of these cells on one side of a neuromast (N=12) (**Figure 21**B), nor the entire thread between two adjacent neuromasts (N=8) (**Figure 21**G), triggered the proliferation or migration of remaining interneuromast cells or neighboring neuromast-resident cells over a period of 7 days (**Figure 21**E,J).

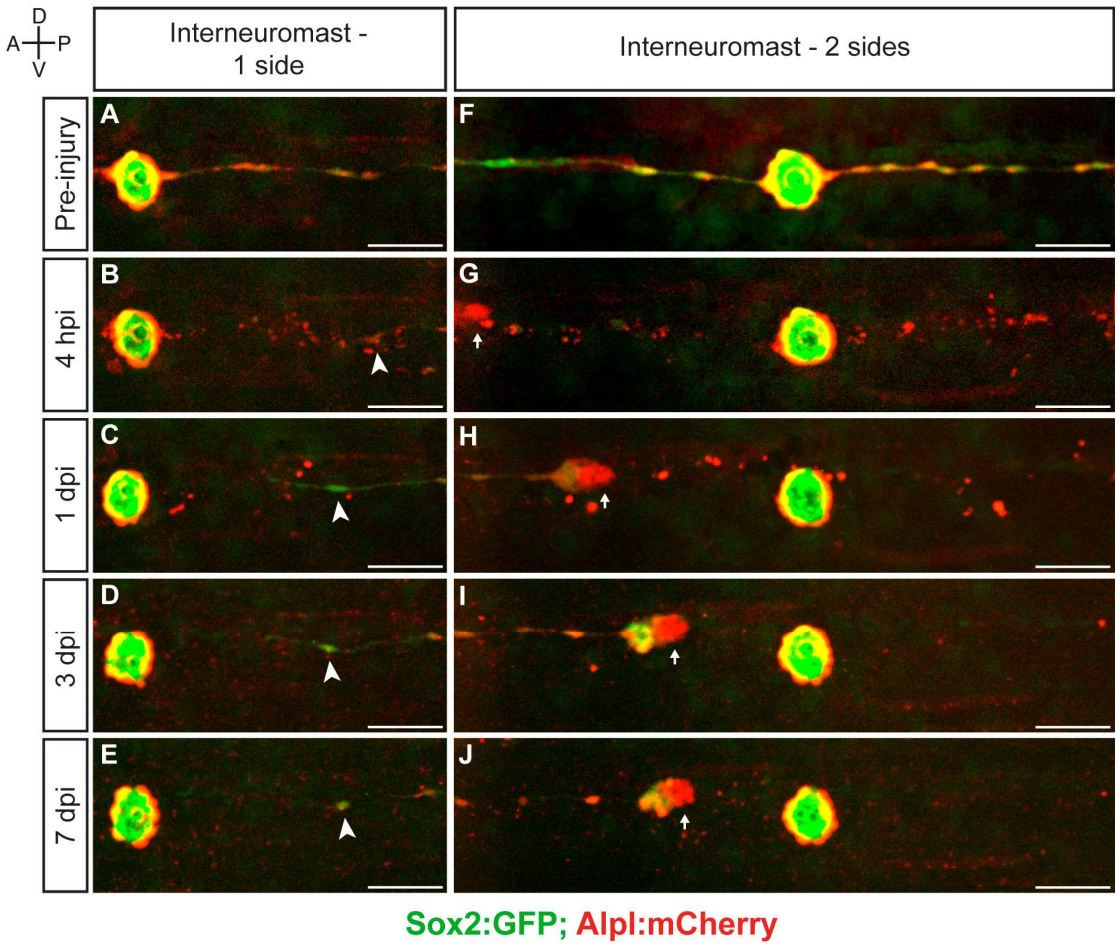

Figure 21. Interneuromast cells do not regenerate. (**A-E**) The ablation of interneuromast cells adjacent to one flank of a neuromast resulted in the stretching of the last undamaged interneuromast cell (arrowhead) but does not trigger interneuromast-cell proliferation nor the engagement of neuromast-resident cells (n=14). (**F-J**) Likewise, the complete ablation of interneuromast cells in both flanks from one neuromast to the next, generates a corresponding gap of interneuromast cells that did not change over 7 days (n=8). Scale bars: 50 µm.

2.14. **Cell location is not affected by the loss of individual cell types**

In light of the previous results, I decided to test the effect of the complete elimination of each cell type on the spatial distribution of the remaining cell types, as well as on epithelial planar polarity. The ablation of mantle cells did not affect the localization of interneuromast, sustentacular or hair cells (N=5) (**Figure 22**A,B). The elimination of interneuromast cells on both sides of a neuromast likewise did not affect the localization of mantle, sustentacular and hair cells (N=5) (**Figure 22**C). The ablation of the hair cells did not shift the spatial arrangement of the other cell types (N=9) (**Figure 22**D).

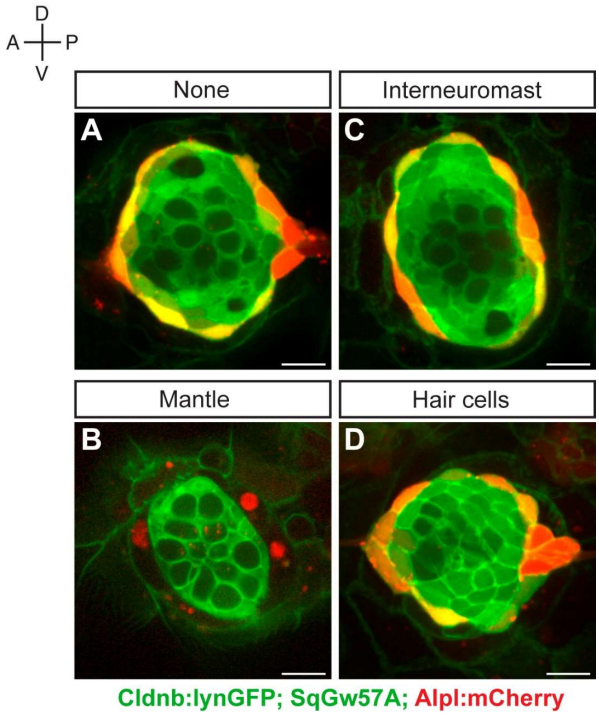

Figure 22. Cell spatial distribution in the absence of individual cell types. (**A**) Representative unperturbed neuromast. (**B**) 8 hours after the mantle cell ablations, sustentacular and hair cells maintain their location compared to control neuromasts. (**C**) Neuromasts without interneuromast cells adopt an oval shape but all cells remain in place. (**D**) 5 hours after hair-cell ablation with neomycin, the spatial distribution of sustentacular, mantle and interneuromast cells remains unperturbed. Scale bars: 10 µm.

This experiment cannot be performed with the sustentacular-cell population because their complete loss will inevitably result in the additional loss of hair cells, simultaneously eliminating two cell types. Also, an epithelium composed exclusively of

mantle cells will lack the essential reference to determine organ proportions and geometry.

Finally, I observed that neuromasts devoid of mantle cells (N=8) or interneuromast cells (N=5) maintained planar polarity (**Figure 23**A-F). Taken together, these results suggest that, with the possible exception of the sustentacular cells, heterotypic cellular interactions do not instruct the spatial relationship between cell types or the coherent planar polarization of the epithelium.

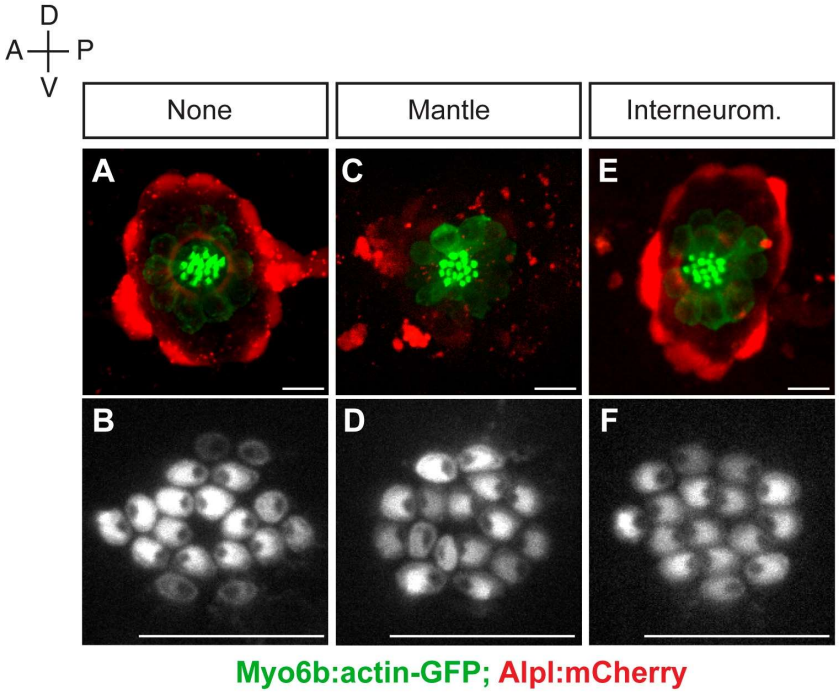

Figure 23. Elimination of individual cell types does not result in hair-cell PCP defects. (**A**) Maximal projection of a control neuromast. (**B**) The orientation of the hair bundles from the above neuromast, show stereotypical planar polarization. (**C**) Neuromast 8 hours after mantle-cell elimination. (**D**) Detail of hair bundles shows no defects in epithelial planar polarity. (**E**) Neuromast without interneuromast cells. (**F**) Hair bundle magnification demonstrates normal planar polarization of the hair cells. Scale bars: 10 μm.

2.15. **Neuromasts have isotropic regenerative capacity**

To explore the regenerative capacity of neuromasts I decided to use milder injury regimes. To systematically produce damage of well-defined scale and location I employed laser-mediated cell ablations in transgenic lines expressing the pan-supporting cell markers Cldnb:lynGFP or Sox2:GFP, and the mantle-cell marker Alpl:mCherry. I found that the ablation of one half of the neuromast involving all three cells types was followed by the rapid elimination of dead cells and cellular debris, the closure of the wound, and the re-epithelialization of the damaged area (**Figure 24**A-C). At 3dpi, the targeted neuromasts regained normal cell-type distribution (**Figure 24**D). At 7dpi, these neuromasts had regenerated approximately 70% of their original cell counts (N=6) (**Figure 24**E,Z). Regeneration occurred equally after the concurrent ablation of one half of the neuromast and the flanking interneuromast cells (N=5) (**Figure 24**F-J,Z). The elimination of equatorial or polar halves of the neuromast resulted in identical outcome, indicating that the neuromast epithelium is symmetric in its regenerative capacity (N=6) (**Figure 24**K-O,Z).

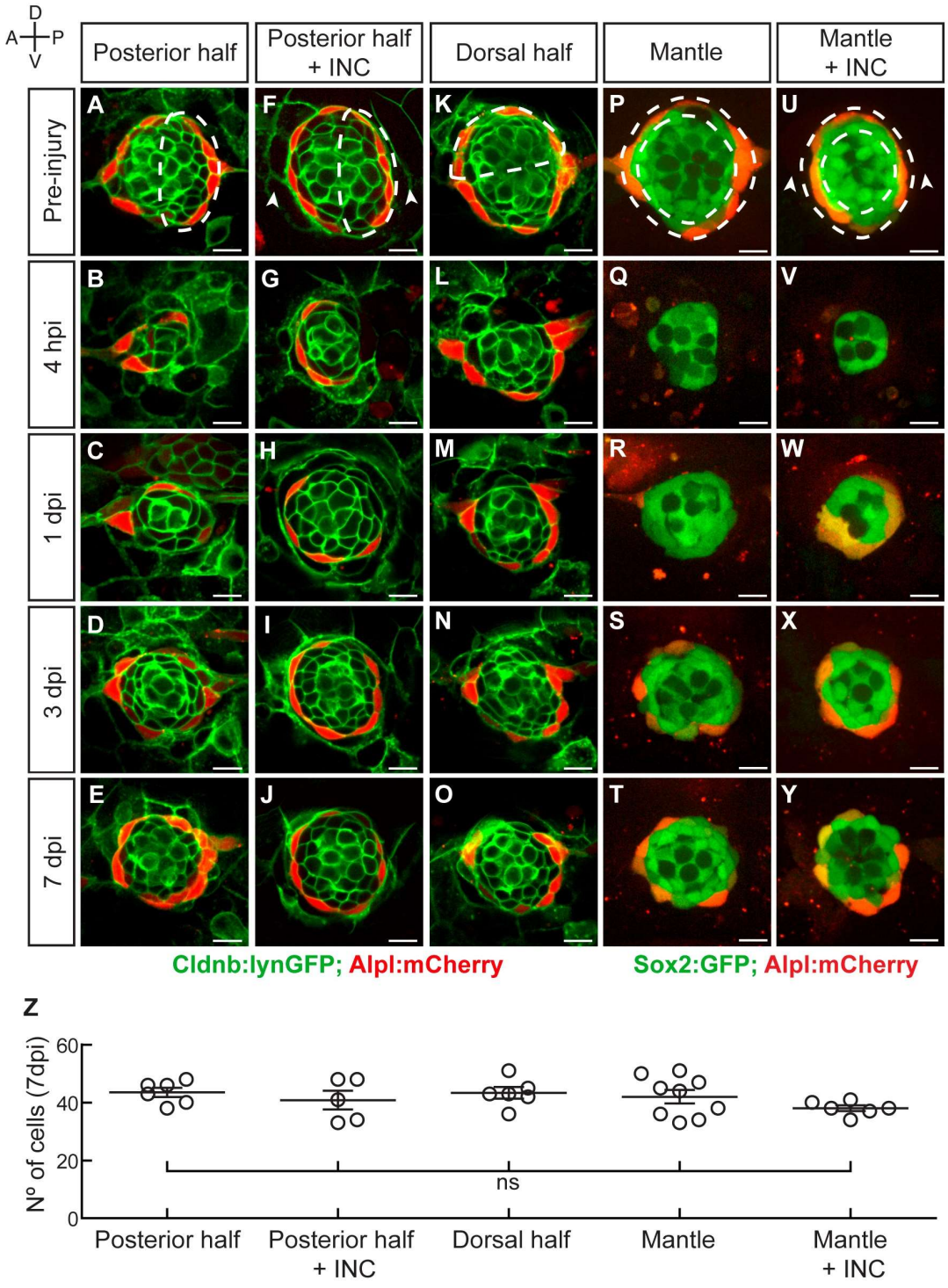
D
A
P
V
Posterior half
Posterior half + INC
Dorsal half
Mantle
Mantle + INC
Pre-injury
4 hpi
1 dpi
3 dpi
7 dpi
A
F
K
P
U
B
G
L
Q
V
C
H
M
R
W
D
I
N
S
X
E
J
O
T
Y
Cldnb:lynGFP; Alpl:mCherry
Sox2:GFP; Alpl:mCherry
Z
Nº of cells (7dpi)
60
40
20
0
ns
Posterior half
Posterior half + INC
Dorsal half
Mantle
Mantle + INC

Figure 24. Neuromasts have isotropic regenerative capacity. (**A)** Ablation of the posterior half of a neuromast. (**B-C**) The damage is resolved by cellular movement from the undamaged site 1dpi. (**D**) Neuromasts recover geometric order after 3 days and (**J**) return to homeostasis by 7dpi. Dashed lines in **A,F,K,P,U** delineate the ablated area. (**F-J**) Simultaneous ablation of the posterior half of a neuromast and the interneuromast cells flanking its anterior and posterior sides led to a regeneration outcome identical to that of the experiment in **A-E**. Arrowheads in **F** point the location normally occupied by the interneuromast cells. (**K-O**) Neuromasts depleted from their dorsal half also recover epithelial size, proportions and geometry in a manner indistinguishable from equatorial-side ablation after 7 days. (**P-T**) 7 days after their complete laser-mediated ablation, mantle cells regenerated for neuromasts to recover the mantle. (**U-Y**) The ablation of interneuromast cells flanking both sides of neuromasts that were depleted of mantle cells resulted in the same outcome. (**Z**) Quantification of the number of cells in regenerated neuromasts at 7dpi. Number of neuromast cells was no statistically significant between groups of different damage regimes as determined by one-way ANOVA ($F(4,27)=1.013$, $p=0.4183$). Scatter plot shows mean±s.e.m. ns: non-significant. Scale bars: 10 μm.

Next, I decided to assess the regenerative ability of mantle cells after the complete elimination of their cell type. The ablation of the entire mantle-cell population was followed by their re-emergence 3dpi, and the complete reconstitution of the outer rim of the neuromast 7dpi (N=15) (**Figure 24**P-T,Z). The simultaneous ablation of mantle and adjacent interneuromast cells led to the same outcome (N=6) (**Figure 24**U-Z), indicating that mantle cells regenerate from sustentacular cells and not from interneuromast cells. Taken together with previous findings that Sox2(+) sustentacular cells are the source of hair cells in regenerating neuromasts (Behra *et al.*, 2009; López-Schier & Hudspeth, 2006; Ma *et al.*, 2008; Wibowo *et al.*, 2011), these results yielded three important and novel findings: 1) that interneuromast cells are neither necessary nor sufficient for neuromast regeneration in larval zebrafish, 2) that neuromasts are symmetric in their regenerative capacity, 3) that Sox2(+) sustentacular cells are tripotent progenitors able to generate every neuromast cell type.

2.16. **Cell type proportions recover after total loss of tissue integrity**

I next tested the limits of neuromast regeneration by systematically ablating increasing number of cells. The ablation of all except 4 to 10 cells, generally reducing the organ to a combination of 2-3 mantle and 2-7 sustentacular cells, allowed regeneration (**Figure 25**A), whereas more extreme ablations (leaving 1-3 cells) almost always led to complete neuromast loss. After losing over 95% of their cellular content, injured neuromast recovered an average of 45 cells at 7dpi, with exceptional cases reaching 60 cells (N=15) (**Figure 25**B-E,K). The regenerated organs were radial symmetric as early as 3dpi (**Figure 25**D), and had normal cell-type composition and proportions 7dpi (**Figure 25**E,L-M). A time-course quantification of cell-type number during regeneration revealed a reproducible pattern of tissue growth and morphogenesis (**Figure 25**K-M). During the first 24hpi, laser-targeted cells are cleared from the injury site and the remaining cells recover a circular epithelium. From 1dpi to 3dpi, cell numbers increase and organ proportions begin to be restored. After 3dpi, cell numbers continue to increase but at a slower pace (**Figure 25**K-M). The concurrent ablation of the interneuromast cells (INCs) flanking the injured neuromasts lead to smaller organs but with normal cell composition, distribution and proportions (N=6) (**Figure 25**F-J,N-P). Remarkably, all neuromasts had normal cell-type composition and proportions despite having a much reduced cell number (**Figure 25**L-M,O-P), revealing that each cell type assumes an appropriate position despite reduced epithelial size and proportional imbalance.

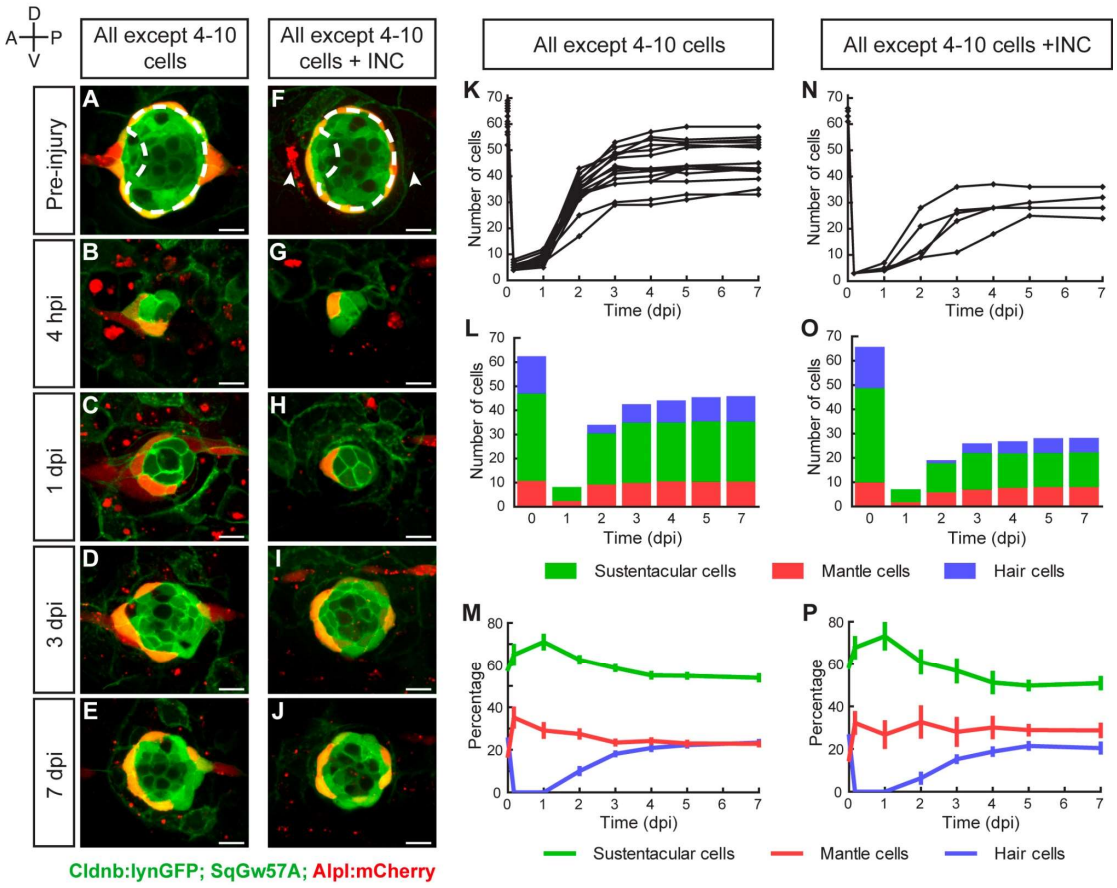

Figure 25. Recovery of organ proportions after loss of tissue integrity. (**A-B**) Severe neuromast ablations led to the survival of 4-10 cells (**C-D**) Neuromasts recover radial symmetry 3dpi and (**E**) original organ proportions at 7dpi. (**F-G**) Neuromasts reduced to 4-10 cells that were previously deprived from adjacent interneuromast cells (INCs) (arrowheads), (**H-J**) regenerated and reformed radial symmetry and proportions 7dpi, despite maintaining a reduced size. Dashed circles in **A,F** illustrate damaged areas. Scale bars: 10 µm. (**K,N**) Total cell numbers in regenerating neuromasts over 7 days in the two conditions depicted in **A-J**. (**L,O)** In the first 2dpi, neuromasts consist of almost exclusively supporting cells (green and red). Hair cells (blue) begin to appear 2dpi. (**M,P**) Percentages of cell types during a 7-day regeneration period. Right after damage, neuromast experience an imbalance of cell proportions that is re-established over the course of 3 days. Afterwards, neuromasts continue to slowly increase all cell numbers at similar rates. The final proportion of cell types recapitulates that of the starting condition. Time points show mean±s.e.m. $N_{\text{All except 4-10 cells}}$ =15, $N_{\text{All except 4-10 cells + INC}}$ =6.

2.17. **Apicobasal polarization recovers during regeneration**

Next, I tested if the orthogonal polarity axes of the neuromast epithelium are re-established after the severest of injuries. To assess neuromasts' apicobasal polarity I used a combination of transgenic lines that allows the identification of asymmetric subcellular structures, including the invariant basal position of the cellular nucleus, and the apical adherens junctions (**Figure 26**A,C) (Ernst *et al.*, 2012; Harding & Nechiporuk, 2012; Hava *et al.*, 2009). I found correct position of these markers in the regenerated epithelium (N=4) (**Figure 26**B,D).

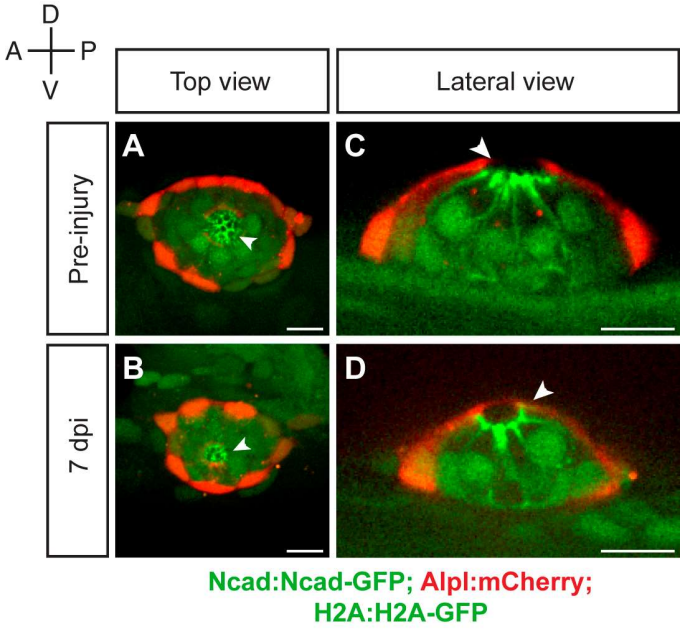

Figure 26. Apicobasal polarity of regenerated neuromasts. (**A**) Top and (**C**) lateral views of a neuromast before injury showing apical N-cadherin enrichment (arrowheads) and basal nuclei position. (**B**) Top and (**D**) lateral views of a regenerated neuromast 7dpi with proper apicobasal polarization. The accumulation of N-cadherin in regenerated neuromasts reveals proper re-establishment of apical constrictions during the process. Scale bars: 10 µm.

To assess hair-cell planar polarity, I looked at hair-bundle orientation using a phalloidin actin staining. This revealed that regenerated neuromasts were plane-polarized in a manner indistinguishable from unperturbed organs 7dpi, including coherent local planar polarity and global orientation relative to the main body axes of

the fish (N=10) (**Figure 27**A-C). This result suggests that as few as 4 surviving supporting cells can autonomously organize the planar polarization of the hair cells. An alternative explanation, however, is that these supporting cells have access to extrinsic polarizing information during regeneration. One potential polarizing cue are anisotropic mechanical forces exerted by the interneuromast cells that flank every neuromast and that are always aligned to its axis of planar polarity. To test this idea, I ablated all the interneuromast cells around an identified neuromast, and concurrently killed the hair cells with the antibiotic toxin neomycin (**Figure 27**D,E). In the absence of interneuromast cells, the hair cells recovered normal local and global planar polarity (N=16) (**Figure 27**F). Collectively, these findings reveal that as few as 4 Sox2(+) sustentacular cells can autonomously initiate and sustain integral organ regeneration, including cell-type proportions, cellular distribution and epithelial polarization.

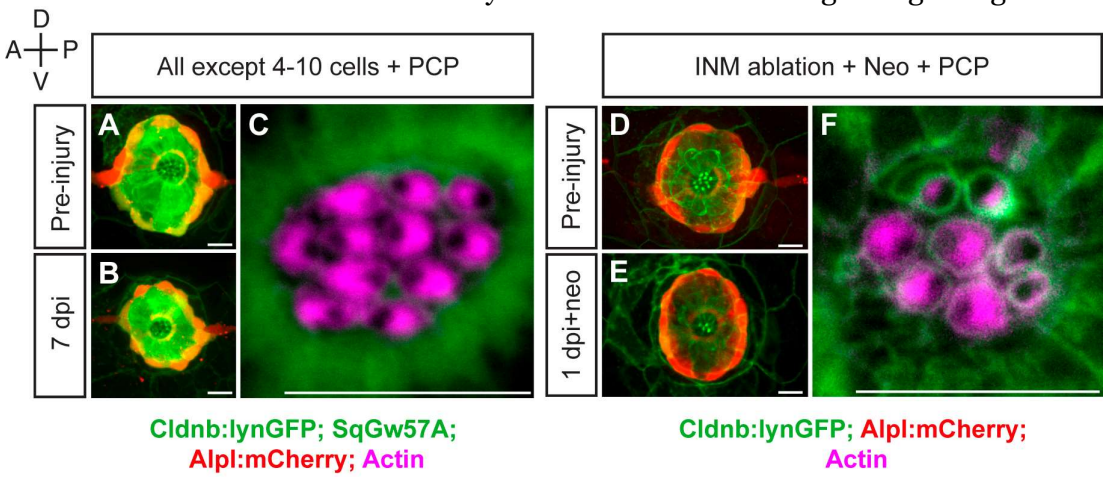

Figure 27. Hair-cell PCP in regenerated neuromasts. (**A**) Neuromast in the triple transgenic line *Tg[Cldnb:lynGFP; SqGw57A; Alpl:mCherry]* prior to severe ablation. (**B**) Regenerated neuromast 7dpi. (**C**) Hair-bundle staining with rhodamine-phalloidin (pink) reveals the coherent planar polarization of hair cells in the regenerated neuromast shown in **B**. (**D**) Neuromast before the removal of flanking interneuromast cells. (**E**) Neuromast during hair-cell regeneration, 48 hours after interneuromast-cell ablation and 24 hours after neomycin treatment. (**F**) Hair-cells regenerated in the absence of interneuromast cells recover coherent epithelial planar polarity. Scale bars: 10 μm.

2.18. **Differential transgene behavior suggests maturity reversal**

During these experiments I consistently observed a decay of cytoplasmic fluorescence, corresponding to the genetically-encoded marker SqGw57A:EGFP, in intact sustentacular cells during the first 24hpi (**Figure 25**C), and fluorescence recovery from 1dpi to 3dpi (**Figure 25**D). I did not see any change in fluorescence when using the Sox2:GFP marker (**Figure 28**A-E). This observation is interesting because I also found that during embryonic development, Sox2:GFP is expressed in lateral-line primordial cells before than the SqGw57A marker (**Figure 28**F-G'). Accordingly, the levels of SqGw57A expression are weak right after neuromast deposition, and increase rapidly during the maturation of the organ (**Figure 28**J-L). In contrast, Sox2:GFP expression levels remain constant during neuromast maturation (**Figure 28**M-O). Thus, SqGw57A is a live sensor of immediate cellular responses to tissue damage that suggests that Sox2(+) sustentacular cells dedifferentiate towards an embryonic status following tissue injury.

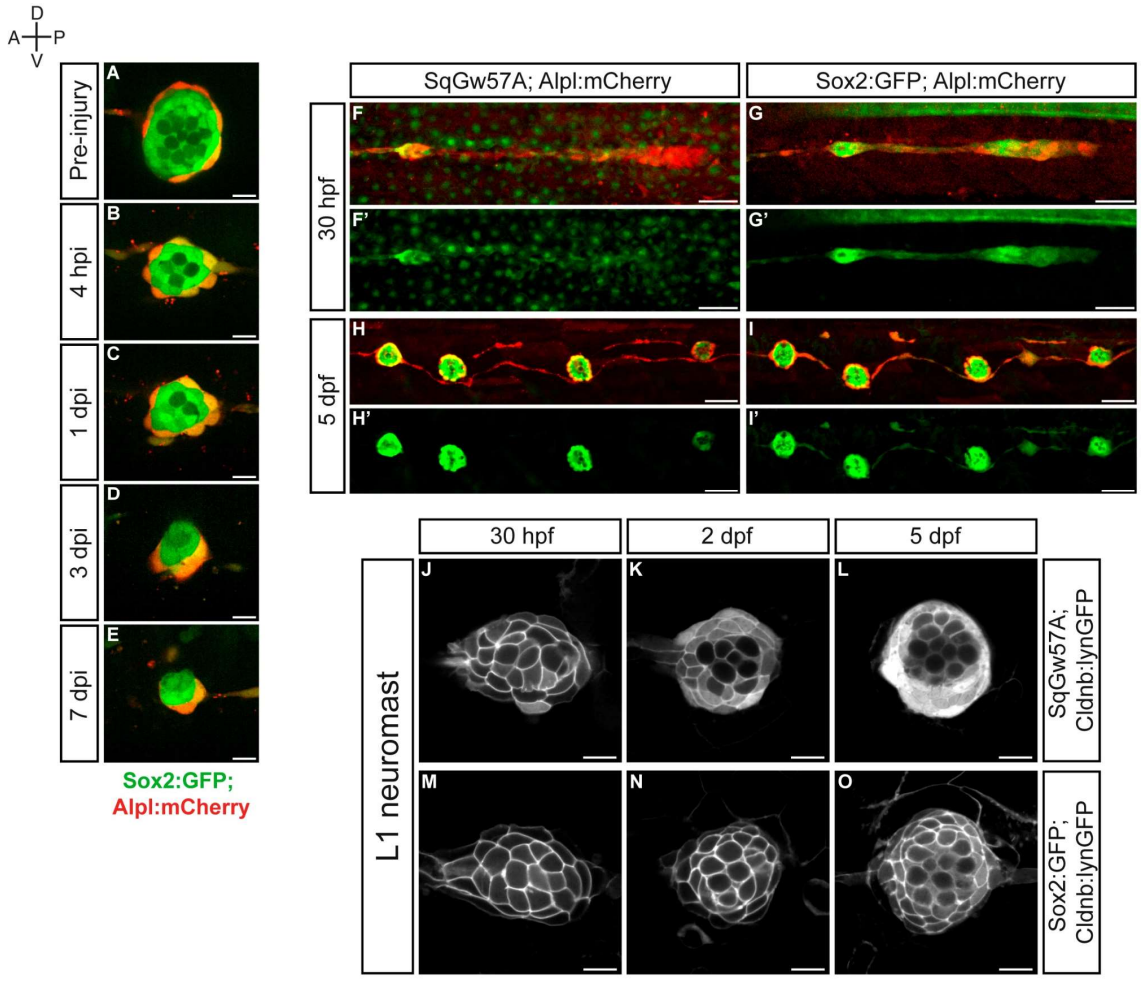

Figure 28. Differential expression profiles of supporting cell markers Sox2:GFP and SqGw57A during development and regeneration. (**A-E**) Neuromasts from a *Tg[Sox2:GFP; Alpl:mCherry]* specimen regenerating from 4-8 cells during a period of 7 days. (**B-C**) Sox2:GFP expression is not downregulated during the first 24hpi. (**F-G'**) Migrating posterior lateral line primordium after the deposition of L1 in the double transgenic lines (**F**) *Tg[SqGw57A; Alpl:mCherry]* and (**G**) *Tg[Sox2:GFP; Alpl:mCherry]*. (**F'**) SgGw57A expression is predominantly observed at the recently deposited L1 neuromast. (**G'**) Sox2:GFP is expressed in the migrating primordium, and the trail of deposited cells and neuromasts. (**H-I'**) Anterior segment of the posterior lateral line. (**H'**) The expression of SqGw57A marker is restricted to neuromast supporting cells. (**I'**) Sox2:GFP labels supporting cells in neuromasts and interneuromast cells along the trunk of the larvae. Scale bars: 50 µm. (**J-O**) Dynamics of expression levels of (**J-L**) Sqgw57A and (**M-O**) Sox2:GFP markers in maturating L1 neuromasts from 30hpf to 5dpf. The intensity of the membrane-tagged GFP from Cldnb:lynGFP marker helps the visual identification expression level dynamics over time. SqGw57A is weakly expressed from (**J**) 30hpf to (**K**) 2dpf and (**L**) increases dramatically by 5dpf, suggesting that its behavior correlates with the maturation state of supporting cells. (**M-O**) Sox2:GFP expression levels show virtually no fluctuation during the same period of time. Scale bars: 10 µm.

2.19. **Wnt/β-catenin is essential for regeneration initiation and termination**

An interesting question raised by these results, is how the final size of regenerated neuromasts is regulated. I have previously shown that the pharmacological activation of the Wnt/β-catenin signaling pathway during development and homeostasis generates hypertrophic neuromasts containing supernumerary sustentacular, hair and mantle cells. To test the putative contribution of Wnt/β-catenin during neuromast regeneration, I treated zebrafish larvae with pharmacological modulators of this signaling pathway after severely injuring neuromasts (**Figure 29**). AZK treatment (N=10) overshot the production of neuromast cells and led to organs that are on average 35% bigger than controls (**Figure 29**B) (N=15), a phenotype not observed in any of the previous regenerative conditions. Contrarily, treating injured organs with the Wnt/β-catenin inhibitor IWR1-endo, a small molecule that reduces the amount of β-catenin available by stabilizing an essential component of its degradation complex, blocks regeneration completely (**Figure 29**C) (N=4).

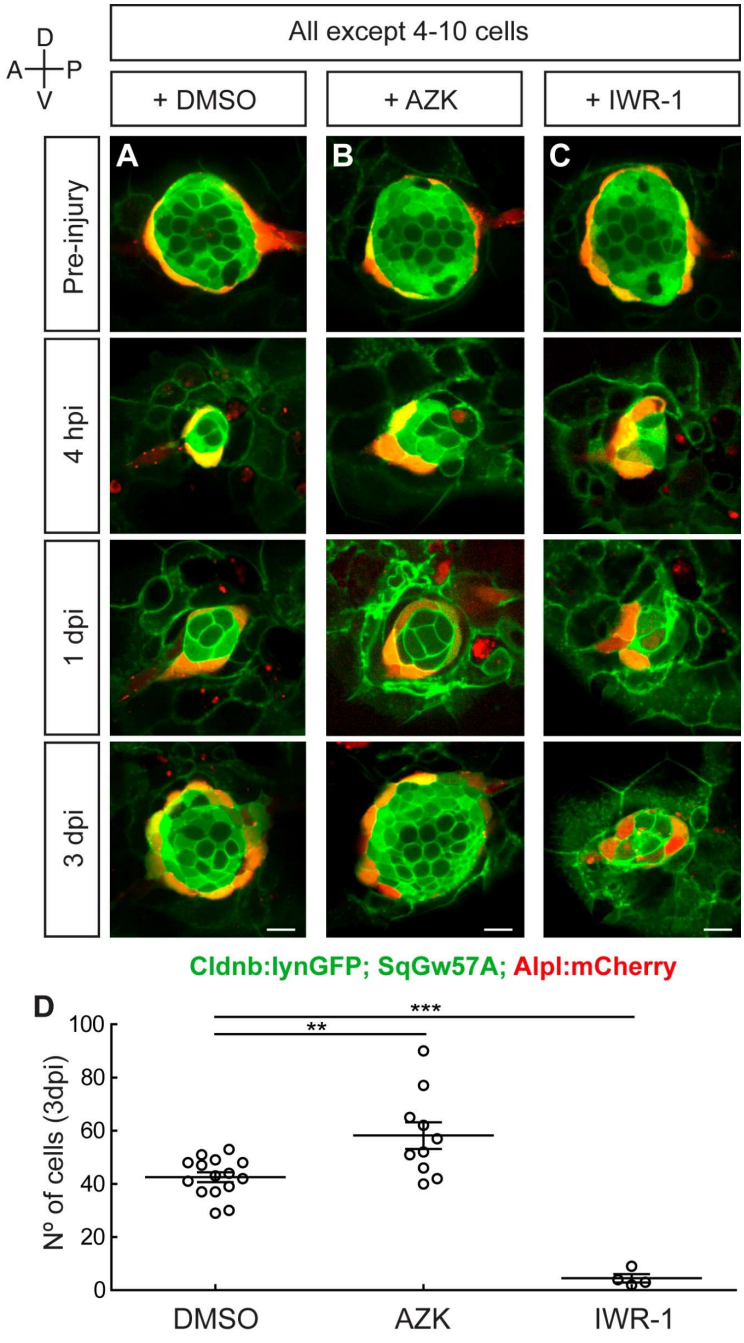

Figure 29. Role of Wnt/β-catenin during neuromast regeneration. (A) Control neuromast regenerating after severe ablation. (**B**) Ablated neuromasts under AZK treatment regenerated supernumerary cells. (**C**) 1-IWR-endo treatment blocked regeneration completely. (**D**) 3dpi, control neuromasts had 43±7 cells (N=15), AZK-treated neuromasts had 58±16 cells (N=10), and IWR1-endo-treated neuromasts 5±3 (N=4) (mean±s.d.). Means are significantly different based on a 1-way ANOVA test [$F(2,26)= 35.58$, $p < 0.0001$] with Tukey's Multiple Comparison Test. Scale bars: 10 μm.

Interestingly, the increase in cell number is exclusively due to an excessive production of sustentacular cells (25±6 cells in controls, 40±11 cells in AZK-treated, mean±s.d.), as hair- and mantle-cell numbers are not significantly different when compared to control neuromasts (**Figure 30**). These results indicate that Wnt/β-catenin is involved in neuromast regeneration by promoting the proliferation of sustentacular cells independently of hair or mantle cell differentiation and, eventually, determining the size of the recovered organ.

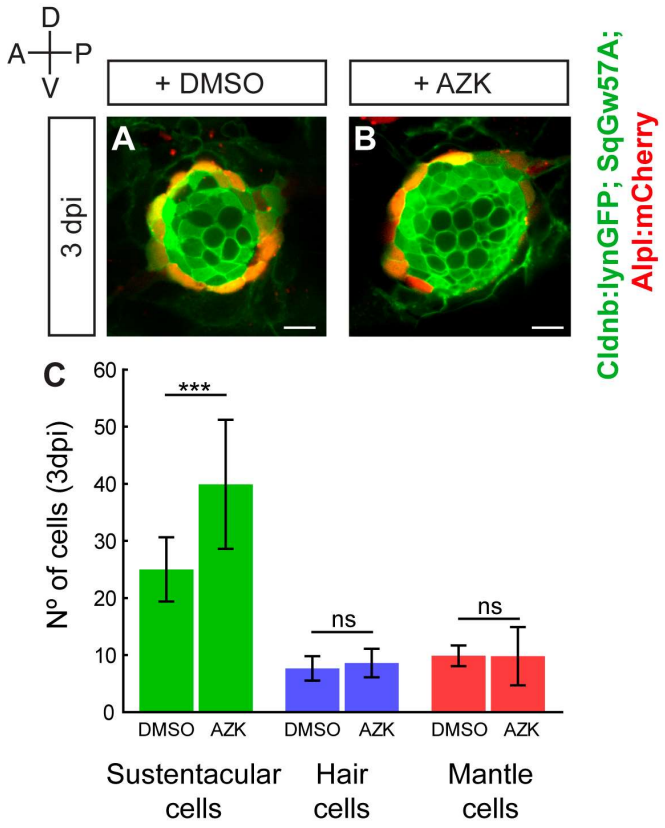

Figure 30. Wnt over-activation promotes sustentacular cell proliferation but not differentiation. (**A**) Example a control regenerated neuromast 3dpi. (**B**) Example of an AZK-treated regenerated neuromast with excessive production of sustentacular cells. (**C**) Pharmacological Wnt activation promotes proliferation of sustentacular cells ($p < 0.0001$, t-test) but does not affect hair or mantle cell differentiation ($N_{DMSO}=15$, $N_{AZK}=10$). Scale bars: 10 µm.

2.20. **Original neuromast size does not influence regeneration outcome**

I hypothesized that another factor that could determine the final size of regenerated neuromasts, is the original size of the organ before the injury. To test this idea, zebrafish larvae were treated with AZK from 2-6dpf to induce the generation of hypertrophic neuromasts. Subsequently, these neuromasts were reduced to a small group of 4-10 surviving cells and larvae were let recover in drug-free medium during 5 dpi (**Figure 31**A). Surprisingly, none of the hypertrophic neuromasts regenerated to a cell count that was near their original cell count (**Figure 31**B) (N=4). As observed in the previous regeneration assays (**Figure 25**), the dynamics of organ growth showed that most cell proliferation took place during the first 3 days and that neuromast growth continues later at a much slower pace. These observations, although still preliminary, suggest that neuromasts' original size does not determine the eventual size of regenerated organs.

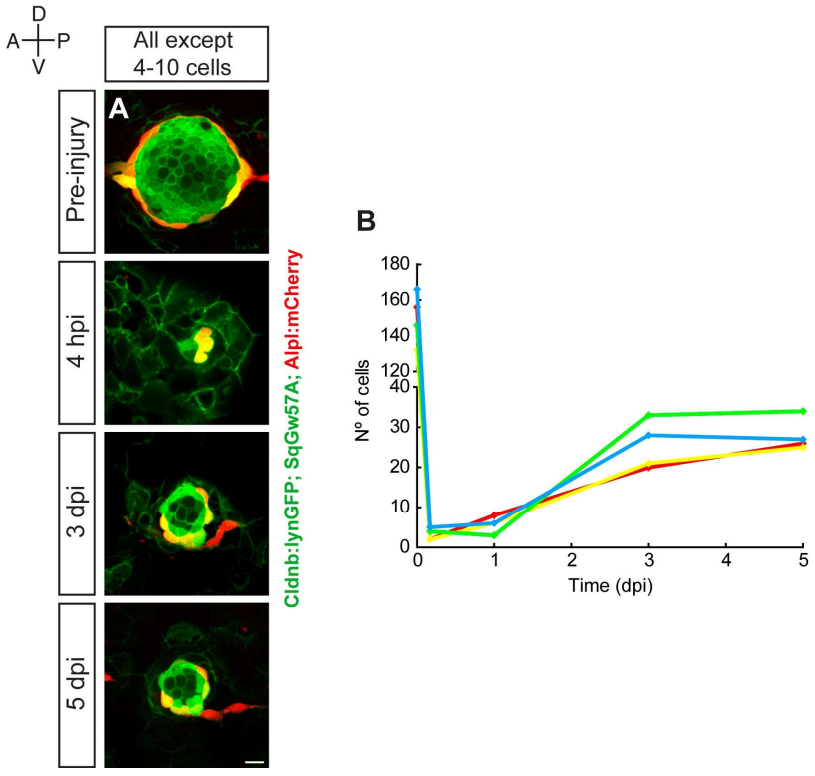

Figure 31. Hypertrophic neuromasts regenerate normal size after severe ablation. (**A**) 5day follow up of the regeneration of a hypertrophic neuromast after the ablation of all except 4-10 cells. (**B**) Although having an excessive number of initial cells, injured neuromasts recover an amount of cells that resembles that of homeostatic neuromasts. Scale bars: 10 μm.

2.21. **Generation of a new Gal4 driver and setup of clone tracing strategy**

To understand cell fate transitions during neuromast regeneration, I turned into classic single-cell tracing approaches. For this purpose, I generated a new transgenic line that drives the expression of the transcriptional activator Gal4-VP16, specifically in cells of the lateral line epithelium on a cell type-independent basis. I took advantage of a previously published plasmid (Gerety *et al.*, 2013) containing an inducible form of Gal4-VP16 whose expression is driven by the CldnB promoter. This Gal4-VP16 version is conveniently fused downstream of the human estrogen receptor (variant ERT2), that drives the translocation of the protein complex to the nuclei upon induction with 4-hydroxy-tamoxifen (4-OHT). By establishing the *Tg[CldnB:ERT2-Gal4]* transgenic line, I could reliably use this sophisticated expression system to temporally control of the onset of Gal4 activation in all neuromast cells. Zebrafish eggs were injected into 1-cell stage with plasmid DNA and transposase mRNA, raised to adulthood, and crossed with *Tg[UAS:RFP1]*. Then, progeny was incubated with 4-OHT to screen for germ-line transgene transmission and positive larvae were selected and raised to adulthood as founders. Because transgene expressivity depends strongly on the number of inserted copies and the genomic landing sites, four different adult founders were screened. They were crossed to *wild type* zebrafish, their progeny incubated with 4-OHT and imaged under a confocal microscope. The founder with the most homogenous transgene

expression levels was selected and established as permanent zebrafish line (**Figure 32**A).

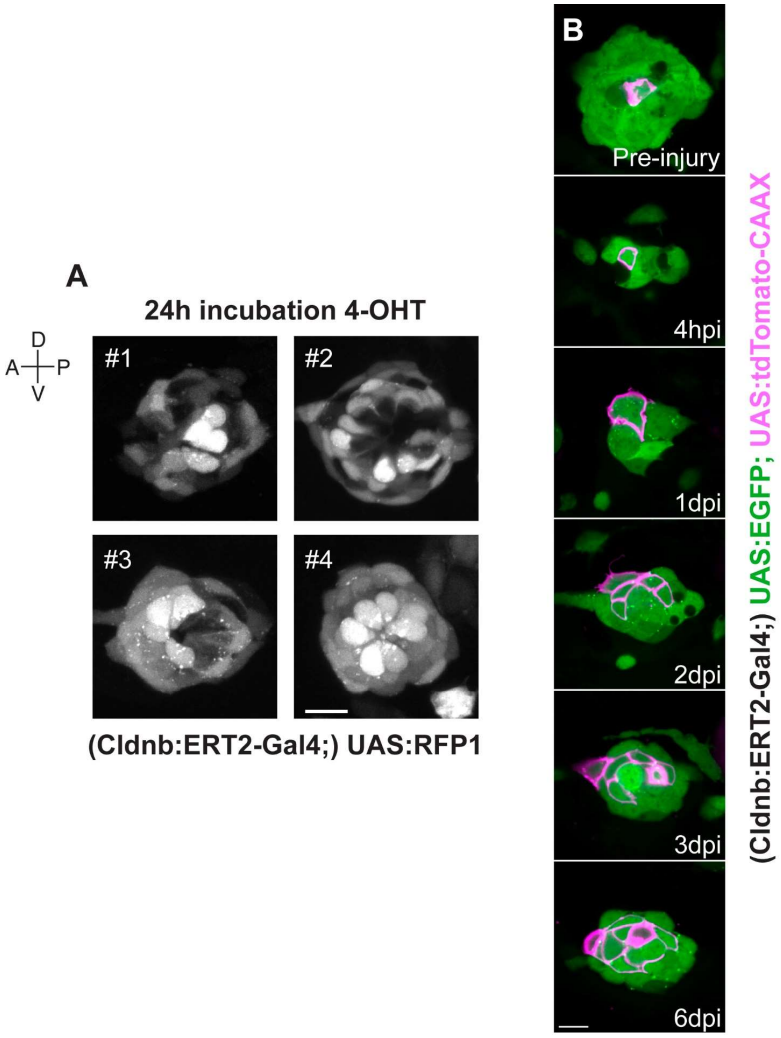

Figure 32. Generation of a neuromast-specific Gal4 driver line and clonal tracing approaches. (A) Gal4 induction with 4-OHT demonstrates variable transgene expressivity among different founder zebrafish. Founder #4 was selected to establish a new zebrafish strain. **(B)** Series of images that follow the regeneration of a neuromast in the triple-transgenic line *Tg[CldnB:Ert2-Gal4; UAS:EGFP; UAS:tdTomato-CAAX]*. A singly-marked sustentacular cell originally residing at the center of a neuromast (pre-injury) eventually produces a clone (1dpi-3dpi) of cells that are localized to the corresponding position of all three cell types in the regenerated neuromast (6dpi). Scale bars: 10 μm.

To sparsely label single neuromast cells, I used the *Tg[CldnB:ERT2-Gal4; UAS:EGFP; UAS:tdTomato-CAAX]* triple transgenic line. In these lines, the UAS:EGFP is expressed homogenously in all the cells of the organ, whereas the expression of UAS:tdTomato is highly mosaic. Importantly, transgene expression is cell-type independent, allowing the tracking of cells of interest and their entire progeny independently of their fate. Severe neuromast ablation led singly marked sustentacular cells to proliferate and contribute to the regeneration of the organ. Marked clones grew both inwards and outwards, generating cells that occupied from the center to the outermost area of the organ which is suggestive of, respectively, hair and mantle cells (**Figure 32**B). These results support the notion that sustentacular cells are tripotent progenitors able to generate all three neuromast cell types but remain still somewhat inconclusive.

2.22. **Long-term live imaging and cell-lineage tracing**

The previously described single-cell tracing approach presented two major handicaps: 1) the combination of transgenic lines used for sparse cell labeling did not allow a precise identification of cell types and 2) the temporal resolution was not enough to resolve most cellular behaviors. To overcome these inconveniences and shed new light into the cellular mechanisms underlying neuromast regeneration, I systematically quantified individual cellular behaviors such as movement, proliferation and differentiation in the context of whole-organ regeneration by means of long-term live videomicroscopy. I used the *Tg[Cldnb:lynGFP; SqGw57A; Alpl:mCherry]* triple-transgenic line to manually trace in time and space cell lineages of cells that remain after damage (from now on called “founder cells”).

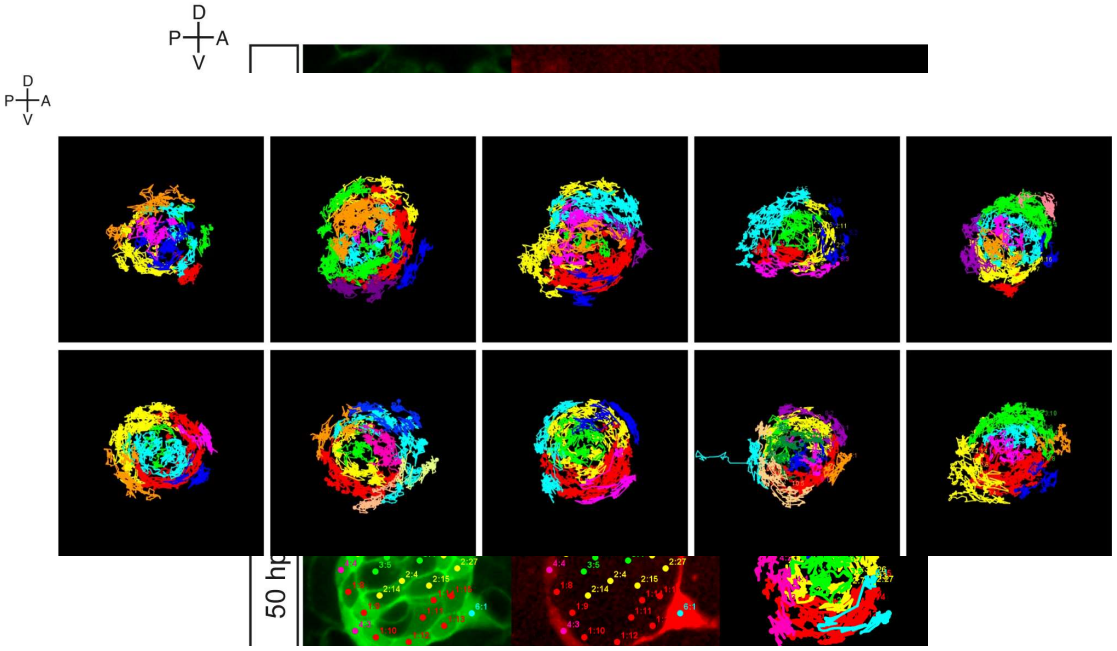

Figure 34. Cell trajectories of founder cells and their progeny reveal a concentric growth pattern. Examples of cell tracings at the last recorded time points for eight regenerated neuromasts. Cellular clones with a shared founder cell are color coded.

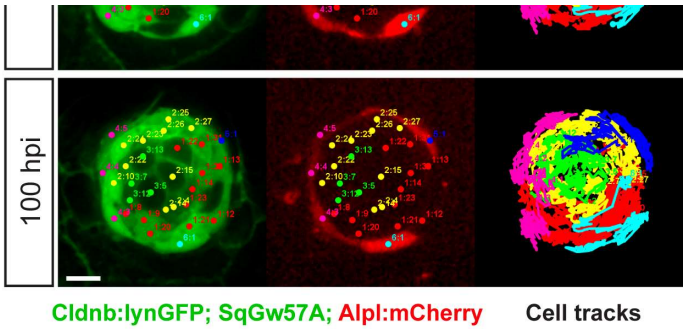

Figure 33. Long-term whole-organ cell-lineage tracing. Still images showing a representative 100 hours time-lapse recording of a regenerating neuromast in *Tg[Clndb:lynGFP; SqGw57A; Alpl:mCherry]* larva (left and middle panels). Cellular clones that share a common founder cell are clustered and color-coded. Cell trajectories reveal a concentric growth pattern (right panel). Scale bars: 10 μm.

I conducted 15 independent time-lapse recordings of the regenerative process after the ablation of all except 4-10 cells, ranging from 65 to 100 hours of continuous imaging (**Figure 33**, **Figure 34**), resulting in a total of 763 cells and 104,863 cell coordinate

points. These data were analyzed in collaboration with Dr. Carsten Marr and Valerio Lupperger from the Single Cell Dynamics Group, of the Institute of Computational Biology at the Helmholtz Zentrum München. To facilitate the interpretation of the time-lapse data, each clone was graphically represented with a tree illustrating the division dynamics and fate choices of each founder cell (**Figure 35**).

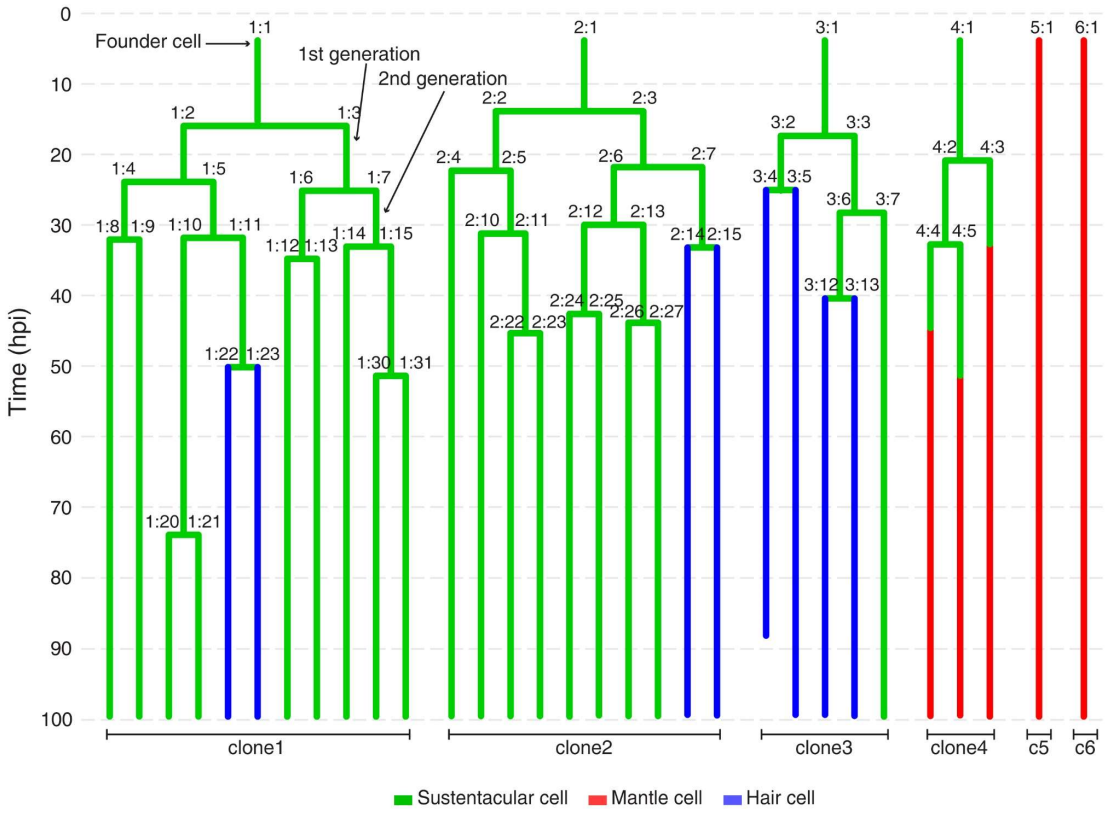

Figure 35. Cell lineages from the time-lapse movie shown in Figure 33. Branching points symbolize cell divisions. The division of a founder cell generates two cells of the 1st generation. Subsequent divisions produce cells of the 2nd, 3rd and 4th generation. Cell types are indicated with green (sustentacular), blue (hair) and red (mantle) colors.

2.23. **Sustentacular and mantle cells exhibit different regenerative potential**

Analyzing all 15 recordings, we obtained a total of 76 founder sustentacular and 30 founder mantle cells. We found that most sustentacular founder cells undergo 3 division rounds over 7dpi, with some diving up to 5 times, whereas almost half of the

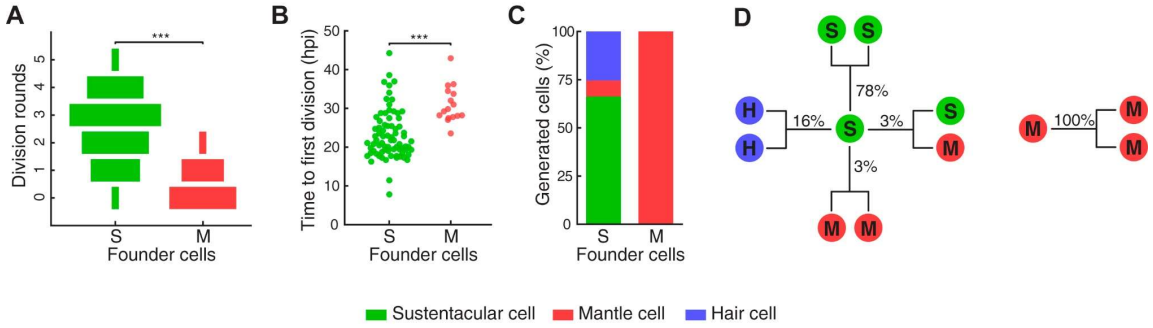

founder mantle cells (14 out of 30) do not divide at all (**Figure 36**A). Founder sustentacular cells require on average 19±6 hours (mean±s.d., n=76) for the first mitosis, whereas the mantle cells that divided required on average 27±5 hours, (mean±s.d., n=30) (**Figure 36**B). Also cell types that derived from sustentacular and mantle founder cells were different: while sustentacular founders produced three cell types (sustentacular, mantle and hair cells), mantle founders produced only their own type (**Figure 36**C).

Figure 36. Long-term whole-organ cell-lineage tracing reveals distinct cellular behaviors during neuromast regeneration. (**A**) Sustentacular founder cells undergo significantly more (p=3.59e-06, Mann-Whitney test) division rounds than mantle founder cells during 100 hours of neuromast regeneration. (**B**) The first division of sustentacular founder cells (n=76) occurs significantly earlier (p=1.13e-5, Mann-Whitney test) than that of mantle founder cells (n=16). (**C**) Sustentacular founder cells (n=76) generate all three neuromast cell types whereas mantle founder cells (n=30) produce only mantle cells. (**D**) Out of 307 sustentacular cell divisions, 78% were self-renewing, 16% produced a pair of hair cells, 3% produced sustentacular cells that both became mantle cells within the next generation and 3% generated two sustentacular cells of which only one transited to mantle cell fate within the next generation. Oppositely, all 20 observed mantle cell divisions were self-renewing.

Next, we categorized all observed cell divisions according to the fate of the two daughter cells at the time of the next division or at the end of the time-lapse recording. This analysis revealed that 97% of the sustentacular-cell divisions were symmetric: 78% producing two sustentacular cells (SS), 16% produced a pair of hair cells (HH) and 3% generated two mantle cells (MM). The few asymmetric divisions (3%), generated one sustentacular and one mantle cell (SM) (**Figure 36**D) (n=307). On the contrary, all mantle-cell divisions (n=20) were symmetric (MM), even when the founder progenitor was a sustentacular cell (**Figure 36**D). Together, these results evidence drastic differences in potency and proliferation between sustentacular and mantle cells, and establish a new cell lineage hierarchy for neuromast regeneration.

2.24. **Sustentacular cells are equipotent**

The previous results do not resolve the long-standing question of whether the sustentacular-cell population is homogeneous or if, on the contrary, consists of a mix of coexisting sub-types with distinguishable identities (Cruz *et al.*, 2015; Romero-Carvajal *et al.*, 2015; Wada *et al.*, 2013; Wibowo *et al.*, 2011). I reasoned that we could answer this question by characterizing the different types of observed clones. Sustentacular founder cells were able to produce four different types of clones: containing sustentacular cells only (S), sustentacular and mantle cells (SM), sustentacular and hair cells (SH), and all cell types (SHM). On the contrary, mantle founder cells only produced clones that contain other mantle cells (M) (see **Figure 37**A for illustrative examples). We found that 37/72 of the clones were SH, 21/72 were S, 12/72 were SM and only 2/79 were SHM (**Figure 37**B). By analyzing the contribution of each clone to the final cellular composition of each regenerated

neuromast, we found that the numbers and proportions of sustentacular founder cell-derived clones diverged strongly among samples (**Figure 37**C).

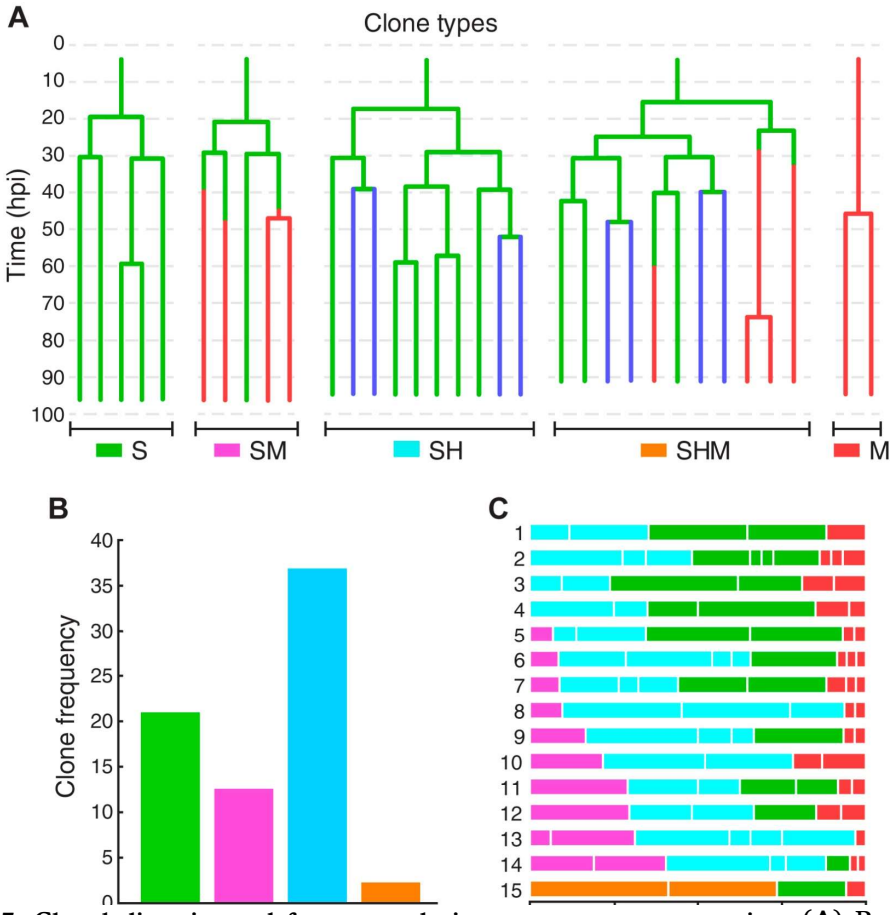

Figure 37. Clonal diversity and frequency during neuromast regeneration. (**A**) Representative examples of different clone types extracted from time-lapse data. Sustentacular cells give rise to S, SM, SH, and SHM clones (color coded respectively with green, pink, cyan and orange) whereas mantle cells produce only pure mantle cell clones. (**B**) The clone composition of the 15 regenerated neuromasts is not stereotypic. The length of each bar represents the proportion of neuromast cells that belong to each clone. Neuromast 8 has been shown in Figure 33. (**C**) The most frequent clones contain sustentacular and hair cells (SH, n=37 clones), followed by those with only sustentacular cells (S, n=21 clones). The third most frequent are composed by sustentacular and mantle cells (SM, n=12 clones). Clones containing all three cell types are very rare (SHM, n=2 clones).

This suggests either that sustentacular cells are homogeneous but behave non-stereotypically during regeneration or, on the contrary, that they are a heterogeneous population. I hypothesized that if the latter was true, sustentacular cell subpopulations may display different proliferative potentials or may require different times to start dividing. However, we did not find significant differences in the average number of cells in S, SH and SM cell clone types (**Figure 38**A) nor in the time to the first division of their respective founder cells (**Figure 38**B), indicating that differences in the proliferative capacity or the time required to start dividing are unlikely to explain differences within sustentacular cells. The representation of the spatial localization of the 72 sustentacular founder cells after damage, relative to the center of their respective founder cell clusters, pointed out that extrinsic cellular features, like position or local environment could determine the clone type of each sustentacular founder cell (**Figure 38**C).

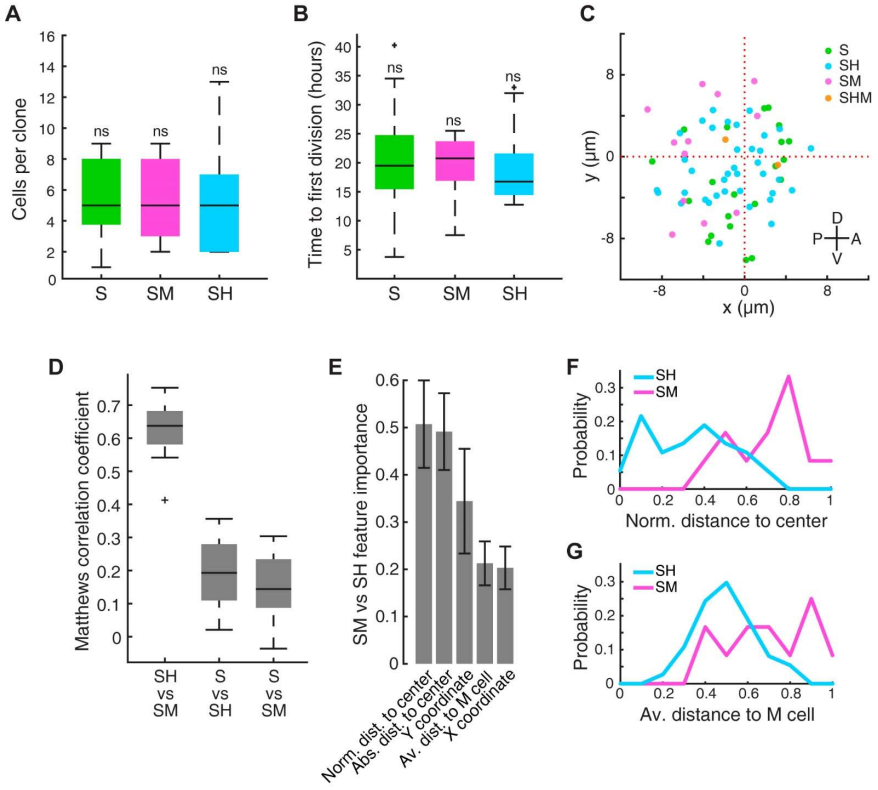

Figure 38. Clonal variability does not reflect plasticity differences within the sustentacular cell population. (**A**) S, SM and SH clones produce similar number of cells (p=0.68, Kruskal Wallis test) (**B**) Sustentacular founder cells of S, SM, and SH clones divide similarly early (p=0.42, Kruskal Wallis test) after approximately 18 hours after neuromast injury. (**C**) Sustentacular founder cells that produce SH (cyan) and S clones (green) are distributed similarly around the center of the organ (at x=y=0). Those that generate SM clones (pink) are localized further away from the center and are biased towards the posterior side. (**D**) Sustentacular founder cell choices between SH vs. SM clones can be predicted with high accuracy (MCC=0.6277±0.0869, mean±s.d., n=15 bootstrapped samples) whilst choices between S and SH or SM clones are highly inaccurate (MCC=0.1927±0.1059 and 0.1514±0.0961, mean±s.d., respectively, n=15 bootstrapped samples), based on 32 calculated features. (**E**) Features relative to the position of the founder cells and their nearest cellular environment can discriminate between SM and SH clone types. (**F**) Feature distribution for normalized distance to neuromast center. (**G**) Feature distribution for average distance to other mantle cells.

To quantitatively analyze and identify several of the variables that possibly determine clone type, we established a machine learning approach using 31 observable cellular features, including among others, absolute and normalized measurements of location, movement and distances to neighboring cell types (see Materials and Methods for complete feature list). We chose this approach because once the number of components in a system reaches a certain threshold, understanding the system without formal analytical tools becomes exceedingly difficult. With these data, we trained a random forest algorithm in the prediction of sustentacular founder cell pairwise choices between the three most common clone types (S vs SH, S vs SM and SM vs SH) via generation of decision trees. To evaluate the quality of these binary clone type predictions, we used Matthews correlation coefficient (MCC). We chose this coefficient because it compensates for size imbalances between the two predicted categories (**Figure 37**B). We were able to predict sustentacular founder cell choices between SM and SH clones with high accuracy (42 out of 49 clones were correctly predicted, MCC=0.63±0.09, mean±s.d., n=15 bootstrapped samples), while neither SH nor SM clones could be discriminated when compared to S clones (**Figure 38**D). Random

forest algorithms allow the individual evaluation of the predictive power of each of the 31 features used for the decision process. The features with highest predictive value for discriminating SM vs SH clones were the distance to the neuromast center and the distance to surrounding mantle cells (**Figure 38**E-G). For details of the predictive power estimations of all features in the 3 binary predictions, see **Figure 39**.

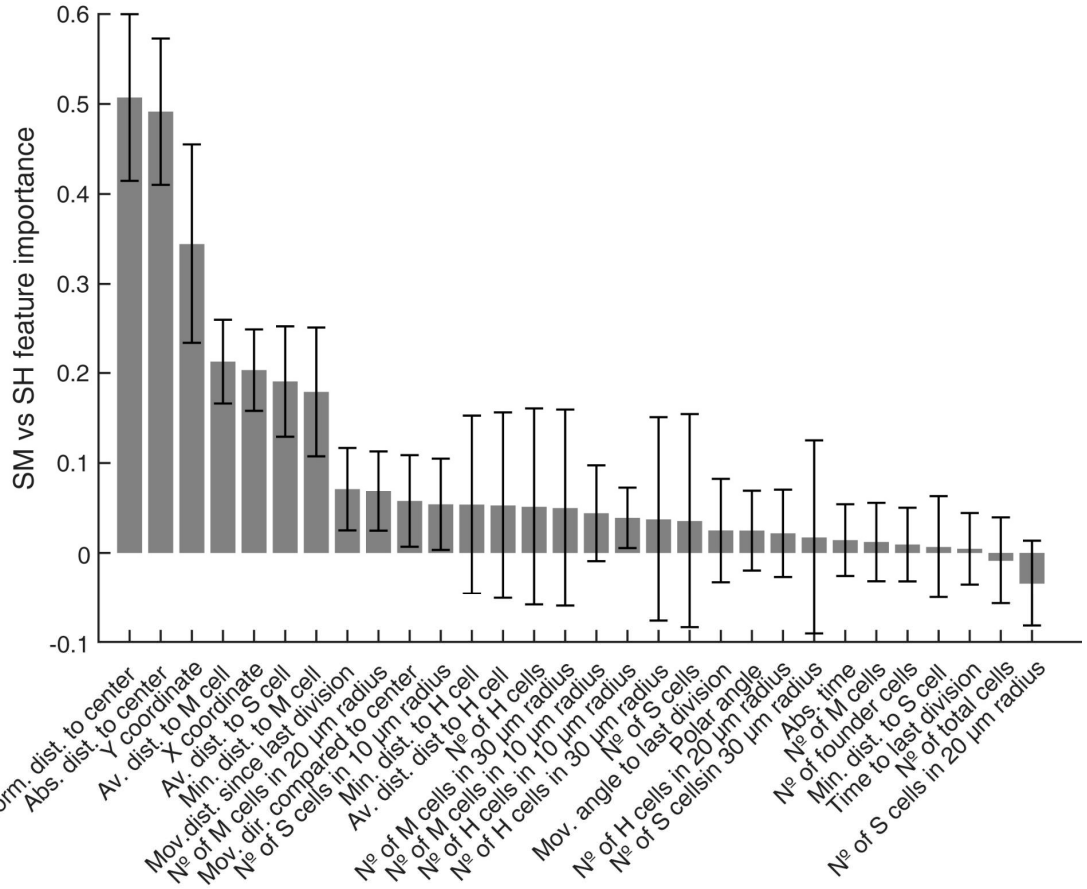

Figure 39. Features used to predict SM vs SH clones sorted by predictive importance.

Finally, I wondered if the sustentacular founder cells that regenerate mantle or hair cells are cell type-specific progenitors. I reasoned that if this was the case, the number of either mantle or hair cells in a SM or SH clone should grow proportionally with the total number of cells in their clones. However, we found no significant correlation

between the number of total cells in SH or SM clones and the number of hair or mantle cells in each clone (**Figure 40**). Together, these data do not support the idea of distinct subpopulations of sustentacular cells, and indicate instead that position and local environment of the founder cell at the start of the regeneration process determines the binary choice between producing an SH or an SM clone.

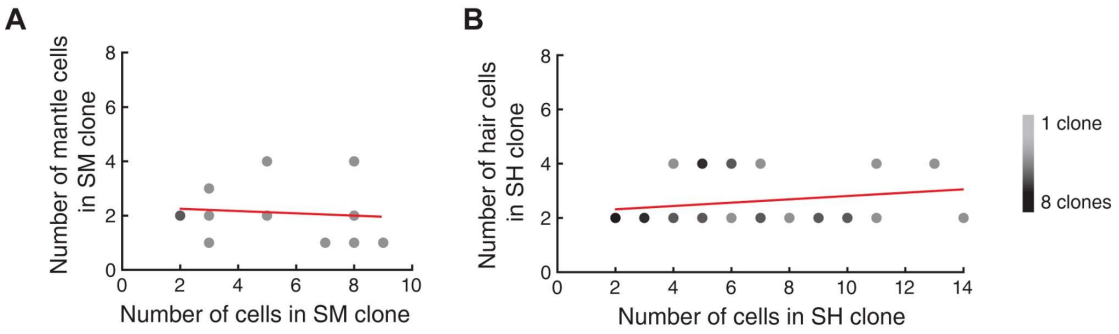

Figure 40. The number of differentiated cells in a clone does not correlate with its total cell number. (**A**) The number of mantle cells that appear in a SM clone does not correlate with its total cell count (Spearman r=-0.21, p=0.51, n=12 clones). (**B**) Similarly, the number of differentiated hair cells in a SH clone does not correlate with its total cell number (Spearman r=0.31, p=0.055, n=39 clones). Color gradient describes the frequency of clones in each position. ns: non-significant.

2.25. Spatiotemporal regulation of cycle length and fate decisions underlies organ regeneration

Because in some developmental contexts, cell-cycle length or proliferative rate can determine the fate of the daughter cells (Calegari *et al.*, 2005; Rossi *et al.*, 2017), I decided to use our cell-tracking data to quantify the kinetics of proliferation during neuromast regeneration. We found three pronounced waves of sustentacular cell divisions spaced by approximately 8 hours (**Figure 41**A). The division frequency of subsequent generations derived from proliferating founder cells revealed pronounced

proliferation peaks at 20h, 28h, and 38h, respectively (**Figure 41**B), suggesting that the cell cycle length early in regeneration is strictly regulated. Indeed, cell cycle lengths in the 1st generation are sharply peaked at 8 hours (mean±s.d at 11±5h.) (**Figure 41**C) regardless of the time to the first division of their founder mother cell. Cell-cycle lengths begin to diffuse in the 2nd generation (peak at 8h, mean±s.d. at 14±9h.) and even more in the 3rd generation (mean±s.d. at 26±18h.) (**Figure 41**C). Therefore, it became clear that cells respond to some cue to switch from strict to relaxed control of cell cycle length between the 1st and the 3rd generations. To identify the transition point between regulated and diffuse cell cycle lengths, we tested the goodness of fit of two-segment regression models with variable change points. This approach allows the quantitative determination of the changing point in the correlation of two independent variables that exhibit different relationships. We found that the length of cell cycles is strictly maintained to 11±3 hours (mean±s.d.) hours up until 47hpi. Afterwards, cell cycle length increases linearly with regeneration time (**Figure 41**D). I hypothesized that another extrinsic influence on the length of the cell cycle may be the size of the organ. To test this assumption, we used a similar two-segment regression model to define when cell cycles lose strict length regulation, and discovered that the vast majority of the cell cycles (76%) span between 7-13h below a threshold of 24 cells (**Figure 41**E). Above this number, cell cycles lengths vary strongly. These results suggest that neuromast damage triggers the activation of a sustentacular cell regenerative program that promotes a switch from quiescence to a proliferative state, in which cells cycle approximately every 11 hours.

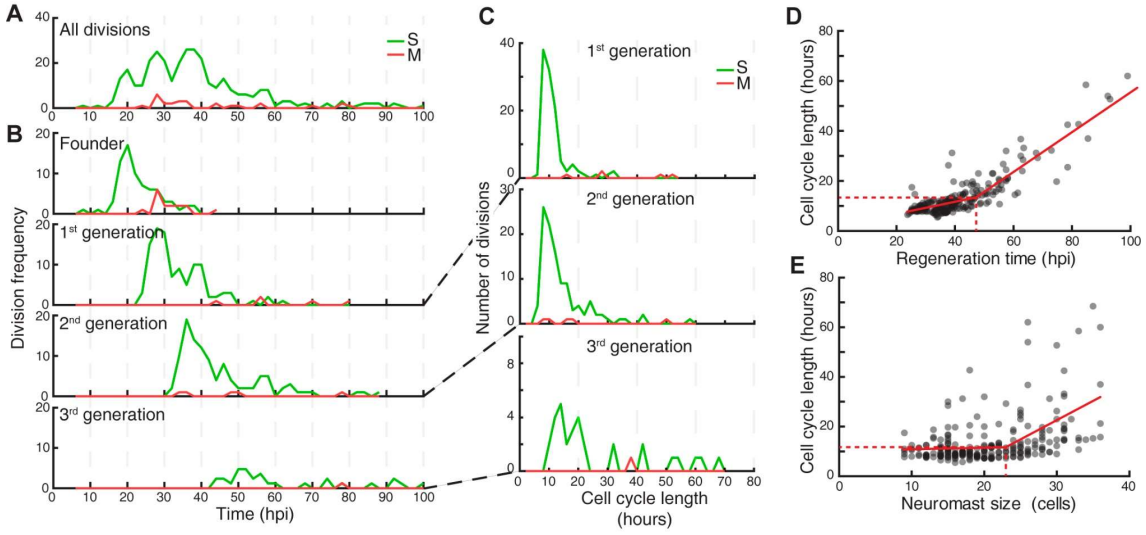

Figure 41. Sustentacular cells drive neuromast regeneration by bi-phasic regulation of cell cycle length. (**A**) Equally-spaced waves of coordinated sustentacular cell divisions (green) underlie the recovery of neuromast cell size. Mantle cell divisions (red) occur occasionally and do not follow the pattern of sustentacular cells. (**B**) Proliferative waves correspond to the coordinated divisions of cells from independent generations. (**C**) Cells from 1st and 2nd generation divide on average after cell cycles of 11±5 and 14±9 hours respectively (mean±s.d.). Coordination is lost at the 3rd generation when cell cycles start to lengthen (26±18 hours, mean±s.d.). (**D**) Cell cycle length (11±3 hours, mean±s.d.) is marginally influenced by regeneration time until 47 hours after injury, when cycle length starts increasing proportionally with regeneration time. (**E**) Cell cycle lengths (12±6 hours, mean±s.d.) do not correlate directly with neuromast size until 24 neuromast cells.

To reveal the features that influence sustentacular cell's fate choices and to facilitate their analysis, we focused on their decision-making process at the time of division. Hair cells regenerate exclusively after the differentiating division (HH division) of a hair-cell progenitor that derives from sustentacular cells that have ceased to receive Notch signaling (Wibowo *et al.*, 2011). However, our time-lapse data show that the transition from sustentacular to mantle cell fate is not determined before nor during the originating division but that, instead, it occurs independently in either one daughter cell (SM division) or the two daughter cells (MM division). For ease of classification, we called these divisions transition-associated divisions (SM/MM), and encompass

both SM and MM divisions. This time, we trained a random forest algorithm in the prediction of binary choices between self-renewing divisions (SS), differentiating divisions (HH) and transition-associated divisions (SM/MM). Here, the choice between differentiating and transition-associated divisions (HH vs SM/MM) was highly predictable (63 out of 66 divisions correctly predicted, MCC=0.91±0.07, mean±s.d., n=15 bootstrapped samples), while the discrimination between self-renewing and differentiating or transition-associated divisions (SS vs HH or SM/MM) was much less accurate (MCC=0.49±0.05 and 0.38±0.15, respectively, mean±s.d., n=15 bootstrapped samples) (**Figure 42**A).

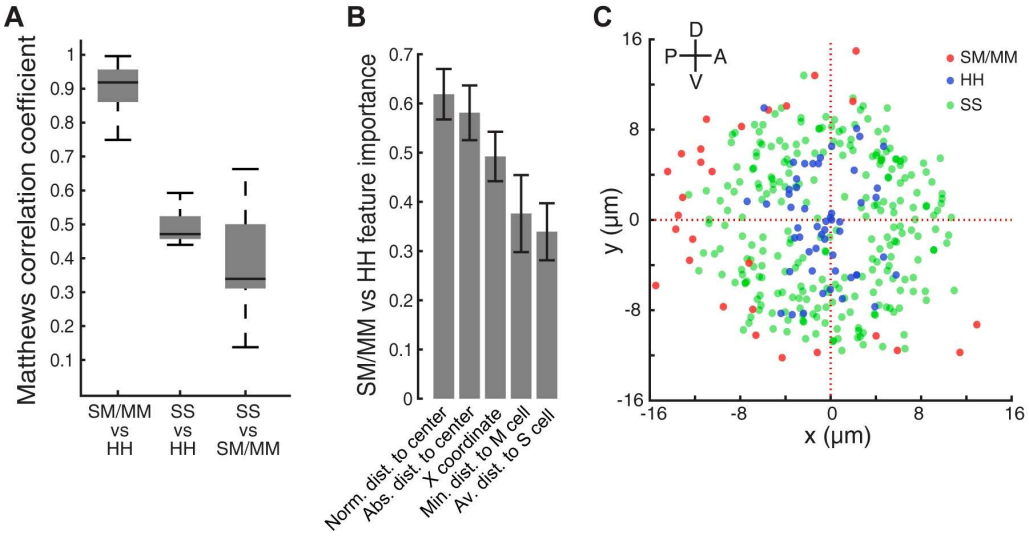

Figure 42. Spatially directed differentiation. (**A**) Choices between SM/MM and HH divisions can be predicted with high accuracy (MCC = 0.9119±0.0699, mean±s.d., n=15 bootstrapped samples) while those between SS and HH or SM/MM have low accuracy (MCC=0.4935±0.0458 and 0.3750±0.1487, respectively, mean±s.d., n=15 bootstrapped samples) (**B**) Features describing the cell's position in relation to the neuromast center and their proximity to other mantle cells have the highest influence on the cell fate choices of a sustentacular cell. (**C**) SM/MM divisions (red) appear predominantly at the periphery of the organ whereas HH divisions (blue) appear proximal to the center. Sustentacular cell self-renewing divisions (SS, green) occur mostly around the neuromast center, generating a ring-like pattern.

The individual estimation of the predictive power of the features revealed that the highest predictive variables were the distance to the neuromast center and the distance to the next mantle cell (**Figure 42**B). For details of the predictive power estimations of all features for the 3 binary predictions, see **Figure 43**. The representation of the Cartesian coordinates of all divisions revealed that transition-associated divisions occur consistently at the outer perimeter of the neuromast, whereas differentiating divisions take place near the center and self-renewing divisions occupy the area between the two differentiated cell types (**Figure 42**C). Importantly, the lack of transition-associated divisions in the anterior-most region, further indicates that neuromasts are able to route sustentacular cells into mantle cell fate specifically in those areas of the organ perimeter that lack other mantle cells.

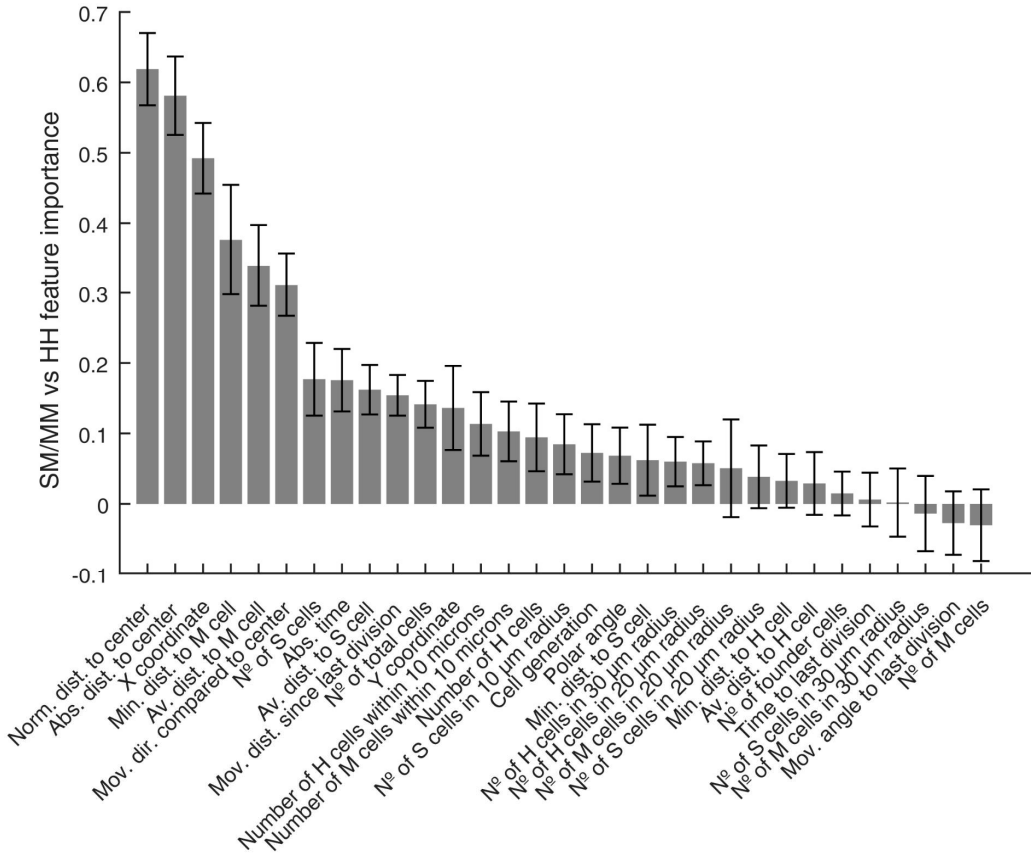

Figure 43. All features used to predict SM/MM vs HH divisions sorted by predictive importance.

Additionally, the temporal profile of differentiating and transition-associated divisions and their prevalence at each cell generation, revealed no bias for either type of division in any generation (**Figure 44**A,B). Also, most transitions to mantle cell occur after the 2nd and 3rd waves of proliferation. Therefore, it appears as if the multicellular cohort senses cell-type composition and re-routes differentiation to achieve normal cell-type proportions. The observation that hair and mantle cells are produced directly by some founder cells further supports the idea that all sustentacular cells are initially equipotent. Together, these results suggest that sustentacular cells self-renew by

default and that different cell-fate choices are driven by the constant evaluation of their local environment.

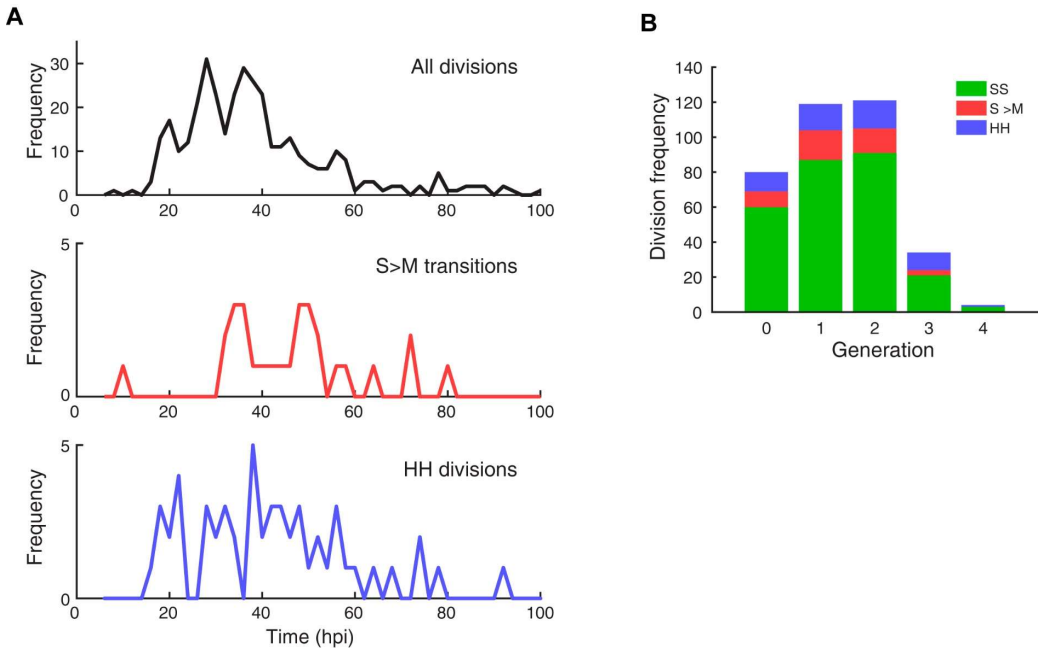

Figure 44. Temporal and generational profile of sustentacular cell differentiation. (**A**) Most transition-associated divisions (SM and MM) take place after the second and third proliferation waves. HH divisions occur steadily until approximately 60hpi. (**B**) Divisions that produce a pair of hair cells (HH) occur in all generations, even in founder cells. Similarly, divisions that produce cells that transit to mantle cell fate within the next generation (SM/MM) occur also at all generations.

2.26. **Founder cells acquire a new spatial identity during regeneration**

Hair-cell regeneration is strongly anisotropic, in that hair-cell progenitors are produced almost exclusively in dorsoventral areas in horizontal neuromasts (Romero-Carvajal *et al.*, 2015; Wibowo *et al.*, 2011). Therefore, I wondered whether whole-organ regeneration also shows directional bias and, if so, whether bias can be predicted from observable cellular behavior. I divided the epithelium in four quarters of equal area so that each territory (dorsal, ventral, anterior and posterior) was fully contained by each quarter. Such divisions also reflect the known territorialization of neuromasts based

on transgene expression and Notch signaling (Ma *et al.*, 2008; Villablanca *et al.*, 2006; Wibowo *et al.*, 2011). First I looked at the localization of cell divisions during the first 60 hours of regeneration and found no consistent spatial pattern (**Figure 45**A). However, after 60 hpi most divisions (74%) took place in the dorsoventral quarters (**Figure 45**B). These data suggest that the tissue is territorialized by around 60 hpi. Importantly, the localization of these territories relative to the main body axes of the fish was identical to that of the neuromast before the ablation. This reveals that horizontal neuromasts faithfully regenerate their global orientation.

Finally, I reasoned that territorialization could occur either by the migration and

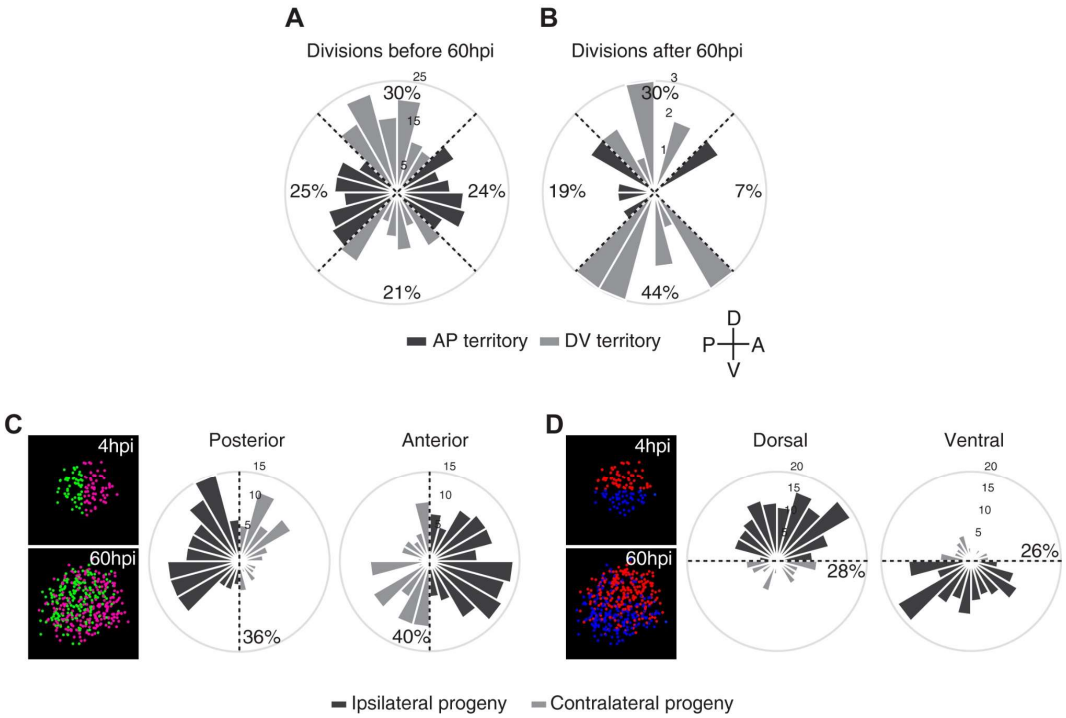

coalescence of equivalent cells that are initially scattered throughout the tissue, or by

Figure 45. Strong maintenance of dorsoventral (DV) identity. (**A**) Proliferation is markedly isotropic during the first 60 hours of neuromast regeneration (n=348). (**B**) Homeostatic, dorsoventral (DV) proliferative territories are restored after 60hpi (n=27). (**C**) 40% and 36% of the progeny from anterior (n=202) and posterior (n=173) founder cells cross to the contralateral side (light grey) after 60 hours of regeneration. (**D**) Only 28% and 26% of the progeny from dorsal (n=199) and ventral (n=176) founder cells cross to the contralateral side (light grey) during the same period of time.

position-adaptive differentiation of an intrinsically homogeneous group of equipotent cells. To disambiguate between these possibilities, I used a virtual Cartesian coordinate system, to fit all founder cells in anterior/posterior and dorsal/ventral halves. Next, I analyzed the localization of the progeny of each founder cell at 60 hpi. I found that 40% of the progeny of anterior-located founders were located in the posterior side of the resulting epithelium, whereas 36% of the progeny of posterior-located founders were found in the anterior side (**Figure 45**C). I also found that only 28% of cells derived from dorsal founders and 26% of cells from ventral founders had crossed the virtual dorsoventral midline (**Figure 45**D). These results suggest that most of the cells in the clone remain ipsilateral to the clone-founder cell, and organ territorialization occurs by location-adaptive cellular differentiation.

3. Discussion

3.1. **Exploring the regenerative limits of the lateral-line epithelium**

The amenability of the zebrafish as a model organism for experimental *in vivo* research, prompted the lateral-line system to the forefront of sensory hair-cell regeneration investigation. Here, I undertook work to address several important long-standing questions by exploring the limits of the regenerative capacity of the system. In doing so, I exposed the potential of neuromasts to contribute to the understanding of cellular mechanisms that govern organ regeneration, thus expanding the applicability of this model beyond the investigation of hair-cell recovery and into the study of organ repair.

The results that I present here provide a singular and original view of how a typical vertebrate sensory organ recapitulates its three-dimensional architecture after severe disruptions of tissue integrity.

3.2. **Stem cell considerations**

Adult stem cells are present in organs and tissues of virtually every multicellular organism. Historically, most histological methods have been unable to unambiguously discriminate these cells from their most immediate differentiated progeny. Thus, understanding the criteria that define adult stem cell identity in tissues and organs has been the focus of extensive research in the recent years (Greco & Guo, 2010; Krieger & Simons, 2015; Simons & Clevers, 2011). Often, stem-cell behaviors have been identified in specific anatomic regions or domains within an organ (Scadden, 2006). The specialized cellular microenvironment of these domains, or niches, is thought to be responsible for the regulation of stem-cell behavior during homeostasis and regeneration (Simons & Clevers, 2011). Stem-cell niches were first conceptualized as

anatomically defined and specialized cellular microenvironments within a tissue that confer self-renewing properties to the cells that reside in them (Schofield, 1978). It follows that stem-cell identity is actively maintained inside the niche by a combinatorial network of paracrine signaling pathways. Cells within the niche have been traditionally assumed to represent a homogenous population characterized by a defined and constant pattern of gene expression. However, studies in some mammalian tissues suggest that stem-cell niches contain cells with heterogeneous transcriptional profiles that are able to function as a single equipotent stem-cell pool with respect to their capacity to differentiate into other cell types (Krieger & Simons, 2015; Simons & Clevers, 2011). As we learn more about organ homeostasis and regeneration, the concept of niche also evolves to encompass a more exhaustive definition of the cell behaviors that characterize stem cell identity. Niches can be differently organized, comprising restricted anatomical regions that facilitate stem cell clustering, or can spread along larger domains, involving the contact of cells with a basement membrane, and thus allowing facultative stem-cell behavior (Simons & Clevers, 2011; Xin *et al.*, 2016). Additionally, recent *in vivo* studies are revealing unexpected plasticity of differentiated cells following tissue injury, allowing tissue regeneration in the absence of a stem cell pool (Krieger & Simons, 2015; Tetteh *et al.*, 2015; Wabik & Jones, 2015). Thus, it is becoming evident that the classic definitions of a stem-cell niche and stem-cell identity struggle to accommodate the broad spectrum of cellular behaviors that underlie organ homeostasis and regeneration *in vivo*.

3.3. **Inexhaustible source of hair-cell progenitors**

I have found that neuromasts of the zebrafish lateral line regenerate mechanosensory hair cells efficiently and inexhaustibly and that this capacity does not diminish with

age. In agreement with a similar recent publication (Cruz *et al.*, 2015), my recurrent ablations of hair cells showed that neuromasts are able to replace approximately 8 hair cells per day without dismantling their epithelial architecture, suggesting that they must persistently produce at least 4 progenitors per day. An outstanding question in the field is how the specification of hair-cell progenitors is achieved, and whether these cells represent a distinguishable identity within the supporting-cell population. Besides, it remains still unclear whether hair-cell progenitors are spatially restricted to defined regions or sparsely located, intermingling with other non-progenitor cells.

It has been proposed that the source of sensory cell progenitors is the Sox2 positive population of supporting cells located beneath the hair cells (Hernandez *et al.*, 2007). Sox2 is a transcription factor that sits at the top of the gene-expression cascade in hair cells. Generally, Sox2 establishes pro-sensory domains in the neuroepithelium of the mammalian and zebrafish inner ears by being expressed in the supporting and hair-cell populations at early stages of development, and down-regulated in mature hair cells (Kiernan *et al.*, 2005; Millimaki *et al.*, 2010; Neves *et al.*, 2013). In particular, during zebrafish otic development, Sox-2 establishes pro-sensory competence in the neuroepithelium for the generation of neurons and hair cells by: 1) the direct activation of Atoh1 expression and, 2) the activation of negative regulators of Atoh1 function (Neves *et al.*, 2013; Sweet *et al.*, 2011). Although Sox2 is known to promote the expression of some components of the Notch signaling pathway in the zebrafish inner ear (Neves et al., 2011), the spatial profile of Sox-2 expression and of Notch activity in neuromasts suggests that they do not directly regulate each other (Wibowo *et al.*, 2011).

In neuromasts, Sox2 is expressed homogeneously in all supporting cells, including sustentacular and mantle cells, but only a few sustentacular cells located basally and

around hair cells show *atoh1a* expression. I observed that the pharmacological inhibition of Notch signaling during hair-cell regeneration increases the domain of *atoh1a*-expressing cells, resulting in the excessive production of hair cells. This occurs because the inhibition of Notch impairs lateral inhibition and allows an excessive number of Sox2-expressing sustentacular cells to stabilize Atoh1a and differentiate into hair cells. Thus, in neuromasts, two parallel inputs appear to control the spatiotemporal profile of Atoh1a expression and, as a consequence, the specification of hair-cell progenitors: a constitutive and un-patterned activation by Sox2, and a patterned inhibition by Notch. In contrast to the ear, the neuromast epithelium does not produce neurons, which may account for the differences between the two organs.

The results shown above suggest that patterned Notch signaling determines the balance of neuromast cell-types without affecting neuromast territorialization or hair-cell polarization. Similar to the Drosophila ovary and the mammalian skin (Blanpain & Fuchs, 2014; Xie & Spradling, 2000), neuromast regions that allow commitment to hair-cell progenitor are spatially fixed, resulting in the preferential production of hair cells in permissive polar areas. This observation provides a mechanistic explanation for the sequence and spatiotemporal pattern of sustentacular-cell conversion into hair-cell progenitor and may explain the inexhaustible production of hair cells upon recurrent hair-cell loss: the mitotic division of sustentacular cells is symmetric with regard to the progenitor potential of the two daughter cells. However, the independent movement of the daughter cells within the epithelium places them in different signaling environments: the cell remaining in an equatorial zone will continue to be exposed to high levels of Notch signaling and maintain a sustentacular-cell character, whereas those entering a polar zone with low Notch activity will stabilize *atoh1a*

expression and become hair-cell progenitors. A default broad expression of *atoh1a* provides a robust mechanism that ensures neuromasts' capacity to rapidly route several sustentacular cells to become sensory progenitors upon acute loss of hair cells.

3.4. **Sustentacular cells**

Up until now, neither a specialized stem-cell population nor a stem-cell niche have yet been identified in lateral-line neuromasts. Previous studies have described three distinct supporting-cell behaviors during hair-cell regeneration that are linked to a specific location within the organ. Specifically, cell-lineage tracing by live imaging and BrdU incorporation assays revealed that supporting-cell divisions at the dorsal and ventral poles of the neuromast are biased towards the production pairs of hair cells, whereas those in the center and anteroposterior areas are biased towards self-renewal (Romero-Carvajal *et al.*, 2015; Wibowo *et al.*, 2011) Additionally, a label-retaining assay demonstrated that supporting cells located in the anterior-most area of the neuromast undergo qualitatively less mitoses during hair-cell regeneration than those in the rest of the organ (Cruz *et al.*, 2015). These studies found an important obstacle in the identification of neuromasts stem cells, in that cellular behaviors were described entirely on the basis of their contribution to hair-cell regeneration, which, inevitably, biases cell production towards the replenishment of this particular cell type. Additionally, to which extent sustentacular and mantle cells constitute discrete cell lineages and contribute differently to regeneration is not understood. The difficulty to unambiguously distinguish between these two types has led to seemingly contradictory results regarding the function of the mantle cells (Dufourcq *et al.*, 2006; Kniss *et al.*, 2016; Romero-Carvajal *et al.*, 2015).

3.4.1. Stem cell competence

Previous observations have led to the current belief that neuromasts contain a dedicated set of cells that predominantly participates in repair. Interestingly, albeit the known functional territorialization of supporting cells during hair-cell replenishment, my injury regimes of different scale and location show that neuromasts regenerate efficiently after injuries that affect disparate organ regions, suggesting that stem-cell behavior is not spatially confined to a particular region. Rather, this behavior indicates that stem-cell competence is broad and symmetric and that neuromasts' regenerative capacity is isotropic (from the Greek *isos* ("equal") and *tropos* ("way"). One explanation for this behavior is that direct cell contact with the basal membrane of the neuromasts confers stem-cell competence. However, I found striking differences in the behavior of mantle and sustentacular cells during neuromast regeneration that suggest that other cell-intrinsic factors regulate stemness of supporting cells. In particular, I found that only sustentacular cells display stemness behavior, whereas mantle cells respond poorly to cell loss. Even following severe injuries that eliminate around 95% of neuromast constituent cells, half of the traced mantle cells remained quiescent, and the other half contributed to regeneration with a unique self-renewing division and did not generate other cell types. These observations support the notion that mantle cells represent a committed population unable to display stem-cell character. Furthermore, their complete elimination demonstrates that these cells do not represent a niche for cell proliferation because sustentacular cells are able to proliferate normally in their absence. On the contrary, sustentacular cells showed remarkable lineage plasticity and self-renewal capacity, which is indicative of stem-cell identity. My data reveal that

sustentacular cells are tripotent progenitors capable of autonomously regenerating entire neuromasts from just a few founder cells.

3.4.2. Equipotency

My clonal analysis reveals different types of sustentacular cell clones based on their cellular composition, which is suggestive of cell heterogeneity. Yet, the predictive algorithms that I have used fail to discriminate between them through the use of more than 30 observable cell features, including time to first division, proliferation rate and frequency or cell movement. Instead, it seems that the type of a given sustentacular-cell clone is a direct consequence of position-dependent cell differentiation events assessed at the single-cell level, that occur later on within its progeny during regenerative process. The non-stereotypic pattern of the overall clone composition of regenerated neuromasts reveals indicates that no hardwired program dictates how cell clones unfold during regeneration, and suggests that sustentacular cells are not lineage-restricted. Nevertheless, although the data cannot unequivocally exclude the possibility that sustentacular cells are transcriptionally heterogeneous, they firmly support the idea that they conform a cell population that is able to function as a single equipotent stem-cell pool. As new stem cell-specific molecular markers are identified, a possible, yet unidentified, heterogeneity among sustentacular cells may be revealed.

3.4.3. Behavioral switch

Organ homeostasis is only achieved if the rate of cell death is paired with the rate of cell proliferation. In organs with low cell turnover, most stem cells are maintained in a

slow-cycling sate. However, to cope with a massive loss of cells during major injury, stem cells must switch to a highly proliferative state (Wabik & Jones, 2015). My time-lapse recordings reveal that all sustentacular cells undergo a dramatic switch from quiescence to a highly proliferative state during neuromast regeneration. Interestingly, the time between injury and the first division of sustentacular cells in a neuromast is remarkably synchronized. This behavior of cell cycle synchrony is specially intriguing because 1) no synchronic cell division has ever been reported during neuromast development and 2) continuous cell turnover during neuromast homeostasis should inevitably break any cell cycle synchrony reminiscent from development. Thus, a reasonable assumption is that the cell cycles in the sustentacular-cell population are presumably not synchronized. However, the synchronization of cell cycles following injury suggests that cells in later stages of their cell cycle are halted, whereas those in early stages are quickly mobilized.

One possible explanation for this behavior is that founder cells need to reassemble intercellular contacts to recreate a three-dimensional scaffold to anchor organ growth. In fact, one constant feature of neuromast regeneration following severe injury is that remaining cells reconstitute a circular structure before the onset of proliferation. Another possible explanation is that cellular proliferation requires important transcriptional changes to reset the spatial rearrangement of key components of intercellular signaling pathways such as Notch or Wnt. Supporting this notion, the pharmacological inhibition of Wnt after severe injury impaired neuromast regeneration by blocking cell proliferation. Rather than being mutually exclusive, both explanations could coexist and even act synergistically. Finally, an additional interesting observation is that, after neomycin treatment, division of hair-cell

progenitors occurs as soon as 8 hours after hair-cell death (Wibowo *et al.*, 2011), almost half the time required for sustentacular cell division after severe injury, but the same time observed between the subsequent divisions. Altogether, these observations indicate that the switch from quiescence to proliferation is an actively regulated cellular behavior, and that the signals that trigger this transition must be accessible to every cell. I propose that proliferative behavior is a facultative state that every sustentacular cell can acquire or abandon upon disruption of organ integrity.

3.4.4. Dedifferentiation

The above observations invite the question of whether sustentacular cells are a differentiated cell population that exhibits transient stemness during regeneration or if, on the contrary, they remain in an undifferentiated state during the entire lifespan. In general, the likelihood of a committed cell lineage to dedifferentiate and acquire stemness is inversely proportional to their progression into a state of maturity (Blanpain & Fuchs, 2014).

In this regard, I noted that the onset of regeneration was invariably characterized by the down-regulation of the supporting cell marker SqGw57A. I do not believe that this is an artifact of laser treatments, microscopy imaging, or a general feature of supporting-cell markers because green fluorescence remained unperturbed in the Sox2:GFP transgenics under the same experimental conditions. Instead, I realized that the expression profile of these markers during neuromast regeneration matches that of embryonic neuromast development. Sox2:GFP labels homogenously immature cells in the moving primordium, whereas SqGw57A is not expressed until neuromasts are deposited and cell-fate determination begins. Thus, the expression of the latest may

function as a *bona fide* readout of supporting cell maturity. The dynamics of transgene expression of these two markers following neuromast injury, suggest that sustentacular cells undergo transcriptional changes during regeneration, which may be indicative of dedifferentiation. I suggest that genome-wide single-cell transcriptomic analyses should be used in the future to reveal the degree of de-differentiation of these cells at the onset of regeneration.

Dedifferentiation of cells has been observed in a wide range of regenerative systems, where cells committed to a differentiated lineage re-acquire hallmark features of adult stem cells, including the capacity of long-term self-renewal, and participate in organ repair (Blanpain & Fuchs, 2014; Krieger & Simons, 2015; Tetteh *et al.*, 2015). Examples of tissue and organ regeneration where dedifferentiation is known to play a key role include the regeneration of germ cells in the *Drosophila* ovaries (Kai & Spradling, 2003, 2004), zebrafish heart (Jopling *et al.*, 2010) and caudal fin (Knopf *et al.*, 2011; Stewart & Stankunas, 2012), mouse brain (Magnusson *et al.*, 2014), and a bewildering number of mammalian epithelial in organs like skin (Rompolas & Greco, 2014; Rompolas *et al.*, 2013), trachea and lung (Tata *et al.*, 2013), stomach (Stange *et al.*, 2013), intestine (Buczacki *et al.*, 2013; Ritsma *et al.*, 2014; Van Es *et al.*, 2012), and liver (Kusaba *et al.*, 2014; Schaub *et al.*, 2014). This modality of regeneration seems to occur after severe injury, and especially when endogenous stem cell populations are lost, to ensure a quick an efficient recovery of organ integrity.

3.4.5. Recapitulation

Altogether, my observations suggest that neuromasts do not contain anatomically restricted regions that confer stem-cell identity to a select group of cells. Instead, they

support the idea that the predominant cell population, the sustentacular cells, is endowed with equipotent stem-cell competence. Thus, I propose that stemness potential is an intrinsic property of sustentacular cells that allows them to reversibly commute between functionally distinct states, in which they become temporally biased for either proliferation or quiescence. My observations suggest that this switch involves transcriptional changes, suggesting that cells are not readily available or primed to perform this behavior.

During neuromast homeostasis, sustentacular cells function in dynamic and noisy transcriptional environments, in which levels of gene expression are spatially restricted by a complex regulatory network of signaling pathways that result in the regionalization of cell behaviors. Severe injuries, however, are likely to dismantle the spatial organization of such network, resulting in the loss of patterning cues and precipitating the synchronization of sustentacular cell states. Through the reversible transfer of cells between transcriptionally distinct states, a population spatially organized in functional territories is able to behave as a single equipotent pool.

In this regard, neuromast stem-cell identity may emerge as a functional state that a large population of cells can acquire according to organ demands. At the molecular level, initiation of identity acquisition may not be an abrupt binary decision, but rather occur progressively as a result of dynamic interactions between cell-intrinsic fluctuations of gene expression levels and extrinsic signals from local environment. By maintaining a large pool of cells ready to be mobilized under the appropriate cues, neuromasts ensure their resilience to injuries and their capacity to comply with the unpredictable extent and location of damage. This regeneration-permissive capacity of epithelial cells is not unique to neuromasts, however, because it resembles

physiological homeostasis or repair of other fast-repairing adult tissues including the gut (Antonello *et al.*, 2015; Gregorieff *et al.*, 2015), the esophagus (Doupé *et al.*, 2012), and the hair follicles of the mammalian skin (Beck & Blanpain, 2012; Blanpain & Fuchs, 2014; Donati & Watt, 2015; Ouspenskaia *et al.*, 2016; Roshan *et al.*, 2016; Tetteh *et al.*, 2015).

3.5. **Mantle cells**

The behavior of mantle cells during neuromast homeostasis and regeneration is especially intriguing. It has been well established that hair-cell progenitors arise from sustentacular cells located at the poles of the dorsoventral axis in horizontal neuromasts. However, it has remained elusive if mantle cells contribute to hair-cell regeneration (Romero-Carvajal *et al.*, 2015; Wibowo *et al.*, 2011). Furthermore, experiments in which large parts of the lateral line were eliminated during tail fin amputation showed that mantle cells are able to proliferate and generate a new primordium that migrates into the regenerated fin and reforms neuromasts (Dufourcq *et al.*, 2006). This observation suggests that mantle cells are capable of producing all cell types that constitute a normal neuromast. Another recent study suggests that mantle cells constitute a quiescent pool that only re-enters cell cycle in response to severe depletion of sustentacular cells. Alternatively, the authors of the study suggest that these cells may conform a stem-cell niche for proliferation of sustentacular cells (Romero-Carvajal *et al.*, 2015). Yet, the contribution of mantle cells to regeneration has remained unclear.

In this regard, my long-term cell lineage tracing assay does not support the previous hypothesis. During regeneration following severe neuromast injury, mantle cells did

not give rise to any lineage other than their own, and their complete elimination did not impair proliferation of sustentacular cells. Yet, neuromasts strive to regenerate them. Is it a mere collateral effect from regeneration or are these cells relevant for the function of the organ? A whole-transcriptome microarray analysis of FACS-sorted mantle cells revealed that following hair-cell elimination, these cells quickly up-regulate expression of membrane-spanning proteins such as transmembrane receptors, cytoskeletal regulators and adhesion molecules (Steiner *et al.*, 2014), providing evidence for an active role during regenerative processes. The nature of these proteins suggests that mantle cells may be involved in structural maintenance of the three dimensional architecture of neuromasts, by virtue of differential intercellular adhesion that confer mechanical anchor for neuromast growth.

3.6. **Interneuromast cells**

Another surprising conclusion that derives from my observations concerns the behavior of interneuromast cells. I have shown that interneuromast cells are unable to produce a new neuromast after its complete elimination. Moreover, the elimination of the interneuromast cells, did not trigger the proliferation or aggregation of adjacent intact interneuromast cells. This suggests that the mere interruption of the continuity of the epithelium is not sufficient to initiate a regenerative response by interneuromast cells. The quiescence of these cells is surprising because they are known to drive neuromast production in several biological contexts (Ghysen & Dambly-Chaudière, 2007; López-Schier & Hudspeth, 2005; Lush & Piotrowski, 2014). However, we systematically observed smaller regenerated organs when interneuromast cells were ablated. These observations suggest that these peripheral cells may yet help

regeneration, either directly by contributing progeny, or by producing mitogenic signals to neuromast-resident cells. Additionally, my results show that quiescent behavior of interneuromast cells cannot be explained by the action of local ErbB-mediated inhibitory signaling emanating from neighboring Schwann cells. Of note, the blockade of ErbB during development or homeostasis had different effects on the behavior of interneuromast cells, suggesting that their stemness behavior may be context-dependent.

A recently published study on neuromast regeneration , concluded that two single interneuromast cells suffice to regenerate an entire new neuromast after its complete elimination, and that Schwann cells act as negative regulators of this process (Sánchez *et al.*, 2016). Intuitively, my results appear to be in disagreement with these statements. First, I have observed that interneuromast cells are not capable of regenerating a new neuromast upon its complete elimination and, second and more importantly, I showed that regeneration by a few remaining neuromast cells, occurs independently of Schwann cells or ErbB signaling. I believe these discrepancies may be the result of different experimental approaches. A possible explanation is the age of the larvae used for the regeneration analysis. While Sánchez et al., used 3dpf larvae, all my ablations were performed at 5 and 6dpf, in order to outrun any bias produced by early developmental processes. Many cellular behaviors, and particularly regeneration, may be heavily influenced by the homeostatic state of the tissue and this may account for differences in the outcome of the two studies. Another possibility is that the method used for cellular ablations results in differential damage to the surrounding tissue. As none of the studies addressed the putative contribution of extracellular matrix and other external environmental cues, this possibility remains to be tested.

3.7. **Regeneration mechanisms**

During organ homeostasis and regeneration, the engagement of stem cells results in restoration of original organ size, cell type proportions and three-dimensional structure. Inherent to this phenomenon is the notion that organs are able to somehow measure each of these attributes (Stanger, 2008). After the sporadic loss of individual cells, characteristic of homeostasis, the physical displacement of neighboring cells could be enough to trigger cell proliferation and compensation without the need for long-range sensing mechanisms. However, severe injuries that eliminate entire organ regions, generally mobilize cells that are not in direct contact with the lost areas, which indicates the existence of long-range mechanisms. In these cases, intercellular communication between stem cells and the rest of the organ is essential to preserve global structure and function.

By systematically measuring the kinetics of cellular behavior, I revealed a consistent hierarchical process that begins immediately after injury. First, surviving cells reassemble contacts to repair the continuity of the epithelium. Second, cells recreate a circular structure that anchors tissue growth and acquire a new positional identity. Third, sustentacular cells switch from quiescence to a progenitor-like state and become highly proliferative. Here, sustentacular cells differentiate into hair-cell progenitor or mantle cell based on the continuous evaluation of their local environment. And finally, once organ size and cell-type proportions are restored, the epithelium returns to a homeostatic state that is characterized by low mitotic rate and rare events of cellular intercalation. Interestingly, I did not observe regenerative overshoot of any cell type or compensatory cell elimination (Agarwala *et al.*, 2015), suggesting the existence of a

mechanism that senses the total number of cells and their fate, and that the balance of cell-type loss biases cell-fate acquisition during repair. These novel findings, which rely on the quantitative spatiotemporal analysis of regeneration data, could not have been predicted from previous studies using static and largely qualitative information (Cruz *et al.*, 2015; Dufourcq *et al.*, 2006; López-Schier & Hudspeth, 2005, 2006; Ma *et al.*, 2008; Romero-Carvajal *et al.*, 2015; Steiner *et al.*, 2014; Wada *et al.*, 2013; Wibowo *et al.*, 2011; Williams & Holder, 2000).

3.7.1. Fate decisions

In order to achieve stereotyped proportions of cell types, organs must keep a strict balance between cell differentiation and self-renewal. The strategies adopted by tissues and organs to maintain this balance are typically classified by two complementary criteria: 1) the level at which asymmetry is achieved (single cell asymmetry *vs*. population asymmetry) and 2) the mechanisms of regulation of such asymmetry (intrinsic *vs*. extrinsic). Single cell asymmetry follows a strict pattern in which every division results invariably in two cells of different type; one commits to a differentiation pathway whereas the other maintains the fate of its progenitor. Contrarily, population asymmetry maintains the balance between differentiation and self-renewal at a global level, where divisions do not follow a strict asymmetric pattern but the average probability of each outcome is balanced (Simons & Clevers, 2011). Interestingly, this strategy leads to a particular pattern of clonal dynamics called "neutral drift", by which, with time, the stochastic loss of stem cells through terminal differentiation and cell death results in the contraction and elimination of specific clones and the compensatory expansion of others. Both modalities may rely on internal

or external regulatory mechanisms. In the former, the asymmetric segregation of polarity proteins and cell fate determinants may result in division asymmetry, whereas, in the latter, cell-adhesion molecules or paracrine signals derived from the local environment may establish and direct fate acquisition (Krieger & Simons, 2015).

In this context, research has focused on the mode of division and on whether the fates of the resulting cells are symmetric or asymmetric. I have shown that sustentacular cells cycle fast and continuously during neuromast regeneration, and that almost 80% of divisions are self-renewing. Only one type of divisions, namely those producing hair cells, seem to be defined shortly prior to or during the division of sustentacular cells. On the other hand, sustentacular cells that commit to mantle cells are not the product of invariable symmetric or asymmetric divisions, suggesting that the decision to differentiate into this lineage is specified after their division. Thus, in our particular context, the classification of symmetric versus asymmetric divisions may, in itself, be a matter of semantics. The algorithms that I have used identified local neighborhood features and position along the radial axis as the predictors with highest confidence value of cellular specification. This finding suggests that commitment to differentiation is not linked to division but may instead emerge in daughter cells from particular combinations of long-range positional cues and short-range signals emanating from the local cellular environment. I propose that all sustentacular cell divisions are equal in terms of potency and that daughter cells do not follow a stereotyped pattern of differentiation. The low degree of cell intercalation and intermingling that I have observed during neuromast regeneration further support the notion that neuromast cells acquire their fate based on their position, but that they do not actively migrate to acquire predefined cell type-specific locations.

Altogether, these observations reveal that neuromasts recover their architecture following a strategy of population asymmetry, regulated, at least in great measure, by external cues. Recent advances in lineage tracing and live imaging in numerous model organisms are revealing a striking preference for population asymmetry mechanisms during homeostasis and regeneration of tissues with high turnover rate (Krieger & Simons, 2015; Wabik & Jones, 2015).

3.7.2. Positional identity

The above results raise the question of how regeneration is controlled spatially. For organs to restore their original architecture, surviving cells must accurately coordinate organ growth with pattern formation. Regeneration from as few as 4-10 cells from the anterior side of a neuromast requires that some surviving cells acquire a new positional identity in the recovered organ. By way of example: a sustentacular cell located initially near the neuromast center ends up at the periphery of the reduced group of cells that survives a severe injury, such that it becomes a "periphery" cell. Because of its condition of sustentacular cell, it engages in proliferation to restore organ size. As the neuromast grows, those cells among its progeny that remain at the periphery of the organ, begin to express mantle-cell markers and acquire their characteristic morphology. On the contrary, other progeny cells located interiorly keep self-renewing and producing new sustentacular cells. Occasionally, a cell taking a more central position will commit to hair-cell progenitor and proceed to a terminal division to gives rise to a pair of hair-cells. This process inevitably involves reprograming of positional information. The low degree of contralateral cell movement and clone intermingling evidences that this information is originally plastic and that cells do no retain memory

of their original position within the organ. The concentric, layered pattern of cell-clone growth suggests that surviving cells organize around a self-generating organ center to quickly reconstitute an iso-symmetric circular structure. New-born cells gradually expand the area of each clone by occupying positions in a perpendicular direction to the center of the organ, supporting the idea that cells recognize their positional identity in relation to the organ radius. These observations resemble distalization processes observed during regeneration of urodele's limb, planarian or hydra, where the distal portion of the lost structure is formed at the cut surface and induces the reorganization of the positional information of the remaining cells (Agata *et al.*, 2007).

3.7.3. Size determination

For any regenerative process to be complete, sensing of cell deficiency is as fundamental as sensing cell recovery, for the restitution of the original size. Is size information contained in the tissue itself? What is the unit of measurement: cell number, cell-type proportions, area/volume occupied? Almost hundred years ago, elegant transplantation experiments during limb development in the salamander revealed that identity of the donor tissue dictated the final size of the limb, suggesting that size information can be contained within the tissue itself (Twitty & Schwind, 1931). Although different experimental models have pointed out different answers, some underlying principles may apply universally. These include that constraints to growth during embryogenesis may operate also in adult tissues, and that size acquired during morphogenesis may serve as a target for future regeneration processes (Stanger, 2008).

Neuromasts proved to be a suitable experimental model to address some of these questions. Remarkably, all the injury regimes that I have used triggered regenerative

responses that resulted in neuromasts with an organization, cell-type proportions and architecture that are undistinguishable from an intact organ. As mentioned before, I did not observe overshoot in the number of any cell type followed by compensatory cell elimination, suggesting the existence of a mechanism that senses cell-type balance during repair. These new findings are important because they demonstrate that resident cells contribute to organ repair by dynamically interpreting the localization and extent of the damage to preferentially replace those structures that have been lost. However, the final number of cells in regenerated neuromasts reached only between 70% and 90% of their original cell count, indicating that other measures may be regulating growth termination. During embryonic development, an organ grows proportionately with its surrounding tissues and the corresponding extracellular matrix, until a final size is reached. Thus, one possibility is that, during regeneration, organ size is controlled by a cross-talk between proliferating cells and remnants of the original physical "scaffold". An illustrative example of this behavior is the regeneration of skeletal muscle fibers, where extracellular matrix remnants from injured fibers guide the migration, division and differentiation of muscle stem cells (Webster *et al.*, 2016). The reorientation of these "ghost" fibers resulted in a disorganized tissue, indicating that they serve as templates for laying down new muscle tissue to match the size and organization of the lost portion (Webster *et al.*, 2016). However, I found that pharmacologically-induced hypertrophic neuromasts regenerate to a normal size following severe injury, indicating that remnants of such scaffold are not a major influence on the final size of the regenerated organ. Thus, neuromast regenerative growth appears to be driven by an autonomous program that is insensitive to prior organ size. In that, size recovery during regeneration may be regulated by the same

mechanism that dictates neuromast size during embryonic development, and homeostasis (discussed below) (Agarwala *et al.*, 2015).

3.7.4. Self-organization

The reduction of neuromasts to around 5% of their original cell number shows that a small group of equipotent cells displaying stemness behavior are able to rebuild a complete neuromast. The recapitulation of organ shape, spatial folding, cell layering and cell polarization is a remarkable process that indicates a certain degree of self-organization. In biological systems, self-organization implies the spontaneous formation of highly ordered structures from a homogenous group of cells without the influence of external morphogenetic landmarks, patterning cues, or pre-existent differential gene-expression profiles (Haken, 1983; Sasai, 2013). By definition, the morphogenetic mechanisms that drive this process must be autonomous and exempt from external instructions such as mechanical forces, spatial constraints or morphogen gradients. Nevertheless, external cues may still contribute to self-organization by providing permissive conditions, such as even tissue growth, as long as they are uniform and non-biased (Sasai, 2013). The concept of multicellular self-organization has been gaining increasing popularity since the recent development of many types of organoids from three-dimensional stem cell cultures (Hariharan, 2016). An interesting example is the recent success in the generation of inner ear organoids from mice embryonic stem-cells or human pluripotent stem-cells (Koehler *et al.*, 2013; Koehler *et al.*, 2017). In these particular cases, stem-cell aggregates self-organize into otic-vesicle-like structures and eventually develop inner ear organoids that display structural and functional characteristics of the membranous labyrinth and vestibular

systems of the inner ear. These organoids give rise to supporting cells and hair cells bearing stereocilia bundles and a kinocilium that form specialized synapses with sensory neurons (Koehler et al., 2013; Koehler et al., 2017). In *in vitro* systems, the contribution of external cues to the recapitulation of organ structure can be easily controlled and monitored. However, assessing the significance of extrinsic control to self-organization *in vivo* is challenging because it is exceedingly difficult to control and measure all possible external influences. Therefore, the collective evidence that I have acquired is suggestive, but not yet confirmatory, of a self-organizing capacity of cells during neuromast regeneration.

3.7.5. Planar polarization

Interestingly, recent studies have identified a transcription factor called Emx2 that regulates the orientation of hair cells in neuromasts of the zebrafish (Jiang *et al.*, 2017). Emx2 is expressed in one half of the hair cells of the neuromast (those oriented towards the tail) and absent in the other half (which are coherently oriented towards the head). Loss- and gain-of-function of Emx2 alter planar cell polarity in a predictable manner: loss of Emx2 leads to neuromasts with every hair cells pointing towards the head of the animal, and Emx2 broad expression orients hair cells towards its tail. Because the coherent local axis of polarity is not affected by these genetic perturbations, Emx2 may act in hair cells as a decoder of global polarity cues. This evidence, together with our results, suggests that during neuromast regeneration founder cells autonomously organize the variegated expression of Emx2 in the re-growing epithelium with consequent recovery of a coherent axis of planar polarity and with one half of the hair cells pointing opposite to the other half. The future development of live markers of

Emx2 expression will be able to test this prediction. I would like to highlight that we do not currently understand the global polarization of the neuromast epithelium relative to the main body axes of the animal. External sources of polarity may impinge in the recovery of these global axes during neuromast regeneration. Previous work has demonstrated that local and global polarization occur independently of innervation (López-Schier & Hudspeth, 2006), but other potential polarizing cues remain untested. Therefore, at present I can only support the notion that local coherent polarity is self-organizing, whereas global orientation may be controlled externally.

3.7.6. Tissue plasticity

During self-organization, the stereotyped distribution of cell-types and the generation of cell diversity from a homogeneous cell population requires local symmetry-breaking events that polarize cell behaviors. In neuromasts, self-organization may function on the basis of self-generated morphogen gradients and auto-regulatory feedback loops that regulate intercellular communication. Such mechanisms ensure permanent sensitivity to disturbances on the signaling network caused by loss of cells or organ regions and sustains a robust and autonomous regenerative response. Supporting this hypothesis, the pharmacological modification of Wnt/β-catenin or Notch activity levels in regenerating neuromasts led to aberrant organs with unbalanced proportions of cell types. The resulting imbalances, however, were reversible, supporting the notion that cellular identities are plastic and that stereotyped proportions of cell types are dynamically maintained by continuous intercellular signaling.

Although we know very little about emergence of symmetry breaking events, it is likely that stochastic variations of expressivity levels initiate the formation of gradients or

self-regulatory loops that are quickly magnified throughout the organ. To reveal novel principles underlying regenerative processes, it will be crucial to complement known molecular mechanisms with aspects relevant to tissue mechanics, like the origin and progression of cell forces and mechanical strains during regeneration *in vivo*.

3.8. **Making sense of signaling networks**

Recent studies are progressively adding new layers of complexity to the crowded network of signaling pathways that regulate cell behaviors in lateral line neuromasts. My results not only confirm the current models, but also contribute to our understanding of how these networks translate into actual cell behaviors by integrating local neighborhood inputs and accurately defining the plasticity of the different cell types.

During neuromast homeostasis, the expression profile of several Wnt components suggests that a negative feedback loop between *dkk2* and *wnt2* regulates the levels of Wnt activity and prevents the superfluous proliferation of supporting cells (Romero-Carvajal *et al.*, 2015; Wada *et al.*, 2013). Under this scenario, it has been proposed that *dkk2* may articulate the interaction between Notch and Wnt/β-catenin signaling. Indeed, neomycin-induced hair-cell ablation leads to Notch downregulation and *atoh1a* activation and, in parallel, promotes downregulation of *dkk2* and the subsequent upregulation of the Wnt ligands *wnt2* and *wnt10a* (Romero-Carvajal *et al.*, 2015). My pharmacological treatments during neuromast regeneration demonstrated that over-activation of Wnt results in exceeding sustentacular cell proliferation but does not affect hair or mantle cell differentiation, suggesting that Notch levels are not directly regulated by Wnt signaling. On the other hand, inhibition of Wnt halts

regeneration completely by, most likely, preventing sustentacular cell proliferation. Thus, a reasonable explanation is that severe neuromast injury triggers the downregulation of *dkk2* to allow a long period of Wnt activation that drives organ growth through sustained sustentacular cell proliferation. As in development, differentiation into hair-cell progenitor during neuromast regeneration may rely on a constitutive activation of *atoh1a* expression by Sox2(+) sustentacular cells and a restricted stabilization via Notch-mediated lateral inhibition mechanisms (discussed below). Supporting this interpretation, pharmacological inhibition of Notch demonstrated that a single change in intercellular signaling can route a large pool of sustentacular cells into acquiring a hair-cell progenitor fate, resulting in the ectopic production of supernumerary hair cells. Commitment to mantle cell fate, however, seems to follow purely from cell location parameters (belonging to the outer cell layer) and neighbor composition (not being encircled by other mantle cells). Approximately two days after neuromast injury, the re-establishment of Notch activity and the return to homeostatic levels of *atoh1a* may lift *dkk2* inhibition and restore the negative feedback that restrains Wnt activity levels. An interesting observation, however, is that in the absence of neuromast injury, the upregulation of Wnt ligands through the pharmacological inhibition of Notch does not suffice to stimulate cell proliferation (Ma *et al.*, 2008; Romero-Carvajal *et al.*, 2015; Wibowo *et al.*, 2011). This suggests that additional intercellular communication signals are necessary for the regulation of cellular proliferation and differentiation during organ homeostasis.

In fact, additional levels of neuromast territorialization complexity have been recently identified. Central sustentacular cells have been found to express the Notch ligand *jagged2* and its downstream target *her4.1*, whose location matches the expression of a

live reporter of Notch activity (Jiang *et al.*, 2014; Romero-Carvajal *et al.*, 2015). Similarly, several components of the FGF signaling pathway such as *fgf3*, *fgf10a* and their downstream target *pea3*, along with the receptors *fgfr1a* and *fgfr2* have been identified, respectively, in central cells and in the polar regions of mature neuromasts (Jiang *et al.*, 2014; Lee *et al.*, 2016; Rubbini *et al.*, 2015; Steiner *et al.*, 2014). I believe that future experimental setups that allow cell type-specific modulation of the expression levels of Wnt, Notch and other candidate signaling pathways such as FGF or Hippo, will undoubtedly shed new light into the mechanisms that regulate proliferation, quiescence, self-renewal and differentiation during neuromast regeneration.

4. Concluding remarks

Understanding the mechanisms that govern the three-dimensional organization and patterning of tissues during morphogenesis and regeneration has far reaching implications in many areas of biology and medicine. As we shed light into such mechanisms, new approaches for treating disease, restoring lost tissue parts or hampering tumor growth will come into focus. Here, I present several novel findings that improve our appreciation of the complex events of whole-organ regeneration. I show that:

- Hair-cell regenerative capacity does not diminish with age.
- Neuromasts' source of hair-cell progenitors is virtually unlimited.
- A spatially-restricted *Atoh1a* domain highlights "primed" hair-cell progenitors.
- Neuromasts' geometric architecture resists disruptions in Notch signaling.
- Imbalances of cell-type proportions are quickly reversed.
- Wnt/β-catenin is essential for the homeostasis of cell-type proportions.
- Neuromasts regenerate after losing 95% of their constituent cells, accurately recovering original cell-type composition, proportions, location and polarity.
- Sustentacular cells are the main drivers of neuromast regeneration. Stem-cell behavior is a facultative status they can transitorily acquire or abandon during regeneration. They are able to differentiate into any neuromast cell type.
- Machine-learning analytical methods identify mediolateral position within the growing epithelium and distance to mantle cells as the best predictors of cell-fate acquisition.
- Wnt/β-catenin is essential for the correct recapitulation of original cell-type proportions.

- An autonomous mechanism of self-organization underlies the collective behavior of individual cells during neuromast regeneration.

I believe that multidisciplinary approaches like that implemented here will be soon imperative to detect individual cellular behaviors within highly packed organs, that were formerly undetectable by traditional single-cell labeling methods. Since this approach is simple and model-independent, it can be easily applicable to other organs or experimental systems to help understand the mechanisms that coordinate cell proliferation, identity acquisition, localization and polarization. This will be instrumental to improve our understanding of the cellular processes that drive the regeneration of complex tissues in the natural context and to elucidate how disease arises from failed repair.

5. Materials and Methods

5.1. **Zebrafish husbandry**

Zebrafish were maintained under standard conditions. Experiments with wild-type, mutant and transgenic embryos were conducted in accordance with institutional guidelines and under a protocol approved by the Ethical Committee of Animal Experimentation of the *Parc de Recerca Biomèdica de Barcelona*, Spain, and the protocol Gz.:55.2-1-54-2532-202-2014 by the *Regierung von Oberbayern*, Germany. Eggs were collected from natural spawning, maintained at 28.5°C in fish medium (Danieau's solution, see below) and kept in Petri dishes at a density of up to 50 per dish and staged according to Kimmel *et al.* (1995).

Fish medium (Danieau's solution):

	Working conc.
NaCl	58 mM
KCl	0,7 mM
$MgSO_4 \cdot 7H_2O$	0,4 mM
$Ca(NO_3)_2$	0,6 mM
HEPES buffer (Sigma)	5 mM
pH of 7.6	

5.2. **Zebrafish lines**

Line	**Origin**
Tg[Cldnb:lynGFP]	Haas and Gilmour (2006). Originally named Tg[-8.0cldnb:Lyn-EGFP]
Tg[SqEt4]	Parinov, S. *et al.* (2004). Originally named Tg[ET(krt4:EGFP)SqET4]
Tg[SqEt20]	Parinov, S. *et al.* (2004). Originally named Tg[ET(krt4:EGFP)sqet20]
Tg[SqGw57A]	Kondrychyn *et al.* (2011). Originally named Tg[ET(krt4:EGFP)SqGw57A]
Tg[Atoh1a:tdTomato]	Wibowo *et al.* (2011)
Tg[Myo6b:actin-GFP]	Kindt *et al.* (2012). Originally named Tg[myo6b:β-actin-GFP]
Tg[Sox2:GFP]	Shin *et al.* (2014). Originally named Tg[Sox2-2a-sfGFPstl84]
Tg[Alpl:mCherry]	Steiner *et al.* (2014). Originally named Tg[−4.7alpl:mCherry]
Tg[Ncad:Ncad-eGFP]	Revenu *et al.* (2014). Originally named Tg[cdh2:Cdh2-GFP]
Tg[Brn3c:mCherry-CAAX]	López-Schier Laboratory, by Laura Pola-Morell
Tg[202A; UAS:EGFP]	López-Schier Laboratory, by Yan Xiao. Xiao *et al.* (2015)
Tg[SILL1:mCherry]	López-Schier Laboratory, by Adèle Faucherre. Faucherre *et al.* (2009)
Tg[CldnB:Ert2-Gal4]	López-Schier Laboratory, by Oriol Viader-Llargués
Tg[UAS:tdTomato-CAAX]	López-Schier Laboratory, by Marta Lozano-Ortega
Tg[UAS:RFP1]	López-Schier Laboratory, stock
Tg[UAS:EGFP]	López-Schier Laboratory, stock
Tg[H2A:H2A-GFP]	López-Schier Laboratory, stock

5.3. **Zebrafish fixation**

Larvae were anesthetized with a 610µM solution of the anesthetic 3-aminobenzoic acid ethyl ester (MS-222, PHARMAQ.Ltd) and transferred into 4% paraformaldehyde (PFA, Sigma). Samples were incubated for 4h at room temperature (RT) or overnight at 4°C.

5.4. **Phalloidin staining**

Samples were fixed, washed several times in PBS buffer with 0.2% of Tween®20 (Sigma) (from now on called 0.2% PBSTw) and incubated in phalloidin-Alexa 568 or Alexa 488 (Invitrogen) diluted 1:20 in 0.2% PBSTw overnight at 4°C. Samples were washed several times in 0.2% PBSTw and mounted in 0.2% PBSTw with Vectashield Mounting Medium (1/100, Vector Laboratories, Burlingame, CA, USA).

5.5. **DAPI staining**

Samples were fixed, washed several times in 0.2% PBSTw and incubated 5 minutes in DAPI (Thermo Fisher) 1/500 in 0.2%PBSTw. Embryos were stored in 0,2% PBSTw with Vectashield at 4°C.

5.6. **Alkaline phosphatase staining**

Samples were fixed for 4 hours at RT, washed 3 times in 0.2% PBSTw and incubated in Alkaline Tris buffer (see below). Reaction time varies according to developmental stage, ranging from 1 minute to 15 minutes. The reaction was stopped by washing 3X for 10 minutes in 0,2% PBST and the larvae stored at 4°C. For imaging, embryos were

mounted in 100% glycerol and photographed on an Olympus BX61 microscope using a 20X dry objective with transmission light.

Alkaline Tris buffer:

	Volume	**Working conc.**
Tris HCl pH 9,5 1M	10 ml	100 mM
$MgCl_2$ 1M	5 ml	50 mM
NaCl 5M	2 ml	100 mM
Tween 20 20%	0,5 ml	0,10%
H_2O	to 50 ml	

5.7. **Immunolabelling**

Larvae were anesthetized, fixed overnight and washed several times in 0.2% PBSTw to remove excess of fixative. For permeabilization, embryos were dehydrated by sequential incubations in 25%, 50%, 75% methanol in 0,2%PBST and finally to 100% methanol. Samples were then stored at -20°C for at least 4 hours. Embryos were rehydrated in the reverse order and washed twice for 5 minutes in 0,2% PBSTw at RT. Blocking was performed using 10% BSA (Sigma) in 0.2% PBSTw. Primary antibody was incubated overnight at 4°C in 0.2% PBSTw and secondary antibody was incubated overnight at 4°C in 0.2% PBSTw. After several washes with 0.2% PBSTw, samples were mounted in Vectashield mounting medium. Antibodies were used at the following dilutions: rabbit anti-Sox2 (AbCam, Cat# ab97959, Cambridge, UK) at 1:200. Texas Red-labeled donkey anti-rabbit immunoglobulin secondary antibody (Molecular

Probes, Life Technologies, Paisley, UK) and Alexa Fluor® 488 goat anti-rabbit immunoglobulin secondary antibodies (A5040, Sigma) at 1:500.

5.8. **Pharmacology**

Neomycin sulfate: To chemically ablate hair cells, zebrafish larvae were incubated in fish medium containing 250µM of neomycin (Sigma) for 45 minutes at RT. Afterwards, larvae were washed with fish medium to wash out residual neomycin. Larvae were allowed to recover from the neomycin treatment for 2 hours before live imaging and/or treatment with other drugs to prevent high mortality. Sibling fish incubated in fish medium for 45min at RT served as controls.

DAPT: Notch signaling was inhibited using the ɣ-secretase inhibitor DAPT (Sigma). DAPT was reconstituted in 10% DMSO to a stock concentration of 150 mM and then diluted to a final concentration of 50µM solution of DAPT in system water with 1% DMSO. Incubation time varied between 24 to 48h according to the experimental setup. Equivalent amounts of DMSO were diluted in fish medium for control larvae.

Tamoxifen: For chemical induction of Gal4, 4-hydroxy-tamoxifen (4-OHT) (H7904, Sigma) was dissolved at 12.5 mg/ml in 100% ethanol and stored at -20°C. Subsequent dilutions in fish medium were made prior to use to a final concentration of 10 µM. Control larvae were incubated with an equivalent amount of ethanol diluted in fish medium.

AG1478: The ErbB inhibitor AG1478 hydrochloride (Cat. No. 1276, Tocris) was reconstituted in 100% DMSO to a stock concentration of 5mM and diluted in fish

medium to a working concentration of 3µM. Equal amounts of DMSO were diluted in fish medium for control larvae.

Azakenpaullone: To constitutively activate Wnt/β-catenin signaling, larvae were incubated in a 3µM solution of glycogen synthase kinase 3b inhibitor 1-azakenpaullone (Tocris) diluted in fish medium. Stock solutions were made by reconstituting 1-Azakenpaullone in 100% DMSO to a concentration of 10mM. Control larvae were incubated in fish medium with equivalent amounts of DMSO.

IWR-1 endo: To inhibit Wnt/β-catenin signaling, 10 mM stock solutions of IWR-1 drugs (Millipore) diluted in DMSO were used. After severe neuromast ablations, fish were allowed to recover in fish medium supplemented with IWR-1-endo at a final concentration of 75-100 µM. Control fish were incubated in IWR-1-exo or in 0.1% DMSO alternatively.

5.9. **Generation of transgenic fish**

To generate the *Tg[CldnB:ERT2-Gal4]* stable transgenic line, 20pg of the ClaudinB::ERT2-GAL4 plasmid and 20pg of synthetic transposase mRNA were simultaneously injected into 1-cell stage wild type eggs. The ClaudinB::ERT2-GAL4 plasmid was kindly donated by D. Wilkinson (NIRM, UK). The plasmid contains a 4.2kb fragment of the proximal region of the zebrafish ClaudinB gene and was cloned into a miniTol2 backbone to ensure transposon-mediated genomic integration (Gerety *et al.*, 2013). The resulting embryos were raised to adulthood and out-crossed for visual screening of germline transmission of the transgene.

5.10. **Bacterial transformation and plasmid purification**

To obtain large amounts of plasmid DNA, 50 μm of chemically competent cells, *E.coli* DH5α™ Competent cells (Invitrogen), were thawed on ice for 20 minutes and mixed with 5 μl of plasmid DNA. After 30 minutes' incubation on ice, cells were heat shocked for 45 seconds at 42°C in a water bath. Cells were then incubated on ice for 2 more minutes, re-suspended in 950 μl of SOC medium (Invitrogen) and incubated for 1 hour at 37°C. Transformed cells were plated on pre-warmed LB agar selective plates with the antibiotic Ampicillin and cultured overnight at 37°C. From the next morning, the plates could be stored at 4°C for a period of approximately 2 weeks. *E. coli* colonies were grown overnight at 37°C in constant shaking in 5ml of LB medium with the antibiotic Ampicillin. After 18 hours of culture, bacterial cells were centrifuged at 4000 rpm for 10 min at 4°C. Purification was done using the QIAprep Spin Miniprep Kit (Qiagen) following manufacturer's instructions.

5.11. **Confocal microscopy**

Larvae were anesthetized, mounted onto a glass-bottom 3-cm Petri dish (MatTek) and covered with 1% low-melting-point agarose (Bio-Rad) with diluted anesthetic. Images were acquired in a Zeiss LSM 510 (Carl Zeiss Inc., Jena, Germany) using 10X air, 40X air and 63X water-immersion objectives.

5.12. **Laser microsurgery**

For *in toto* microsurgery, I used the iLasPulse laser system Roper Scientific SAS) mounted on a Zeiss Axio Observer inverted microscope equipped with a 63X water-

immersion objective (N.A. = 1.2). Zebrafish larvae were anesthetized, mounted on a glass-bottom dish and embedded in 1% low-melting-point agarose. Three laser pulses (355 nm, 400 ps/2.5 μJ per pulse) were applied to each target cell. After ablations, larvae were removed from the agarose and placed in anesthetic-free embryo medium. All ablations were systematically performed on 6dpf larvae, targeting the second or third parallel neuromasts of the posterior lateral line, except for those in **Figure 20**A-E, in which I targeted the second perpendicular neuromast. In **Figure 26**, I used neuromasts from the dorsal lateral line to assess the recovery of apicobasal polarity,

5.13. **Regeneration analysis and quantification**

For quantification of cell numbers during neuromast regeneration, *Tg[Cldnb:lynGFP; SqGw57A; Alpl:mCherry]* zebrafish larvae were anesthetized, mounted on a glass-bottom dish and embedded in 1% low-melting-point agarose. All samples were imaged before, 4 hours after ablation and every 24-48 hour periods up to 7-days- post-injury. After imaging, larvae were quickly transferred to anesthetic-free medium. Cells were counted using confocal stacks acquired with an inverted spinning-disc confocal microscope (Zeiss by Visitron), under a 63X water-immersion objective. Cell types were manually identified using the following criteria. Interneuromast cells: Cldnb:lynGFP(+), SqGw57A(-), Alpl:mCherry(+). Mantle cells: Cldnb:lynGFP(+), SqGw57A(+), Alpl:mCherry(+). Sustentacular cells: Cldnb:lynGFP(+), SqGw57A(+), Alpl:mCherry(-). Hair cells: Cldnb:lynGFP(+), SqGw57A(-), Alpl:mCherry(-). Hair-cell identity was verified by the concomitant observation of the correct transgene expression pattern, central-apical location and the presence of a hair-cell bundle. All

data was processed and analyzed using GraphPad Prism version 6.04 for Windows (GraphPad Software, La Jolla, CA, USA, www.graphpad.com).

5.14. **Live imaging and cell tracking**

Larvae were anesthetized, mounted onto a glass-bottom 3-cm Petri dish (MatTek) and covered with 1% low-melting-point agarose with diluted anesthetic. Petri dish were located on a chambered-stage with a constant temperature of 28.5°C. Z-stack series were acquired every 15 minutes using a 63X water-immersion objective. Cells were tracked overtime using volumetric Z-stack images with FIJI plugin MTrackJ (Meijering *et al.*, 2012). Movies were registered two times for image stabilization and centered upon the centroid of the surviving group of cells and the subsequent regenerating organs. All images were processed with the FIJI software package.

5.15. **Random forest prediction**

Random forest-based algorithms use the majority vote of numerous decision trees based on selected features to predict choices between given outcomes (Murphy, Kevin P. Machine learning: a probabilistic perspective. MIT press, 2012.). We used a list of spatial, movement and neighborhood features (see below) to perform the random forest prediction. We left out one experiment, trained the random forest on the remaining ones and tested our prediction on the left out experiment. We left out every experiment once, leading to 15 test sets overall. To evaluate our prediction, we

calculated the Mathews Correlation Coefficient (MCC) which accounts for imbalance in our data (e.g. 78% of all divisions are SS divisions). The MCC is calculated by

$$\mathrm{MCC} = \frac{TP \times TN - FP \times FN}{\sqrt{(TP + FP)(TP + FN)(TN + FP)(TN + FN)}}$$

where TP are the true positive, TN the true negative, FP the true positive and FN the false negative predictions. MCC can have values between -1 and +1 where -1 is a completely incorrect, 0 a random and +1 a perfect prediction.

To evaluate the MCC on all 15 test sets we used bootstrapping which is a resampling method to determine the variance in sample estimates. For this purpose, we resampled all test sets with replacement 15 times. With this resampled data we were able to calculate the mean MCC as well as the standard deviation of the test sets.

5.16. **List of predictive features**

Feature name	**Feature description**
Number of total cells	Number of overall cells in the neuromast
Number of S cells	Number of sustentacular cells in the neuromast
Number of M cells	Number of mantle cells in the neuromast
Number of H cells	Number of hair cells in the neuromast
Time to last division	Time-point of current division – time-point of mother cell division or start of the movie (in case of founder cell division)
Absolut time	Current time point (hpi)

X coordinate	Current position on the X axis
Y coordinate	Current position on the Y axis
Absolute distance to center	Euclidean distance of division location to the neuromast center (sqrt((x_div-x_center)^2 + (y_div-y_center)^2))
Normalized distance to center	Euclidean distance of division location to the neuromast center divided by the distance of the current furthest cell compared to the center (to approximate the neuromast size)
Cell generation	Number of divisions that the cell undergone so far
Movement distance since last division	Euclidean distance the cell moved compared to location of mother cell division or start of the movie (in case of founder cell division)
Movement angle to last division	Angle measured between current location, neuromast center and location of mother cell division or start of the movie (in case of founder cell division)
Polar angle	Polar angle is the counterclockwise angle between the x-axis, the neuromast center and the current location
Movement direction compared to center	Comparison of the current location to the location of mother cell division or start of the movie (in case of founder cell division) in terms of distance to the neuromast center. If the Current location is nearer to the center the value is positive in case it is further away the value is negative
Number of founder cells	Number of overall cells the regeneration starts with
Founder Cell Type	Cell type of the founder cell the current cell originates from
Minimum distance to S cell	Minimal Euclidean distance to all current sustentacular cells
Minimum distance to M cell	Minimal Euclidean distance to all current mantle cells
Minimum distance to H cell	Minimal Euclidean distance to all current hair cells
Average distance to S cell	Average Euclidean distance to all current sustentacular cells

Average distance to M cell	Average Euclidean distance to all current mantle cells
Average distance to H cell	Average Euclidean distance to all current hair cells
Number of S cells in 10 μm radius	Number of sustentacular cells within a radius of 10 μm
Number of S cells in 20 μm radius	Number of sustentacular cells within a radius of 20 μm
Number of S cells in 30 μm radius	Number of sustentacular cells within a radius of 30 μm
Number of M cells in 10 μm radius	Number of mantle cells within a radius of 10 μm
Number of M cells in 20 μm radius	Number of mantle cells within a radius of 20 μm
Number of M cells in 30 μm radius	Number of mantle cells within a radius of 30 μm
Number of H cells in 10 μm radius	Number of hair cells within a radius of 10 μm
Number of H cells in 20 μm radius	Number of hair cells within a radius of 20 μm
Number of H cells in 30 μm radius	Number of hair cells within a radius of 30 μm

6. References

Adler, H. J., & Raphael, Y. (1996). New hair cells arise from supporting cell conversion in the acoustically damaged chick inner ear. *Neurosci Lett, 205*(1), 17-20.

Agarwala, S., Duquesne, S., Liu, K., Boehm, A., Grimm, L., Link, S., Konig, S., Eimer, S., Ronneberger, O., & Lecaudey, V. (2015). Amotl2a interacts with the Hippo effector Yap1 and the Wnt/beta-catenin effector Lef1 to control tissue size in zebrafish. *Elife, 4*, e08201. doi:10.7554/eLife.08201

Agata, K., Saito, Y., & Nakajima, E. (2007). Unifying principles of regeneration I: Epimorphosis versus morphallaxis. *Dev Growth Differ, 49*(2), 73-78. doi:10.1111/j.1440-169X.2007.00919.x

Aman, A., & Piotrowski, T. (2008). Wnt/beta-catenin and Fgf signaling control collective cell migration by restricting chemokine receptor expression. *Dev Cell, 15*(5), 749-761. doi:10.1016/j.devcel.2008.10.002

Amsterdam, A., Burgess, S., Golling, G., Chen, W., Sun, Z., Townsend, K., Farrington, S., Haldi, M., & Hopkins, N. (1999). A large-scale insertional mutagenesis screen in zebrafish. *Genes Dev, 13*(20), 2713-2724.

Antonello, Z. A., Reiff, T., Ballesta-Illan, E., & Dominguez, M. (2015). Robust intestinal homeostasis relies on cellular plasticity in enteroblasts mediated by miR-8-Escargot switch. *EMBO J, 34*(15), 2025-2041. doi:10.15252/embj.201591517

Baird, R. A., Burton, M. D., Lysakowski, A., Fashena, D. S., & Naeger, R. A. (2000). Hair cell recovery in mitotically blocked cultures of the bullfrog saccule. *Proc Natl Acad Sci U S A, 97*(22), 11722-11729. doi:10.1073/pnas.97.22.11722

Balak, K. J., Corwin, J. T., & Jones, J. E. (1990). Regenerated hair cells can originate from supporting cell progeny: evidence from phototoxicity and laser ablation experiments in the lateral line system. *J Neurosci, 10*(8), 2502-2512.

Beck, B., & Blanpain, C. (2012). Mechanisms regulating epidermal stem cells. *The EMBO journal, 31*(9), 2067-2075.

Becker, T., Wullimann, M. F., Becker, C. G., Bernhardt, R. R., & Schachner, M. (1997). Axonal regrowth after spinal cord transection in adult zebrafish. *Journal of Comparative Neurology, 377*(4), 577-595.

Behra, M., Bradsher, J., Sougrat, R., Gallardo, V., Allende, M. L., & Burgess, S. M. (2009). Phoenix is required for mechanosensory hair cell regeneration in the zebrafish lateral line. *PLoS genet, 5*(4), e1000455. doi:10.1371/journal.pgen.1000455

Blanpain, C., & Fuchs, E. (2014). Stem cell plasticity. Plasticity of epithelial stem cells in tissue regeneration. *Science, 344*(6189), 1242281. doi:10.1126/science.1242281

Blum, N., & Begemann, G. (2012). Retinoic acid signaling controls the formation, proliferation and survival of the blastema during adult zebrafish fin regeneration. *Development, 139*(1), 107-116. doi:10.1242/dev.065391

Bosch, T. C. G. (2007). Why polyps regenerate and we don't: Towards a cellular and molecular framework for Hydra regeneration. *Developmental biology, 303*(2), 421-433.

Broussonet, M. (1786). Observations sur la régénérations de quelques parties du corps des poissons. *Hist. d. I'Acad. Roy. des Sciences*.

Buczacki, S. J., Zecchini, H. I., Nicholson, A. M., Russell, R., Vermeulen, L., Kemp, R., & Winton, D. J. (2013). Intestinal label-retaining cells are secretory precursors expressing Lgr5. *Nature, 495*(7439), 65-69.

Calegari, F., Haubensak, W., Haffner, C., & Huttner, W. B. (2005). Selective lengthening of the cell cycle in the neurogenic subpopulation of neural progenitor cells during mouse brain development. *J Neurosci, 25*(28), 6533-6538. doi:10.1523/jneurosci.0778-05.2005

Carlson, B. M. (2007a). Chapter 1 - An Introduction to Regeneration *Principles of Regenerative Biology* (pp. 1-29). Burlington: Academic Press.

Carlson, B. M. (2007b). Chapter 12 - Stem Cells, Plasticity, and Regeneration *Principles of Regenerative Biology* (pp. 239-258). Burlington: Academic Press.

Coombs, S., & Montgomery, J. C. (1999). The enigmatic lateral line system *Comparative hearing: Fish and amphibians* (pp. 319-362): Springer.

Corwin, J. T. (1981). Postembryonic production and aging in inner ear hair cells in sharks. *J Comp Neurol, 201*(4), 541-553. doi:10.1002/cne.902010406

Corwin, J. T. (1985). Perpetual production of hair cells and maturational changes in hair cell ultrastructure accompany postembryonic growth in an amphibian ear. *Proceedings of the National Academy of Sciences, 82*(11), 3911-3915.

Corwin, J. T., & Cotanche, D. A. (1988). Regeneration of sensory hair cells after acoustic trauma. *Science, 240*(4860), 1772-1774.

Cruz, I. A., Kappedal, R., Mackenzie, S. M., Hailey, D. W., Hoffman, T. L., Schilling, T. F., & Raible, D. W. (2015). Robust regeneration of adult zebrafish lateral line hair cells reflects continued precursor pool maintenance. *Dev Biol, 402*(2), 229-238. doi:10.1016/j.ydbio.2015.03.019

Cruz, R. M., Lambert, P. R., & Rubel, E. W. (1987). Light microscopic evidence of hair cell regeneration after gentamicin toxicity in chick cochlea. *Archives of Otolaryngology–Head & Neck Surgery, 113*(10), 1058-1062.

Cunningham, T. J., & Duester, G. (2015). Mechanisms of retinoic acid signalling and its roles in organ and limb development. *Nat Rev Mol Cell Biol, 16*(2), 110-123. doi:10.1038/nrm3932

Chardin, S., & Romand, R. (1995). Regeneration and mammalian auditory hair cells. *Science, 267*(5198), 707-711.

Chen, G. D., & Fechter, L. D. (2003). The relationship between noise-induced hearing loss and hair cell loss in rats. *Hear Res, 177*(1-2), 81-90.

Chezar, H. H. (1930). Studies on the lateral□line system of amphibia. II. Comparative cytology and innervation of the lateral□line organs in the urodela. *Journal of Comparative Neurology, 50*(1), 159-175.

Chitnis, A. B., Nogare, D. D., & Matsuda, M. (2012). Building the posterior lateral line system in zebrafish. *Dev Neurobiol, 72*(3), 234-255. doi:10.1002/dneu.20962

Chiu, L. L., Cunningham, L. L., Raible, D. W., Rubel, E. W., & Ou, H. C. (2008). Using the Zebrafish Lateral Line to Screen for Ototoxicity. *JARO: Journal of the Association for Research in Otolaryngology, 9*(2), 178-190. doi:10.1007/s10162-008-0118-y

Davis, R. I., Ahroon, W. A., & Hamernik, R. P. (1989). The relation among hearing loss, sensory cell loss and tuning characteristics in the chinchilla. *Hear Res, 41*(1), 1-14.

Diep, C. Q., Ma, D., Deo, R. C., Holm, T. M., Naylor, R. W., Arora, N., Wingert, R. A., Bollig, F., Djordjevic, G., & Lichman, B. (2011). Identification of adult nephron progenitors capable of kidney regeneration in zebrafish. *Nature, 470*(7332), 95-100.

Dijkgraaf, S. (1963). The functioning and significance of the lateral□line organs. *Biological Reviews, 38*(1), 51-105.

Dinsmore, C. E. (1991). *A history of regeneration research: milestones in the evolution of a science*: Cambridge University Press.

Donati, G., & Watt, F. M. (2015). Stem cell heterogeneity and plasticity in epithelia. *Cell Stem Cell, 16*(5), 465-476.

Doupé, D. P., Alcolea, M. P., Roshan, A., Zhang, G., Klein, A. M., Simons, B. D., & Jones, P. H. (2012). A single progenitor population switches behavior to maintain and repair esophageal epithelium. *Science, 337*(6098), 1091-1093.

Doyon, Y., McCammon, J. M., Miller, J. C., Faraji, F., Ngo, C., Katibah, G. E., Amora, R., Hocking, T. D., Zhang, L., & Rebar, E. J. (2008). Heritable targeted gene disruption in zebrafish using designed zinc-finger nucleases. *Nature biotechnology, 26*(6), 702-708.

Driever, W., Solnica-Krezel, L., Schier, A. F., Neuhauss, S. C., Malicki, J., Stemple, D. L., Stainier, D. Y., Zwartkruis, F., Abdelilah, S., Rangini, Z., Belak, J., & Boggs, C. (1996). A genetic screen for mutations affecting embryogenesis in zebrafish. *Development, 123*, 37-46.

Dufourcq, P., Roussigne, M., Blader, P., Rosa, F., Peyrieras, N., & Vriz, S. (2006). Mechano-sensory organ regeneration in adults: the zebrafish lateral line as a model. *Mol Cell Neurosci, 33*(2), 180-187. doi:10.1016/j.mcn.2006.07.005

Durdu, S., Iskar, M., Revenu, C., Schieber, N., Kunze, A., Bork, P., Schwab, Y., & Gilmour, D. (2014). Luminal signalling links cell communication to tissue architecture during organogenesis. *Nature, 515*(7525), 120-124. doi:10.1038/nature13852

Ernst, S., Liu, K., Agarwala, S., Moratscheck, N., Avci, M. E., Dalle Nogare, D., Chitnis, A. B., Ronneberger, O., & Lecaudey, V. (2012). Shroom3 is required downstream of FGF signalling to mediate proneuromast assembly in zebrafish. *Development, 139*(24), 4571-4581. doi:10.1242/dev.083253

Faucherre, A., Pujol-Marti, J., Kawakami, K., & Lopez-Schier, H. (2009). Afferent neurons of the zebrafish lateral line are strict selectors of hair-cell orientation. *PLoS One, 4*(2), e4477. doi:10.1371/journal.pone.0004477

Froehlicher, M., Liedtke, A., Groh, K., López-Schier, H., Neuhauss, S. C., Segner, H., & Eggen, R. I. (2009). Estrogen receptor subtype β2 is involved in neuromast development in zebrafish (Danio rerio) larvae. *Developmental biology, 330*(1), 32-43.

Gerety, S. S., Breau, M. A., Sasai, N., Xu, Q., Briscoe, J., & Wilkinson, D. G. (2013). An inducible transgene expression system for zebrafish and chick. *Development, 140*(10), 2235-2243.

Ghysen, A., & Dambly-Chaudière, C. (2007). The lateral line microcosmos. *Genes Dev, 21*(17), 2118-2130. doi:10.1101/gad.1568407

Golling, G., Amsterdam, A., Sun, Z., Antonelli, M., Maldonado, E., Chen, W., Burgess, S., Haldi, M., Artzt, K., Farrington, S., Lin, S. Y., Nissen, R. M., & Hopkins, N. (2002). Insertional mutagenesis in zebrafish rapidly identifies genes essential for early vertebrate development. *Nat Genet, 31*(2), 135-140. doi:10.1038/ng896

Grant, K. A., Raible, D. W., & Piotrowski, T. (2005). Regulation of latent sensory hair cell precursors by glia in the zebrafish lateral line. *Neuron, 45*(1), 69-80. doi:10.1016/j.neuron.2004.12.020

Greco, V., & Guo, S. (2010). Compartmentalized organization: a common and required feature of stem cell niches? *Development, 137*(10), 1586-1594.

Gregorieff, A., Liu, Y., Inanlou, M. R., Khomchuk, Y., & Wrana, J. L. (2015). Yap-dependent reprogramming of Lgr5(+) stem cells drives intestinal regeneration and cancer. *Nature, 526*(7575), 715-718. doi:10.1038/nature15382

Greulich, P., & Simons, B. D. (2016). Dynamic heterogeneity as a strategy of stem cell self-renewal. *Proc Natl Acad Sci U S A, 113*(27), 7509-7514. doi:10.1073/pnas.1602779113

Haas, P., & Gilmour, D. (2006). Chemokine signaling mediates self-organizing tissue migration in the zebrafish lateral line. *Dev Cell, 10*(5), 673-680. doi:10.1016/j.devcel.2006.02.019

Haffter, P., Granato, M., Brand, M., Mullins, M. C., Hammerschmidt, M., Kane, D. A., Odenthal, J., van Eeden, F. J., Jiang, Y. J., Heisenberg, C. P., Kelsh, R. N., Furutani-Seiki, M., Vogelsang, E., Beuchle, D., Schach, U., Fabian, C., & Nusslein-Volhard, C. (1996). The identification of genes with unique and essential functions in the development of the zebrafish, Danio rerio. *Development, 123*, 1-36.

Haken, H. (1983). *Synergetics: an introduction : nonequilibrium phase transitions and self-organization in physics, chemistry, and biology*: Springer.

Harding, M. J., McGraw, H. F., & Nechiporuk, A. (2014). The roles and regulation of multicellular rosette structures during morphogenesis. *Development, 141*(13), 2549-2558. doi:10.1242/dev.101444

Harding, M. J., & Nechiporuk, A. V. (2012). Fgfr-Ras-MAPK signaling is required for apical constriction via apical positioning of Rho-associated kinase during mechanosensory organ formation. *Development, 139*(17), 3130-3135. doi:10.1242/dev.082271

Hariharan, I. K. (2016). Size regulation blossoms in Kobe. *Development, 143*(15), 2691-2695.

Harris, J. A., Cheng, A. G., Cunningham, L. L., MacDonald, G., Raible, D. W., & Rubel, E. W. (2003). Neomycin-induced hair cell death and rapid regeneration in the lateral line of zebrafish (Danio rerio). *Journal of the Association for Research in Otolaryngology, 4*(2), 219-234.

Hava, D., Forster, U., Matsuda, M., Cui, S., Link, B. A., Eichhorst, J., Wiesner, B., Chitnis, A., & Abdelilah-Seyfried, S. (2009). Apical membrane maturation and cellular rosette formation during morphogenesis of the zebrafish lateral line. *J Cell Sci, 122*(Pt 5), 687-695. doi:10.1242/jcs.032102

Head, J. R., Gacioch, L., Pennisi, M., & Meyers, J. R. (2013). Activation of canonical Wnt/beta-catenin signaling stimulates proliferation in neuromasts in the zebrafish posterior lateral line. *Dev Dyn, 242*(7), 832-846. doi:10.1002/dvdy.23973

Hernández, P. P., Moreno, V., Olivari, F. A., & Allende, M. L. (2006). Sub-lethal concentrations of waterborne copper are toxic to lateral line neuromasts in zebrafish (Danio rerio). *Hearing research, 213*(1), 1-10.

Hernandez, P. P., Olivari, F. A., Sarrazin, A. F., Sandoval, P. C., & Allende, M. L. (2007). Regeneration in zebrafish lateral line neuromasts: expression of the neural progenitor cell marker sox2 and proliferation-dependent and-independent mechanisms of hair cell renewal. *Dev Neurobiol, 67*(5), 637-654. doi:10.1002/dneu.20386

Howe, K., Clark, M. D., Torroja, C. F., Torrance, J., Berthelot, C., Muffato, M., Collins, J. E., Humphray, S., McLaren, K., Matthews, L., McLaren, S., Sealy, I., Caccamo, M., Churcher, C., Scott, C., Barrett, J. C., Koch, R., Rauch, G.-J., White, S., Chow, W., *et al.* (2013). The zebrafish reference genome sequence and its relationship to the human genome. *Nature, 496*(7446), 498-503. doi:10.1038/nature12111

Huang, P., Xiao, A., Zhou, M., Zhu, Z., Lin, S., & Zhang, B. (2011). Heritable gene targeting in zebrafish using customized TALENs. *Nature biotechnology, 29*(8), 699-700.

Hudspeth, A. J. (1989). How the ear's works work. *Nature, 341*(6241), 397-404. doi:10.1038/341397a0

Huth, M. E., Ricci, A. J., & Cheng, A. G. (2011). Mechanisms of aminoglycoside ototoxicity and targets of hair cell protection. *Int J Otolaryngol, 2011*, 937861. doi:10.1155/2011/937861

Jacques, B. E., Montgomery, W. H. t., Uribe, P. M., Yatteau, A., Asuncion, J. D., Resendiz, G., Matsui, J. I., & Dabdoub, A. (2014). The role of Wnt/beta-catenin signaling in proliferation and regeneration of the developing basilar papilla and lateral line. *Dev Neurobiol, 74*(4), 438-456. doi:10.1002/dneu.22134

Jacques, B. E., Puligilla, C., Weichert, R. M., Ferrer-Vaquer, A., Hadjantonakis, A. K., Kelley, M. W., & Dabdoub, A. (2012). A dual function for canonical Wnt/beta-catenin signaling in the developing mammalian cochlea. *Development, 139*(23), 4395-4404. doi:10.1242/dev.080358

Jiang, L., Romero-Carvajal, A., Haug, J. S., Seidel, C. W., & Piotrowski, T. (2014). Gene-expression analysis of hair cell regeneration in the zebrafish lateral line. *Proc Natl Acad Sci U S A, 111*(14), E1383-1392. doi:10.1073/pnas.1402898111

Jiang, T., Kindt, K., & Wu, D. K. (2017). Transcription factor Emx2 controls stereociliary bundle orientation of sensory hair cells. *Elife, 6*. doi:10.7554/eLife.23661

Jopling, C., Sleep, E., Raya, M., Marti, M., Raya, A., & Izpisua Belmonte, J. C. (2010). Zebrafish heart regeneration occurs by cardiomyocyte dedifferentiation and proliferation. *Nature, 464*(7288), 606-609. doi:10.1038/nature08899

Kai, T., & Spradling, A. (2003). An empty Drosophila stem cell niche reactivates the proliferation of ectopic cells. *Proceedings of the National Academy of Sciences, 100*(8), 4633-4638.

Kai, T., & Spradling, A. (2004). Differentiating germ cells can revert into functional stem cells in Drosophila melanogaster ovaries. *Nature, 428*(6982), 564-569.

Kiernan, A. E., Pelling, A. L., Leung, K. K., Tang, A. S., Bell, D. M., Tease, C., Lovell-Badge, R., Steel, K. P., & Cheah, K. S. (2005). Sox2 is required for sensory organ development in the mammalian inner ear. *Nature, 434*(7036), 1031-1035. doi:10.1038/nature03487

Kikuchi, K., Holdway, J. E., Major, R. J., Blum, N., Dahn, R. D., Begemann, G., & Poss, K. D. (2011). Retinoic acid production by endocardium and epicardium is an injury response essential for zebrafish heart regeneration. *Dev Cell, 20*(3), 397-404. doi:10.1016/j.devcel.2011.01.010

Kimmel, C. B. (1972). Mauthner axons in living fish larvae. *Developmental biology, 27*(2), 272-275.

Kimmel, C. B., Ballard, W. W., Kimmel, S. R., Ullmann, B., & Schilling, T. F. (1995). Stages of embryonic development of the zebrafish. *Dev Dyn, 203*. doi:10.1002/aja.1002030302

Kindt, K. S., Finch, G., & Nicolson, T. (2012). Kinocilia mediate mechanosensitivity in developing zebrafish hair cells. *Developmental Cell, 23*(2), 329-341.

Kniss, J. S., Jiang, L., & Piotrowski, T. (2016). Insights into sensory hair cell regeneration from the zebrafish lateral line. *Curr Opin Genet Dev, 40*, 32-40. doi:10.1016/j.gde.2016.05.012

Knopf, F., Hammond, C., Chekuru, A., Kurth, T., Hans, S., Weber, C. W., Mahatma, G., Fisher, S., Brand, M., Schulte-Merker, S., & Weidinger, G. (2011). Bone regenerates via dedifferentiation of osteoblasts in the zebrafish fin. *Dev Cell, 20*(5), 713-724. doi:10.1016/j.devcel.2011.04.014

Koehler, K. R., Mikosz, A. M., Molosh, A. I., Patel, D., & Hashino, E. (2013). Generation of inner ear sensory epithelia from pluripotent stem cells in 3D culture. *Nature, 500*(7461), 217-221.

Koehler, K. R., Nie, J., Longworth-Mills, E., Liu, X. P., Lee, J., Holt, J. R., & Hashino, E. (2017). Generation of inner ear organoids containing functional

hair cells from human pluripotent stem cells. *Nat Biotechnol, 35*(6), 583-589. doi:10.1038/nbt.3840

Kondrychyn, I., Teh, C., Garcia-Lecea, M., Guan, Y., Kang, A., & Korzh, V. (2011). Zebrafish Enhancer TRAP transgenic line database ZETRAP 2.0. *Zebrafish, 8*(4), 181-182.

Krieger, T., & Simons, B. D. (2015). Dynamic stem cell heterogeneity. *Development, 142*(8), 1396-1406. doi:10.1242/dev.101063

Kroehne, V., Freudenreich, D., Hans, S., Kaslin, J., & Brand, M. (2011). Regeneration of the adult zebrafish brain from neurogenic radial glia-type progenitors. *Development, 138*(22), 4831-4841.

Kusaba, T., Lalli, M., Kramann, R., Kobayashi, A., & Humphreys, B. D. (2014). Differentiated kidney epithelial cells repair injured proximal tubule. *Proceedings of the National Academy of Sciences, 111*(4), 1527-1532.

Langer, T., am Zehnhoff-Dinnesen, A., Radtke, S., Meitert, J., & Zolk, O. (2013). Understanding platinum-induced ototoxicity. *Trends Pharmacol Sci, 34*(8), 458-469. doi:10.1016/j.tips.2013.05.006

Lecaudey, V., Cakan-Akdogan, G., Norton, W. H., & Gilmour, D. (2008). Dynamic Fgf signaling couples morphogenesis and migration in the zebrafish lateral line primordium. *Development, 135*(16), 2695-2705. doi:10.1242/dev.025981

Ledent, V. (2002). Postembryonic development of the posterior lateral line in zebrafish. *Development, 129*(3), 597-604.

Lee, S. G., Huang, M., Obholzer, N. D., Sun, S., Li, W., Petrillo, M., Dai, P., Zhou, Y., Cotanche, D. A., Megason, S. G., Li, H., & Chen, Z. Y. (2016). Myc and Fgf Are Required for Zebrafish Neuromast Hair Cell Regeneration. *PLoS One, 11*(6), e0157768. doi:10.1371/journal.pone.0157768

López-Schier, H., & Hudspeth, A. J. (2005). Supernumerary neuromasts in the posterior lateral line of zebrafish lacking peripheral glia. *Proc Natl Acad Sci U S A, 102*(5), 1496-1501. doi:10.1073/pnas.0409361102

López-Schier, H., & Hudspeth, A. J. (2006). A two-step mechanism underlies the planar polarization of regenerating sensory hair cells. *Proc Natl Acad Sci U S A, 103*(49), 18615-18620. doi:10.1073/pnas.0608536103

López-Schier, H., Starr, C. J., Kappler, J. A., Kollmar, R., & Hudspeth, A. J. (2004). Directional cell migration establishes the axes of planar polarity in the posterior lateral-line organ of the zebrafish. *Dev Cell, 7*(3), 401-412. doi:10.1016/j.devcel.2004.07.018

Lush, M. E., & Piotrowski, T. (2014). ErbB expressing Schwann cells control lateral line progenitor cells via non-cell-autonomous regulation of Wnt/β-catenin. *Elife, 3*. doi:10.7554/eLife.01832

Ma, E. Y., & Raible, D. W. (2009). Signaling pathways regulating zebrafish lateral line development. *Curr Biol, 19*(9), R381-386. doi:10.1016/j.cub.2009.03.057

Ma, E. Y., Rubel, E. W., & Raible, D. W. (2008). Notch signaling regulates the extent of hair cell regeneration in the zebrafish lateral line. *J Neurosci, 28*(9), 2261-2273. doi:10.1523/jneurosci.4372-07.2008

Mackenzie, S. M., & Raible, D. W. (2012). Proliferative regeneration of zebrafish lateral line hair cells after different ototoxic insults. *PLoS One, 7*(10), e47257. doi:10.1371/journal.pone.0047257

Magnusson, J. P., Göritz, C., Tatarishvili, J., Dias, D. O., Smith, E. M., Lindvall, O., Kokaia, Z., & Frisén, J. (2014). A latent neurogenic program in astrocytes regulated by Notch signaling in the mouse. *Science, 346*(6206), 237-241.

Matsuda, M., & Chitnis, A. B. (2010). Atoh1a expression must be restricted by Notch signaling for effective morphogenesis of the posterior lateral line primordium in zebrafish. *Development, 137*(20), 3477-3487. doi:10.1242/dev.052761

Meijering, E., Dzyubachyk, O., & Smal, I. (2012). Methods for cell and particle tracking. *Methods Enzymol, 504*, 183-200. doi:10.1016/b978-0-12-391857-4.00009-4

Meng, X., Noyes, M. B., Zhu, L. J., Lawson, N. D., & Wolfe, S. A. (2008). Targeted gene inactivation in zebrafish using engineered zinc-finger nucleases. *Nat Biotechnol, 26*(6), 695-701. doi:10.1038/nbt1398

Metcalfe, W. K., Kimmel, C. B., & Schabtach, E. (1985). Anatomy of the posterior lateral line system in young larvae of the zebrafish. *J Comp Neurol, 233*(3), 377-389. doi:10.1002/cne.902330307

Millimaki, B. B., Sweet, E. M., & Riley, B. B. (2010). Sox2 is required for maintenance and regeneration, but not initial development, of hair cells in the zebrafish inner ear. *Dev Biol, 338*(2), 262-269. doi:10.1016/j.ydbio.2009.12.011

Montgomery, J., Carton, G., Voigt, R., Baker, C., & Diebel, C. (2000). Sensory processing of water currents by fishes. *Philos Trans R Soc Lond B Biol Sci, 355*(1401), 1325-1327. doi:10.1098/rstb.2000.0693

Montgomery, J. C., Baker, C. F., & Carton, A. G. (1997). The lateral line can mediate rheotaxis in fish. *Nature, 389*(6654), 960-963.

Morgan, T. H. (1898). Experimental studies of the regeneration of Planaria maculata. *Development genes and evolution, 7*(2), 364-397.

Moss, J. B., Koustubhan, P., Greenman, M., Parsons, M. J., Walter, I., & Moss, L. G. (2009). Regeneration of the pancreas in adult zebrafish. *Diabetes, 58*(8), 1844-1851. doi:10.2337/db08-0628

Mullins, M. C., Hammerschmidt, M., Haffter, P., & Nusslein-Volhard, C. (1994). Large-scale mutagenesis in the zebrafish: in search of genes controlling development in a vertebrate. *Curr Biol, 4*(3), 189-202.

Nechiporuk, A., & Keating, M. T. (2002). A proliferation gradient between proximal and msxb-expressing distal blastema directs zebrafish fin regeneration. *Development, 129*(11), 2607-2617.

Nechiporuk, A., & Raible, D. W. (2008). FGF-dependent mechanosensory organ patterning in zebrafish. *Science, 320*(5884), 1774-1777. doi:10.1126/science.1156547

Neves, J., Vachkov, I., & Giraldez, F. (2013). Sox2 regulation of hair cell development: incoherence makes sense. *Hear Res, 297*, 20-29. doi:10.1016/j.heares.2012.11.003

Nicolson, T. (2005). The genetics of hearing and balance in zebrafish. *Annu Rev Genet, 39*, 9-22. doi:10.1146/annurev.genet.39.073003.105049

Nuñez, V. A., Sarrazin, A. F., Cubedo, N., Allende, M. L., Dambly-Chaudière, C., & Ghysen, A. (2009). Postembryonic development of the posterior lateral line in the zebrafish. *Evol Dev, 11*. doi:10.1111/j.1525-142X.2009.00346.x

Ouspenskaia, T., Matos, I., Mertz, A. F., Fiore, V. F., & Fuchs, E. (2016). WNT-SHH antagonism specifies and expands stem cells prior to niche formation. *Cell, 164*(1), 156-169.

Owens, K. N., Cunningham, D. E., Macdonald, G., Rubel, E. W., Raible, D. W., & Pujol, R. (2007). Ultrastructural analysis of aminoglycoside□induced hair cell death in the zebrafish lateral line reveals an early mitochondrial response. *Journal of Comparative Neurology, 502*(4), 522-543.

Parinov, S., Kondrichin, I., Korzh, V., & Emelyanov, A. (2004). Tol2 transposon-mediated enhancer trap to identify developmentally regulated zebrafish genes in vivo. *Dev Dyn, 231*. doi:10.1002/dvdy.20157

Parinov, S., Kondrichin, I., Korzh, V., & Emelyanov, A. (2004). Tol2 transposon□mediated enhancer trap to identify developmentally regulated zebrafish genes in vivo. *Developmental dynamics, 231*(2), 449-459.

Pfefferli, C., & Jazwinska, A. (2015). The art of fin regeneration in zebrafish. *Regeneration (Oxf), 2*(2), 72-83. doi:10.1002/reg2.33

Pinto-Teixeira, F., Muzzopappa, M., Swoger, J., Mineo, A., Sharpe, J., & López-Schier, H. (2013). Intravital imaging of hair-cell development and

regeneration in the zebrafish. *Front Neuroanat, 7*, 33. doi:10.3389/fnana.2013.00033

Pittlik, S., & Begemann, G. (2012). New sources of retinoic acid synthesis revealed by live imaging of an Aldh1a2-GFP reporter fusion protein throughout zebrafish development. *Dev Dyn, 241*(7), 1205-1216. doi:10.1002/dvdy.23805

Poss, K. D., Wilson, L. G., & Keating, M. T. (2002). Heart regeneration in zebrafish. *Science, 298*(5601), 2188-2190. doi:10.1126/science.1077857

Pujol-Marti, J., & López-Schier, H. (2013). Developmental and architectural principles of the lateral-line neural map. *Front Neural Circuits, 7*, 47. doi:10.3389/fncir.2013.00047

Revenu, C., Streichan, S., Dona, E., Lecaudey, V., Hufnagel, L., & Gilmour, D. (2014). Quantitative cell polarity imaging defines leader-to-follower transitions during collective migration and the key role of microtubule-dependent adherens junction formation. *Development, 141*(6), 1282-1291. doi:10.1242/dev.101675

Richardson, R., Slanchev, K., Kraus, C., Knyphausen, P., Eming, S., & Hammerschmidt, M. (2013). Adult zebrafish as a model system for cutaneous wound-healing research. *Journal of Investigative Dermatology, 133*(6), 1655-1665.

Ritsma, L., Ellenbroek, S. I., Zomer, A., Snippert, H. J., de Sauvage, F. J., Simons, B. D., Clevers, H., & van Rheenen, J. (2014). Intestinal crypt homeostasis revealed at single-stem-cell level by in vivo live imaging. *Nature, 507*(7492), 362-365.

Roberson, D., Kreig, C., & Rubel, E. (1996). Light microscopic evidence that direct transdifferentiation gives rise to new hair cells in regenerating avian auditory epithelium. *Auditory Neuroscience, 2*(3), 195-205.

Roberson, D. W., Alosi, J. A., & Cotanche, D. A. (2004). Direct transdifferentiation gives rise to the earliest new hair cells in regenerating avian auditory epithelium. *J Neurosci Res, 78*(4), 461-471. doi:10.1002/jnr.20271

Rojas-Muñoz, A., Rajadhyksha, S., Gilmour, D., Bebber, F., Antos, C., Rodríguez Esteban, C., Nüsslein-Volhard, C., & Izpisúa Belmonte, J. C. (2009). ErbB2 and ErbB3 regulate amputation-induced proliferation and migration during vertebrate regeneration. *Dev Biol, 327*. doi:10.1016/j.ydbio.2008.12.012

Romero-Carvajal, A., Navajas Acedo, J., Jiang, L., Kozlovskaja-Gumbriene, A., Alexander, R., Li, H., & Piotrowski, T. (2015). Regeneration of Sensory Hair Cells Requires Localized Interactions between the Notch and Wnt Pathways. *Dev Cell, 34*(3), 267-282. doi:10.1016/j.devcel.2015.05.025

Rompolas, P., & Greco, V. (2014). *Stem cell dynamics in the hair follicle niche.* Paper presented at the Semin Cell Dev Biol.

Rompolas, P., Mesa, K. R., & Greco, V. (2013). Spatial organization within a niche as a determinant of stem-cell fate. *Nature, 502*(7472), 513-518.

Roshan, A., Murai, K., Fowler, J., Simons, B. D., Nikolaidou-Neokosmidou, V., & Jones, P. H. (2016). Human keratinocytes have two interconvertible modes of proliferation. *Nat Cell Biol, 18*(2), 145-156.

Rossi, A. M., Fernandes, V. M., & Desplan, C. (2017). Timing temporal transitions during brain development. *Curr Opin Neurobiol, 42*, 84-92. doi:10.1016/j.conb.2016.11.010

Rubbini, D., Robert-Moreno, A., Hoijman, E., & Alsina, B. (2015). Retinoic Acid Signaling Mediates Hair Cell Regeneration by Repressing p27kip and sox2 in Supporting Cells. *J Neurosci, 35*(47), 15752-15766. doi:10.1523/JNEUROSCI.1099-15.2015

Rubel, E. W., Furrer, S. A., & Stone, J. S. (2013). A brief history of hair cell regeneration research and speculations on the future. *Hear Res, 297*, 42-51. doi:10.1016/j.heares.2012.12.014

Ryals, B. M., & Rubel, E. W. (1988). Hair cell regeneration after acoustic trauma in adult Coturnix quail. *Science, 240*(4860), 1774-1776.

Sadler, K. C., Krahn, K. N., Gaur, N. A., & Ukomadu, C. (2007). Liver growth in the embryo and during liver regeneration in zebrafish requires the cell cycle regulator, uhrf1. *Proc Natl Acad Sci U S A, 104*(5), 1570-1575. doi:10.1073/pnas.0610774104

Sánchez, M., Ceci, M. L., Gutiérrez, D., Anguita-Salinas, C., & Allende, M. L. (2016). Mechanosensory organ regeneration in zebrafish depends on a population of multipotent progenitor cells kept latent by Schwann cells. *BMC biology, 14*(1), 27. doi:10.1186/s12915-016-0249-2

Sapède, D., Gompel, N., Dambly-Chaudière, C., & Ghysen, A. (2002). Cell migration in the postembryonic development of the fish lateral line. *Development, 129*.

Sasai, Y. (2013). Cytosystems dynamics in self-organization of tissue architecture. *Nature, 493*(7432), 318-326.

Scadden, D. T. (2006). The stem-cell niche as an entity of action. *Nature, 441*(7097), 1075-1079. doi:10.1038/nature04957

Schaub, J. R., Malato, Y., Gormond, C., & Willenbring, H. (2014). Evidence against a stem cell origin of new hepatocytes in a common mouse model of chronic liver injury. *Cell reports, 8*(4), 933-939.

Schofield, R. (1978). The relationship between the spleen colony-forming cell and the haemopoietic stem cell. *Blood cells, 4*(1-2), 7-25.

Shi, F., Hu, L., Jacques, B. E., Mulvaney, J. F., Dabdoub, A., & Edge, A. S. (2014). beta-Catenin is required for hair-cell differentiation in the cochlea. *J Neurosci, 34*(19), 6470-6479. doi:10.1523/jneurosci.4305-13.2014

Shi, F., Kempfle, J. S., & Edge, A. S. (2012). Wnt-responsive Lgr5-expressing stem cells are hair cell progenitors in the cochlea. *J Neurosci, 32*(28), 9639-9648. doi:10.1523/jneurosci.1064-12.2012

Shin, J., Chen, J., & Solnica-Krezel, L. (2014). Efficient homologous recombination-mediated genome engineering in zebrafish using TALE nucleases. *Development, 141*(19), 3807-3818. doi:10.1242/dev.108019

Simons, B. D., & Clevers, H. (2011). Strategies for homeostatic stem cell self-renewal in adult tissues. *Cell, 145*(6), 851-862. doi:10.1016/j.cell.2011.05.033

Song, J., Yan, H. Y., & Popper, A. N. (1995). Damage and recovery of hair cells in fish canal (but not superficial) neuromasts after gentamicin exposure. *Hearing research, 91*(1), 63-71.

Stange, D. E., Koo, B.-K., Huch, M., Sibbel, G., Basak, O., Lyubimova, A., Kujala, P., Bartfeld, S., Koster, J., & Geahlen, J. H. (2013). Differentiated Troy+ chief cells act as reserve stem cells to generate all lineages of the stomach epithelium. *Cell, 155*(2), 357-368.

Stanger, B. (2008). The biology of organ size determination. *Diabetes, Obesity and Metabolism, 10*(s4), 16-22.

Steiner, A. B., Kim, T., Cabot, V., & Hudspeth, A. J. (2014). Dynamic gene expression by putative hair-cell progenitors during regeneration in the zebrafish lateral line. *Proc Natl Acad Sci U S A, 111*(14), E1393-1401. doi:10.1073/pnas.1318692111

Stewart, S., & Stankunas, K. (2012). Limited Dedifferentiation Provides Replacement Tissue during Zebrafish Fin Regeneration. *Dev Biol, 365*(2), 339-349. doi:10.1016/j.ydbio.2012.02.031

Streisinger, G., Walker, C., Dower, N., Knauber, D., & Singer, F. (1981). Production of clones of homozygous diploid zebra fish (Brachydanio rerio). *Nature, 291*(5813), 293-296.

Sweet, E. M., Vemaraju, S., & Riley, B. B. (2011). Sox2 and Fgf interact with Atoh1 to promote sensory competence throughout the zebrafish inner ear. *Dev Biol, 358*(1), 113-121. doi:10.1016/j.ydbio.2011.07.019

Tata, P. R., Mou, H., Pardo-Saganta, A., Zhao, R., Prabhu, M., Law, B. M., Vinarsky, V., Cho, J. L., Breton, S., & Sahay, A. (2013). Dedifferentiation of committed epithelial cells into stem cells in vivo. *Nature, 503*(7475), 218-223.

Tetteh, P. W., Farin, H. F., & Clevers, H. (2015). Plasticity within stem cell hierarchies in mammalian epithelia. *Trends Cell Biol, 25*(2), 100-108. doi:10.1016/j.tcb.2014.09.003

Twitty, V. C., & Schwind, J. L. (1931). The growth of eyes and limbs transplanted heteroplastically between two species of Amblystoma. *Journal of Experimental Zoology Part A: Ecological Genetics and Physiology, 59*(1), 61-86.

Van Es, J. H., Sato, T., Van De Wetering, M., Lyubimova, A., Nee, A., Gregorieff, A., Sasaki, N., Zeinstra, L., Van Den Born, M., & Korving, J. (2012). Dll1+ secretory progenitor cells revert to stem cells upon crypt damage. *Nat Cell Biol, 14*(10), 1099-1104.

Varga, M. (2018). The Doctor of Delayed Publications: The Remarkable Life of George Streisinger (1927-1984). *Zebrafish*. doi:10.1089/zeb.2017.1531

Varshney, G. K., Sood, R., & Burgess, S. M. (2015). Understanding and Editing the Zebrafish Genome. *Adv Genet, 92*, 1-52. doi:10.1016/bs.adgen.2015.09.002

Vihtelic, T. S., & Hyde, D. R. (2000). Light-induced rod and cone cell death and regeneration in the adult albino zebrafish (Danio rerio) retina. *Journal of neurobiology, 44*(3), 289-307.

Villablanca, E. J., Renucci, A., Sapède, D., Lec, V., Soubiran, F., Sandoval, P. C., Dambly□Chaudière, C., Ghysen, A., & Allende, M. L. (2006). Control of cell migration in the zebrafish lateral line: Implication of the gene "Tumour□Associated Calcium Signal Transducer," tacstd. *Developmental dynamics, 235*(6), 1578-1588.

Wabik, A., & Jones, P. H. (2015). Switching roles: the functional plasticity of adult tissue stem cells. *EMBO J, 34*(9), 1164-1179. doi:10.15252/embj.201490386

Wada, H., Ghysen, A., Asakawa, K., Abe, G., Ishitani, T., & Kawakami, K. (2013). Wnt/Dkk negative feedback regulates sensory organ size in zebrafish. *Curr Biol, 23*(16), 1559-1565. doi:10.1016/j.cub.2013.06.035

Wada, H., Ghysen, A., Satou, C., Higashijima, S.-I., Kawakami, K., Hamaguchi, S., & Sakaizumi, M. (2010). Dermal morphogenesis controls lateral line patterning during postembryonic development of teleost fish. *Dev Biol, 340*. doi:10.1016/j.ydbio.2010.02.017

Wada, H., & Kawakami, K. (2015). Size control during organogenesis: Development of the lateral line organs in zebrafish. *Dev Growth Differ, 57*(2), 169-178. doi:10.1111/dgd.12196

Webster, M. T., Manor, U., Lippincott-Schwartz, J., & Fan, C. M. (2016). Intravital Imaging Reveals Ghost Fibers as Architectural Units Guiding Myogenic Progenitors during Regeneration. *Cell Stem Cell, 18*(2), 243-252. doi:10.1016/j.stem.2015.11.005

Wibowo, I., Pinto-Teixeira, F., Satou, C., Higashijima, S., & López-Schier, H. (2011). Compartmentalized Notch signaling sustains epithelial mirror symmetry. *Development, 138*(6), 1143-1152. doi:10.1242/dev.060566

Williams, J. A., & Holder, N. (2000). Cell turnover in neuromasts of zebrafish larvae. *Hear Res, 143*(1-2), 171-181.

Xiao, Y., Faucherre, A., Pola-Morell, L., Heddleston, J. M., Liu, T.-L., Chew, T.-L., Sato, F., Sehara-Fujisawa, A., Kawakami, K., & López-Schier, H. (2015). High-resolution live imaging reveals axon-glia interactions during peripheral nerve injury and repair in zebrafish. *Disease Models & Mechanisms, 8*(6), 553-564. doi:10.1242/dmm.018184

Xie, T., & Spradling, A. C. (2000). A niche maintaining germ line stem cells in the Drosophila ovary. *Science, 290*(5490), 328-330.

Xin, T., Greco, V., & Myung, P. (2016). Hardwiring Stem Cell Communication through Tissue Structure. *Cell, 164*(6), 1212-1225. doi:10.1016/j.cell.2016.02.041

Yang, C.-T., Sengelmann, R. D., & Johnson, S. L. (2004). Larval melanocyte regeneration following laser ablation in zebrafish. *Journal of Investigative Dermatology, 123*(5), 924-929.

Yun, M. H. (2015). Changes in Regenerative Capacity through Lifespan. *International Journal of Molecular Sciences, 16*(10), 25392-25432. doi:10.3390/ijms161025392

7. Appendix

7.1. List of publications

Pinto-Teixeira, F.*, Viader-Llargués, O.*, Torres-Mejia, E., Turan, M., Gonzalez-Gualda, E., Pola-Morell, L., & López-Schier, H. (2015). Inexhaustible hair-cell regeneration in young and aged zebrafish. *Biol Open*, 4(7), 903-909. doi:10.1242/bio.012112

* equally contributing authors

Viader-Llargués, O., Lupperger, V., Pola-Morell, L., Marr, C., & López-Schier, H. (2018). Live cell-lineage tracing and machine learning reveal patterns of organ regeneration. *eLife*, 7. doi:10.7554/eLife.30823

7.2. List of acronyms

4-OHT	4-hydroxy-tamoxifen
actb1	actin b 1
AG1478	*N*-(3-Chlorophenyl)-6,7-dimethoxy-4-quinazolinanine hydrochloride
Atoh1	atonal bHLH transcription factor 1a
AZK	azakenpaullone
BrdU	bromodeoxyuridine
BSA	Bovine Serum Albumin
Cas9	CRISPR-associated protein 9
cdkn1bb	cyclin-dependent kinase inhibitor 1Bb
CRISPR	Clustered Regularly Interspaced Short Palindromic Repeats
API	4′,6-Diamidine-2′-phenylindole dihydrochloride
DAPT	N-[N-(3,5-Difluorophenacetyl)-L-alanyl]-S-phenylglycine t-butyl ester
dkk	dickkopf
DMSO	dimethylsulfoxid
DNA	deoxyribonucleic Acid
dpa	days post ablation
dpi	days post injury
EGFP	Enhanced Green Fluorescent Protein
ErbB2	erb-b2 receptor tyrosine kinase 2
ERT2	Estrogen Receptor T2

FACS	Fluorescence-Activated Cell Sorting
FGF	Fibroblast Growth Factor
FGFR1	Fibroblast Growth Factor Receptor 1
GAL4	yeast transcriptional activator
GFP	Green Fluorescent Protein
GSK3	Glycogen Synthase Kinase 3
her4.1	hairy-related 4, tandem duplicate 1
hpf	hours post fertilization
hpt	hours post treatment
IWR-1	4-(1,3,3a,4,7,7a-Hexahydro-1,3-dioxo-4,7-methano-2H-isoindol-2-yl)-N-8-quinolinyl-Benzamide
kb	kilo-base
krt4	keratin 4
LB	Luria-Bertani
LSM	Laser Scanning Microscopy
MCC	Matthews Correlation Coefficient
mRNA	messenger RNA
ngn1	neurogenin 1
PBS	Phosphate-Buffered Saline
PBST	PBS Tween
PCP	Planar Cell Polarity
PFA	paraformaldehyde
RA	Retinoic Acid

rar	retinoic acid receptor
RFP1	Red Fluorescent Protein 1
RNA	ribonucleic acid
RT	Room Temperature
SILL1	Sensory Innervation of the Lateral Line 1
SOC	Super Optimal broth with Catabolite repression
Sox2	Sex determining region Y-box 2
ET	Enhancer Trap
TALEN	Transcription Activator-Like Effector Nuclease
Tg	transgenic line
UAS	Upstream Activating Sequence
VP16	transactivation domain
Wnt	wingless-related integration site

7.3. **Acknowledgments**

During these years I have had the chance to interact with many good people who offered invaluable support and who helped shape this thesis in one way or another. I am deeply grateful to everyone who made this work possible.

I would like to thank my thesis director Dr. Hernán López-Schier for giving me the opportunity to joining his lab, for sharing his passion for science and for his endless and thorough guidance and mentorship.

I also want to thank my *Doktorvater* Prof. Dr. Wolfgang Wurst for approving and supervising my PhD project as member of my HELENA thesis committee and for representing this thesis at the TUM.

I would also like to thank Dr. Jovica Ninkovic for being an active member of my HELENA thesis committee and steering my research work towards the right direction.

I would also like to thank the HELENA graduate school for all their support and for fostering the development of transferable skills along with the purely scientific ones.

I am thankful to my collaborators, Dr. Carsten Marr and Valerio Lupperger for their excellent work with the machine learning analysis, insightful suggestions and rigorous support. It has been a real pleasure to work together with them.

At this point, I want to extend my gratitude to all members of the López-Schier lab, not only for their scientific support, but also for their sincere friendship. First and foremost, to Elen, one of those friends that are really hard to find, but also to Jesús, Ioannis, Prisca, Petra, Amir, Yan, Marta, Gema, Weili and Eva. Thank you all for making the long hours at the lab a truly enjoyable experience. Also, to former members of the lab, Filipe, Adèle, Alessandro and Andrea for transferring your knowledge onto us

diligently. Last but not least, to the animal caretakers of the zebrafish facility for maintaining the fish lines and stocks in excellent conditions.

Thank you to all the members of the Desbordes' lab: Sabrina, Stefan, Tanja, Theresa and Anna for completing the "family".

I am also grateful to my colleagues from other labs, in particular to Kirill and Christian, for being great buddies on whom I could rely at all times.

Finally, I would like to extend a very special thank you to my family, and in particular to my parents Eulàlia and Armand, for giving me unconditional love and endless courage from afar. Thank you for always fostering my curiosity in science and for instilling in me great work ethics.

Something very unique, however, has made this whole journey absolutely worth it; meeting Laura, the mother of my newborn baby Emma. She hasn't only contributed enormously to this thesis, but she also has filled my life with meaning and purpose.

7.4. **Eidesstattliche Erklärung**

Hiermit erkläre ich an Eides statt, dass ich die vorliegende Dissertation gemäß der Prüfungsordnung der Technische Universität München selbstständig, ohne unzulässige fremde Hilfe und unerlaubte Hilfsmittel angefertigt habe.

München, den

_____

(Oriol Viader-Llargués)